2022-12-01

Continuous Moisture Measurement During Pavement Foundation Construction: Laboratory Measurements

Isaac Esteban Zuniga
University of Texas at El Paso

Recommended Citation

Zuniga, Isaac Esteban, "Continuous Moisture Measurement During Pavement Foundation Construction: Laboratory Measurements" (2022). *Open Access Theses & Dissertations*. 3754.
https://scholarworks.utep.edu/open_etd/3754

CONTINUOUS MOISTURE MEASUREMENT DURING PAVEMENT FOUNDATION CONSTRUCTION: LABORATORY MEASUREMENTS

ISAAC ESTEBAN ZUNIGA

Master's Program in Civil Engineering

APPROVED:

Soheil Nazarian, Ph.D. Chair

Cesar Tirado, Ph.D.

Arturo Bronson, Ph.D.

Mark Baker, D.Sc.

Stephen L. Crites Jr., Ph.D.
Dean of the Graduate School

CONTINUOUS MOISTURE MEASUREMENT DURING PAVEMENT FOUNDATION CONSTRUCTION: LABORATORY MEASUREMENTS

by

ISAAC E. ZUNIGA, B.S.C.E.

THESIS

Presented to the Faculty of the Graduate School of
The University of Texas at El Paso
in Partial Fulfillment
of the Requirements
for the Degree of

MASTER OF SCIENCE

Department of Civil Engineering
THE UNIVERSITY OF TEXAS AT EL PASO
December 2022

ACKNOWLEDGEMENTS

I would like to express my gratitude to Dr. Soheil Nazarian, Professor of Civil Engineering and Director of the Center for Transportation Infrastructure Systems (CTIS) at the University of Texas at El Paso (UTEP), for his guidance and support during my master's career. I also want to thank Dr. Mark Baker for his assistance and guidance throughout my master's research. It was a privilege working with both and a rewarding experience I will cherish. Both taught me so much in the fields of research, geotechnical engineering, and geophysics, making me a better researcher, writer, and engineer.

A special thanks to Sebastian Morales, Undergraduate Research Assistant, for all the help provided during the laboratory testing and all the assistance provided throughout this study. Also, to Sergio Rocha, Laboratory Manager, for his assistance throughout the laboratory research.

I would like to acknowledge the funders of my study, the National Road Research Alliance (NRRA) and the Minnesota Road Research Facility (MnROAD) staff of the Minnesota Department of Transportation, for their financial assistance provided for the study.

Finally, a special thanks to my family for encouraging me and supporting me. To my mother and father; I am very thankful for all the love and support throughout my academic career.

TABLE OF CONTENTS

LIST OF TABLES

LIST OF FIGURES

CHAPTER 1 – INTRODUCTION

1.1 Objective

For successful construction and the long-term durability of pavement constructions, it is essential that the moisture content of earthwork is measured for accurately and promptly during the compacting of foundation layers. The goal of this research was to show a prototype/breadboard of a device that can continually measure moisture throughout the construction of a pavement foundation and evaluate existing devices that can read moisture in a laboratory environment.

The developed device is based on characterizing moisture content by measuring a geomaterials' complex resistivity (CR) as a function of frequency, field strength, and measurement geometry. In complex resistivity measurements, the distortion (phase shift) between the voltage and current is recorded in addition to the resistivity amplitude over a wide frequency range. The resistivity is given by the in-phase amplitude, while the dielectric constant is given by the amplitude with a 90° phase shift.

Complex resistivity measurements can be caused by both the extrinsic properties of charge transfer between metal electrodes to pore water and the intrinsic properties of ionic conduction in the geomaterial. Ionic conduction across free pore water, polarization at the air-water interface, and polarization along adsorbed water at grain boundaries are the targets to be measured by complex resistivity. Void content, moisture content, and pore size distribution control the in-phase and out-of-phase currents. In most cases, dissolved solids or mineral surface charges have an ionic effect that suppresses water permittivity, which causes bias in materials with a high fines content. Water connection across the pore space and saturation levels dominate low-frequency resistivity measurements, with water volume coming in second. If sufficient observations are taken to differentiate between residual moisture on particles, saturation fluctuations, and void changes in compaction, low-frequency resistivity may likely be employed with little calibration, which requires measuring:

1) Material resistivity before watering
2) The resistivity of the water added
3) Pre-and Post-compaction resistivity

With an improved polarization signal with partial saturation, CR at intermediate frequencies should identify saturated and unsaturated situations from charges restricted from movement at air-water interfaces, reducing the requirement to evaluate soil resistivity before and after watering.

1.2 Organization

Chapter 2 will document the current state of knowledge concerning field moisture measurement during pavement foundation construction and case studies demonstrating cost savings resulting from more effective moisture measurements. Chapter 3 will provide the different laboratory procedures and an explanation of each laboratory measurement. Chapter 4 will present the different measuring devices with correlations to moisture content in the laboratory setting on compacted specimens. Chapter 5 will discuss the conclusion made from the study and recommendations.

CHAPTER 2 – CURRENT MOISTURE MEASUREMENT METHODS

A foundation layer for durable rigid pavements should have the following attributes (White et al., 2021):

1) Provide uniform support
2) Be balanced in terms of flexibility and stiffness
3) Provide adequate drainage
4) Not be affected by permanent plastic deformation
5) Utilize sustainable practices and materials

Moisture content is an essential property of geomaterials that must be monitored during and after the construction of unbound pavement layers. Improper quality control and quality assurance (QC/QA) of compacted geomaterials may result in from an inability to estimate the moisture content correctly and rapidly during construction. During the life of a pavement, excessive volume of water in the unbound layers of the pavement structure may contribute to the development of early distress and lead to the structural or functional collapse of the pavement. Water-related damage can result in one or more of the following types of deterioration: weakening of the subgrade, base, and subbase; differential swelling in expansive subgrade soils; frost heave; and weakening of the subgrade, base, and subbase during frost melt; and movement of fine particles into the base or subbase coarse materials, resulting in a decrease in hydraulic conductivity (Liang et al., 2016). During the 1980s, several scholars researched the problem of monitoring the water content of pavement constructions, which sparked an upsurge in interest in this field. The Strategic Highway Research Program (SHRP) examined how fluctuations in moisture content affected pavement structures (Svensson, 1997). Since then, several methods and procedures for measuring the soil moisture content have been presented. Traditional moisture measurement methods, such as physical sampling or installing sensors such as time domain reflectometry (TDR) probes, give only spot measurements, making them impracticable for large-scale research. Professionals in the business are now developing a novel method for detecting soil water content in real-time across a continuous region.

An ideal section of pavement should be laid on a consistent pavement base that extends beyond the driving lane. To achieve consistent pavement construction, it should be constructed upon a uniform embankment. The cross-section of an idealized pavement is seen in Figure 1. It must offer appropriate drainage and be sufficiently compact to withstand various vehicular loads. The subgrade should be properly compacted first.

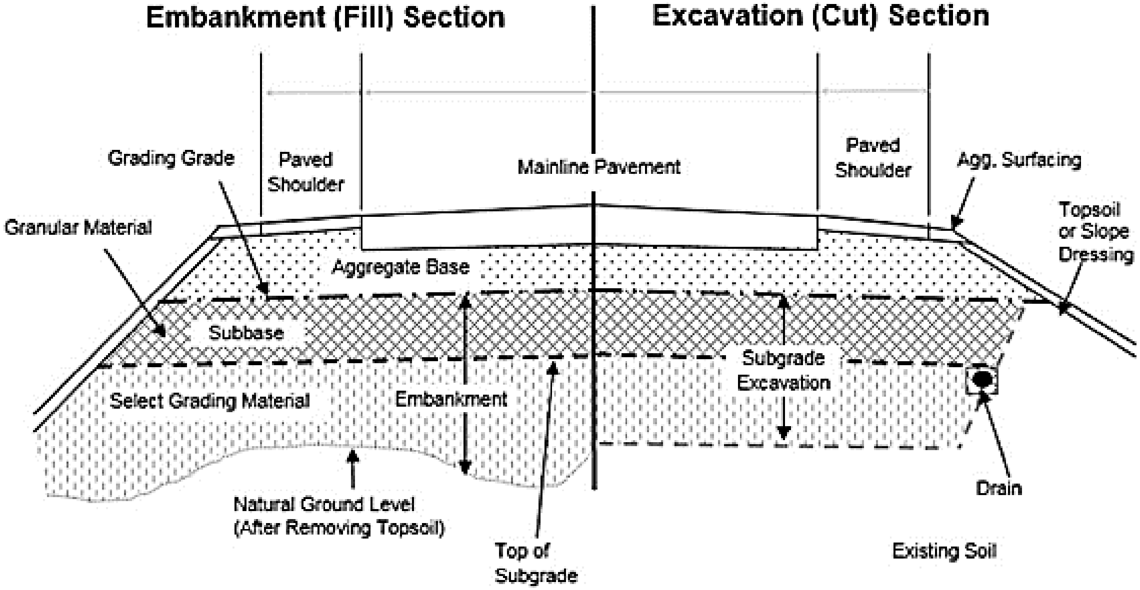

Figure 1: An Ideal Pavement Section

A review of the literature on the various measuring apparatuses is provided next.

2.1 Measuring Methods

Several methods for soil moisture measurement have been developed throughout the years. Based on the technique and measurement principles used, the various methodologies may be divided into direct and indirect categories (Svensson, 1997). The direct approach (i.e., the gravimetric method) entails collecting a soil sample from the site under investigation. The soil sample is weighed before and after drying at 105°C (220°F). This approach is regarded as the "gold standard" for determining the moisture content of substances.

In indirect approaches, a radiation source or a probe put in or on the geomaterial is used to measure a parameter significantly related to the moisture content. Since the soil is only disturbed during installation, the primary benefits of these techniques are that they are more rapid and often nondestructive (Evett et al., 2008).

None of these techniques directly measure the soil water content, but all measure a characteristic highly linked with the soil moisture content. Some of the equipment associated with this research that monitor moisture content only offer point readings, not spatially continuous observations. Examples of these approaches and their principles are presented in Table 1.

ASTM D6938-17a outlines the standard test techniques for in-situ density and soil water content measurement with nuclear methods. The nuclear density gauge (NDG, Figure 2) measures the density and estimates the water content of compacted geomaterials in various ways (Viyanant et al., 2004). The gauge is calibrated to measure soil or aggregate moisture mass per unit volume. The volumetric water content may be calculated by dividing the mass of water per unit volume then multiplying by 100. The nuclear gauge also employs direct transmission and backscatter to determine density and water content.

Thermalizing or slowing fast neutrons that impact hydrogen atoms in the soil, the neutron moisture measurement calculates the water mass per volume. The neutron source and thermal neutron detector are surface-based and can record and convert the slow neutron count rate to estimate the volumetric water content. Thermal neutron capture may also affect the thermal neutron count rate, with iron (Fe) being the most prevalent modifier. Alternative methods are suggested for measuring the moisture content of base and subgrades. (Sebesta et al., 2013).

Table 1: Indirect Tests

Method	Measurement Principle	Explanation
Nuclear Density Gauge (NDG)	Back-scattered or transmitted gamma-ray count-rate	A source of high energy emits gamma rays (Co60) that interact with the geomaterial. A gamma detector counts the returning gamma rays with energies linked to Compton Scattering, which is directly connected to electron density and material density.
Nuclear Moisture Gauge	Thermalized neutron count-rate	A neutron source emits high-energy neutrons, while a neutron detector measures neutrons whose energy has been thermalized by repeated collisions with hydrogen nuclei in water. Neutron capture by some elements affects count rates subsequently.
Nuclear Magnetic Resonance (NMR)	Detection of the weak magnetic moment	After placing a combination of soil and water in the NMR analyzer and inducing a radio frequency, a voltage is supplied to the surrounding coil. This voltage is proportional to the amount of water in the sample and corresponds to the number of atoms that have absorbed energy (Svensson, 1997). When a radio frequency is induced, an atom absorbs a certain amount of energy to reposition itself inside the magnetic field.
Capacitance meters	Oscillating circuit to measure changes in frequency	A capacitor consists of two insulated electrodes, with the soil contributing the most to the dielectric constant. Equipment and dirt compose the measurement circuit. The probe detects and measures the frequency change dominated by the water content of the soil. (Svensson, 1997).
Ground Penetrating Radar (GPR)	Short pulses of electromagnetic through the soil	In addition to its other applications, GPR may be used to assess the soil's water content. Changes in permittivity may also be connected to variations in transmission time and amplitude of the reflected pulse (dielectric constant). After getting the changes in permittivity, it is possible to compute the soil's water content (Svensson, 1997).
Thermal Sensors	Heat conductivity or heat capacity of the soil	A heat pulse is generated, and the subsequent increase or decrease in soil temperature is monitored over time. Since soil is a weak heat conductor compared to water, the heat or heat transfer quantity is proportional to the volumetric water content (Evett et al., 2008).
Conductivity Sensors	Electrical conductivity of a porous medium in contact with the soil	Granular matrix sensors and gypsum blocks include conductivity sensors. Instead of assessing water content by volume, these sensors evaluate soil water tension (Evett et al., 2008). Current measures the conductivity and quantity of water between electrodes by injecting an alternating voltage between two electrodes in a porous medium, facilitating the exchange of soil moisture.
	Voltage measured at two electrodes from current injected at two other electrodes	A low-frequency alternating current is injected between two electrodes, while a voltage is monitored between two electrodes with no current flow. The shape of the electrodes transforms the observed voltage/current ratio to apparent resistivity, while the distance between the electrodes regulates the measurement volume.
	Eddy currents, induced by an alternating magnetic field, increase with conductivity	A magnetic field created by one coil over the ground is measured at a second coil. This secondary field reacts to geometry, magnetic susceptibility of the soil, and eddy currents created in a conductive soil, which are principally governed by soil moisture. The eddy current is related to the frequency and conductivity of the soil.
Resistance measurements	The resistance between two electrodes	The electrical resistance of the soil, which fluctuates depending on its moisture content, is used to quantify its moisture content. As the moisture content of the soil rises, its electrical resistance lowers, and conductance rises. Resistance may range from several hundred k when wet to several hundred M when dry (Sad, 2007).
Tensiometer measurements	Measurement of a pressure differential in the soil	A porous membrane forms the contact between the water-filled pressure sensor and the soil as the significant component of the tensiometer. The negative pressure inside the tube may be measured using a vacuum gauge to determine water tension (Evett, 2008). However, if the relationship between matric potential and soil water content is understood, the water content may be determined (Svensson, 1997).

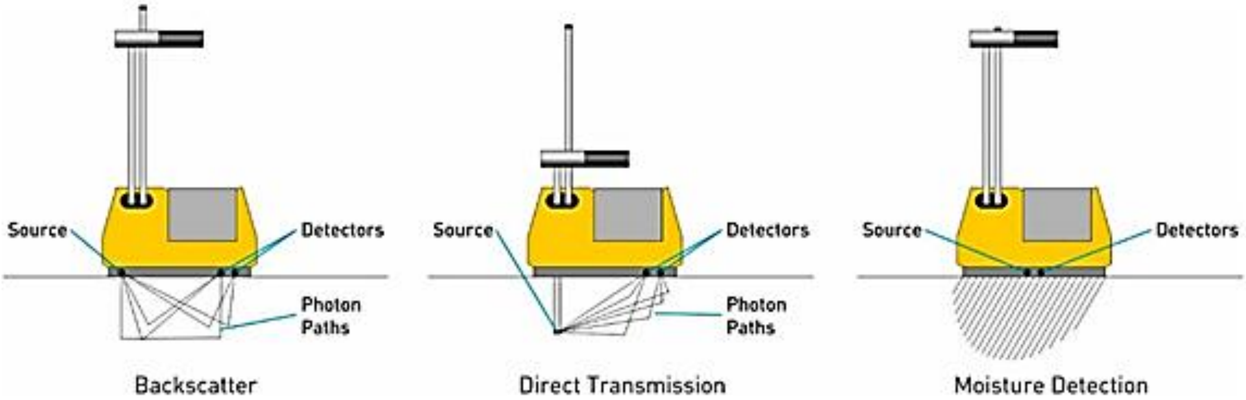

Figure 2: Positioning of a Nuclear Gauge for Three Different Methods (UTEST, 2016)

Time Domain Reflectometry (TDR, Figure 3) is widely used to determine water content and electrical conductivity (Jones et al., 2002). TDR transmits an electromagnetic pulse over a coaxial wire to the probe and detects its reflection. Time to reflection is proportional to cable length, early reflection amplitude is governed by permittivity (dielectric constant), and late reflection features are governed by electrical conductivity. The reflection amplitude is determined chiefly by the dielectric constant of the soil around the probe; the dielectric constant is 1 for air, 2-9 for ordinary dry soil particles, and about 81 for water. Since changes in the TDR-measured dielectric constant are strongly related to changes in the water content of soils, it is relatively easy to determine the soil moisture content for silicate soils (Yu and Yu, 2009). Soils with carbonates, gypsum, and clays have a higher dry permittivity and require local calibration for mineral variations.

Sotelo (2012) evaluated five non-nuclear devices, including a Purdue Time Domain Reflectometer (TDR), Soil Density Gauge (SDG200), Decagon 10HS Moisture Content Sensor (10 HS), Speedy Moisture Tester (SMT), and a DOT600 Roadbed Water Content Meter, to determine their accuracy in measuring moisture content and dry density. Sotelo prepared several small-scale specimens within the laboratory to simulate the construction of five soils ranging from poorly graded gravel to clay (CH). The TDR and SMT were the most accurate devices in measuring moisture content. The other three devices were accurate, with only specific soil samples. The most accurate device in measuring dry density was the TDR, except for a CH material; however, the SDG accurately measured the density of the CH soil but not the remaining soils.

Figure 3: Typical TDR Device

2.2 Evaluation of Technologies Determining Moisture Content over Time

Bogena et al. (2007) examined an ECH$_2$O probe (model EC-5, low-capacitance sensor by Decagon Devices Inc.) utilizing laboratory and field tests. Using TDR and EC-5 sensors, they also compared permittivity and soil water content data. They put four EC-5 sensors and two TDR probes permanently attached to a data recorder in the field. The TDR measurements were conducted using Campbell Scientific TDR100 cable tester equipment, and a sensor reading-permittivity (SRP) model was utilized to determine the EC-5 sensor’s recorded permittivity. Using an equation given by Robinson et al., the researchers calculated the soil moisture content (2003). Figure 4 shows the TDR-measured soil water content and the mean values and standard deviations of all EC-5 sensors throughout seven months. The findings indicated that the data from the EC-5 sensor should be modified using the temperature and conductivity adjustment algorithms.

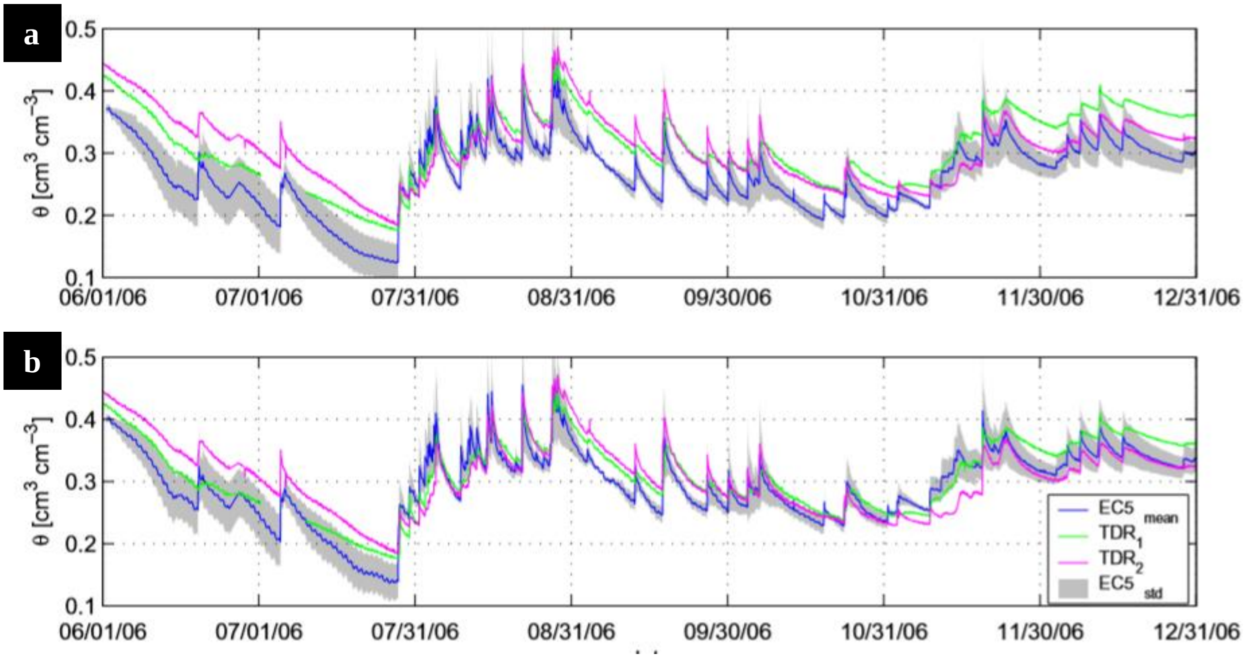

Figure 4: Measured VWC (a) TDR and EC-5 Sensors (b) TDR and Corrected EC-5 Measurements

Mittelbach et al. (2011) examined a distinct capacitance probe (10HS) for measuring volumetric water content (VWC) in the laboratory and the field. The 10HS VWC readings were compared to the matching gravimetric and TDR data (TRIME-EZ and TRIME-IT, IMKO GmbH, Germany). Using gravimetric sample measurements as a reference, the goal of the laboratory tests was to detect the difference in VWC between the 10HS and the TRIME sensors. Figure 5a displays the laboratory VWC measurements. Two calibration functions are presented for the 10HS sensor (Decagon Version 2.0 and best lab fit). According to the findings, TDR values were closer to the standard VWC. The calibration feature of Decagon Version 2.0 produced inaccurate results, particularly over 30-40% moisture content. The finest lab fit enhanced the reading, hence increasing its reliability. Figure 5b depicts the measurement accuracy of sensor reading, illustrating the variation within the 10HS sensor type (blue) and the DV/dVMC of the 10HS sensor (green). The sensor sensitivity for DV/dVWC (mV/Vol.%) decreased significantly as VWC increased. The decrease in sensitivity may be linked to the concept of capacitance sensors, wherein the capacitor charges more slowly at high VWC.

The 10HS sensors were evaluated for the field measurements at the Swiss locations of Oensigen (OEN) and Payerne (PAY). For 13 months, the soil moisture content was monitored at both sites using 10HS and TRIME IT/EZ. Figure 6 depicts precipitation, air temperature, and absolute soil moisture. Absolute soil moisture is the soil moisture integrated across the measured soil column in millimeters. Except for the past two months, using the best field fit considerably improved the calculated absolute soil moisture content, mirroring TDR readings. The researchers determined that the optimal configuration for accurate soil moisture networks comprised parallel capacitance and TDR measurements with the correct calibration of 10HS sensors. They concluded that the differences between the various 10HS sensors were minimal. In addition, they emphasized that the 10HS sensor requires site-specific calibration functions and is optimal for low VWC concentrations.

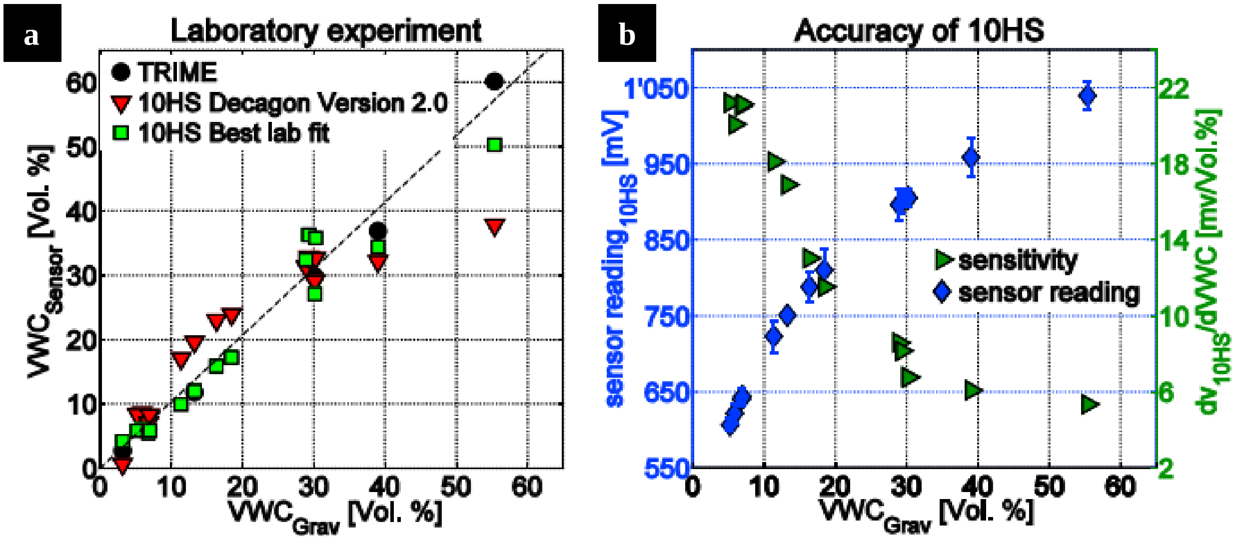

Figure 5: (a) Laboratory Measurements Results with TRIME (TDR) and 10HS (capacitance) Sensors as a Function of VWC of the Gravimetric Samples (b) Accuracy of 10HS Sensors

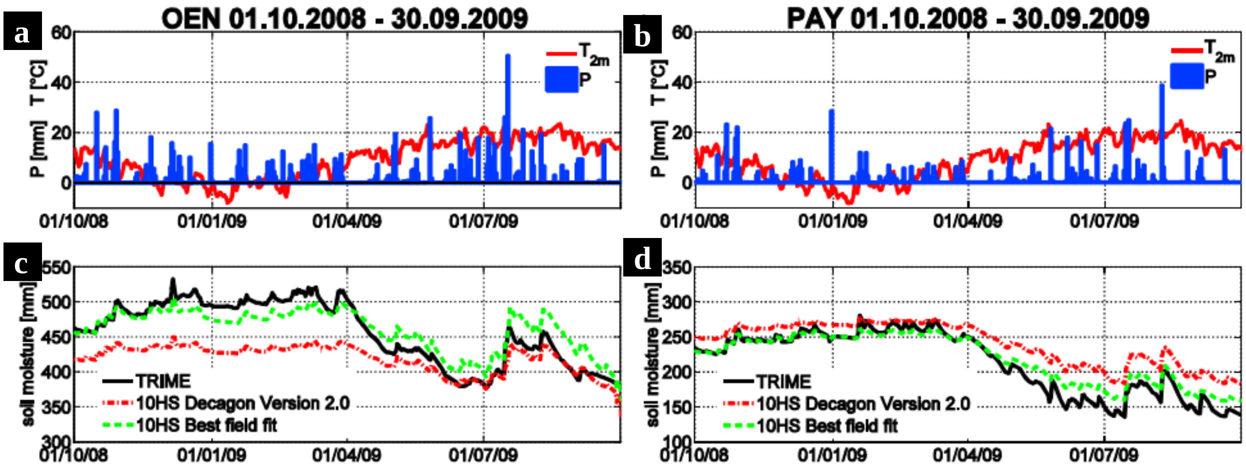

Figure 6: Precipitation and Temperature Measurements of (a) OEN and (b) PAY. Absolute Soil Moisture of (c) OEN and (d) PAY

Hansen and Nieber (2013) examined the accuracy of the DOT600 (moisture content), WP4C dewpoint potentiometer (matric suction), the Button Heat Pulse Sensor (BHPS) (temperature rise vs. moisture content), and an exudation pressure test device in predicting the moisture contents of three subgrade soils typically used in Minnesota roadway construction projects.

In a study, Singh (2017) evaluated the field performance of eight electromagnetic (EM) sensors (TDR315, CS655, HydraProbe2, 5ET, EC5, CS616, Field Connect, and AquaCheck). Specific aims of the research included evaluating EM sensors for VWC and comparing factory calibration to bespoke calibration procedures for VWC. In addition to the factory default calibrations for the EM sensors, the Topp calibration equation (Topp et al., 1980) was evaluated for the TDR315, HydraProbe2, and EC5 sensors. Following Bell et al., the field-calibrated neutron moisture meter (NMM) was adopted as the standard for VWC (1987).

The variance over time between sensor-reported and reference VWC found in this investigation is shown in Figure 7 for single-sensor probes and Figure 8 for multi-sensor probes. Using either the factory calibrations or the included alternative calibrations, these charts indicated that all tested sensors followed the overall trend. However, they all overestimated VWC in comparison to the standard. Using Topp's calibration equation instead of the factory calibration enhanced the performance of TDR315 but not HydraProbe2 or EC5.

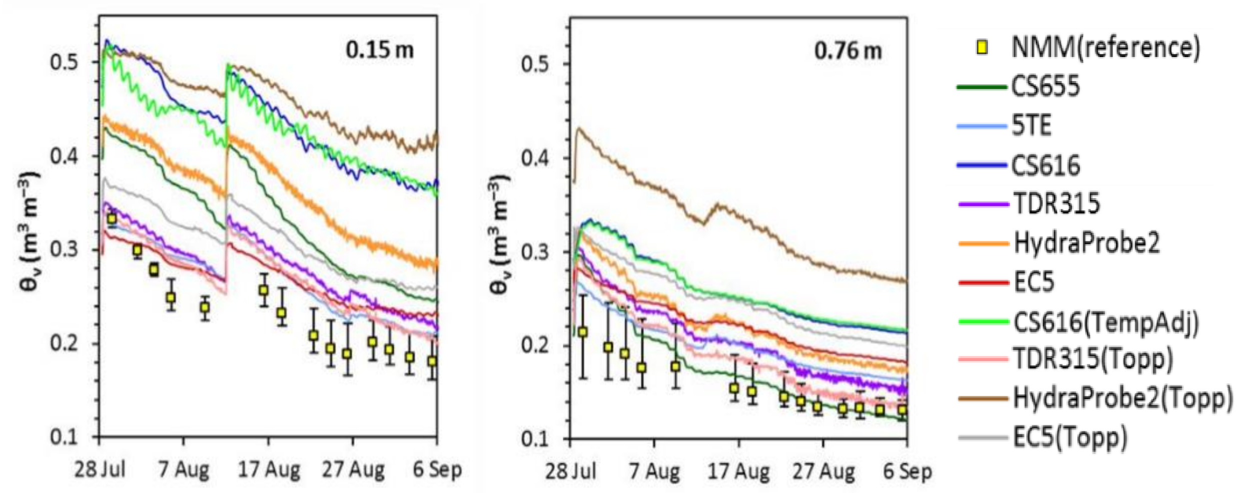

Figure 7: Measurements of VWC at Two Distinct Depths with Single-Sensor Probes as compared with the field-calibrated NMM

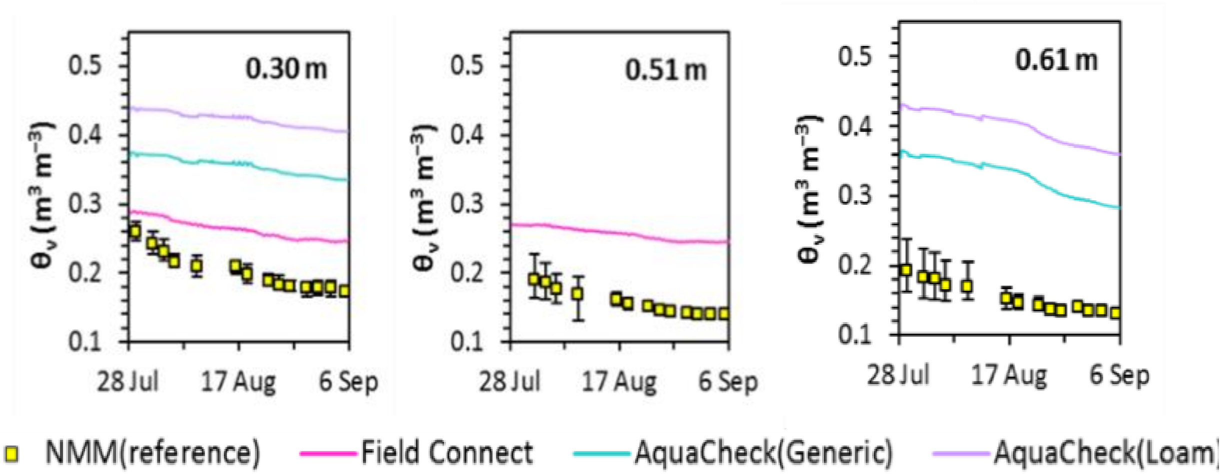

Figure 8: Measurements of VWC at Three Distinct Depths using Multi-Sensor Probes as compared with Field-Calibrated NMM

Shaikh et al. (2018) devised a simple laboratory setup to analyze all six profile probe (PP) sensors for a specific soil type and compaction condition concurrently. Based on TDR and the capacitance technique, PP measurements were conducted on six soils planned for use in a multilayer cover system (MLCS). Figure 9 depicts the experimental setup used to evaluate the performance of the PP. This assessment was accomplished by comparing the measured and calculated (theoretical) VWC; recalibration was undertaken if the comparison was inadequate. The first findings revealed a discrepancy between the measured and calculated VWC for each of the six soil types. Consequently, various calibration constants were utilized to recalculate the recorded VWC from the known voltage values and the square root of the dielectric constant; the recalculated measurements yielded satisfactory findings, as shown in Figure 10.

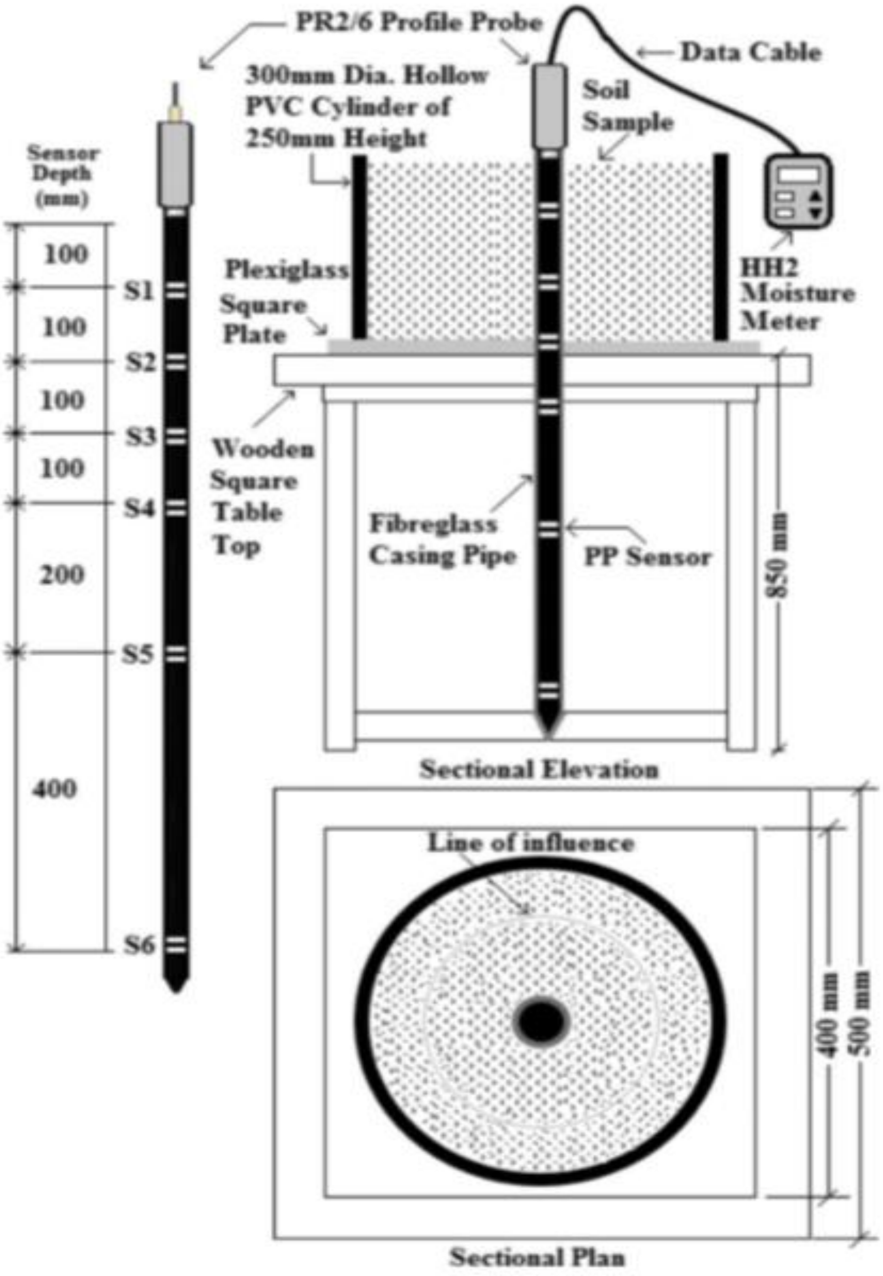

Figure 9: Laboratory Setup for Calibration of PP Sensors

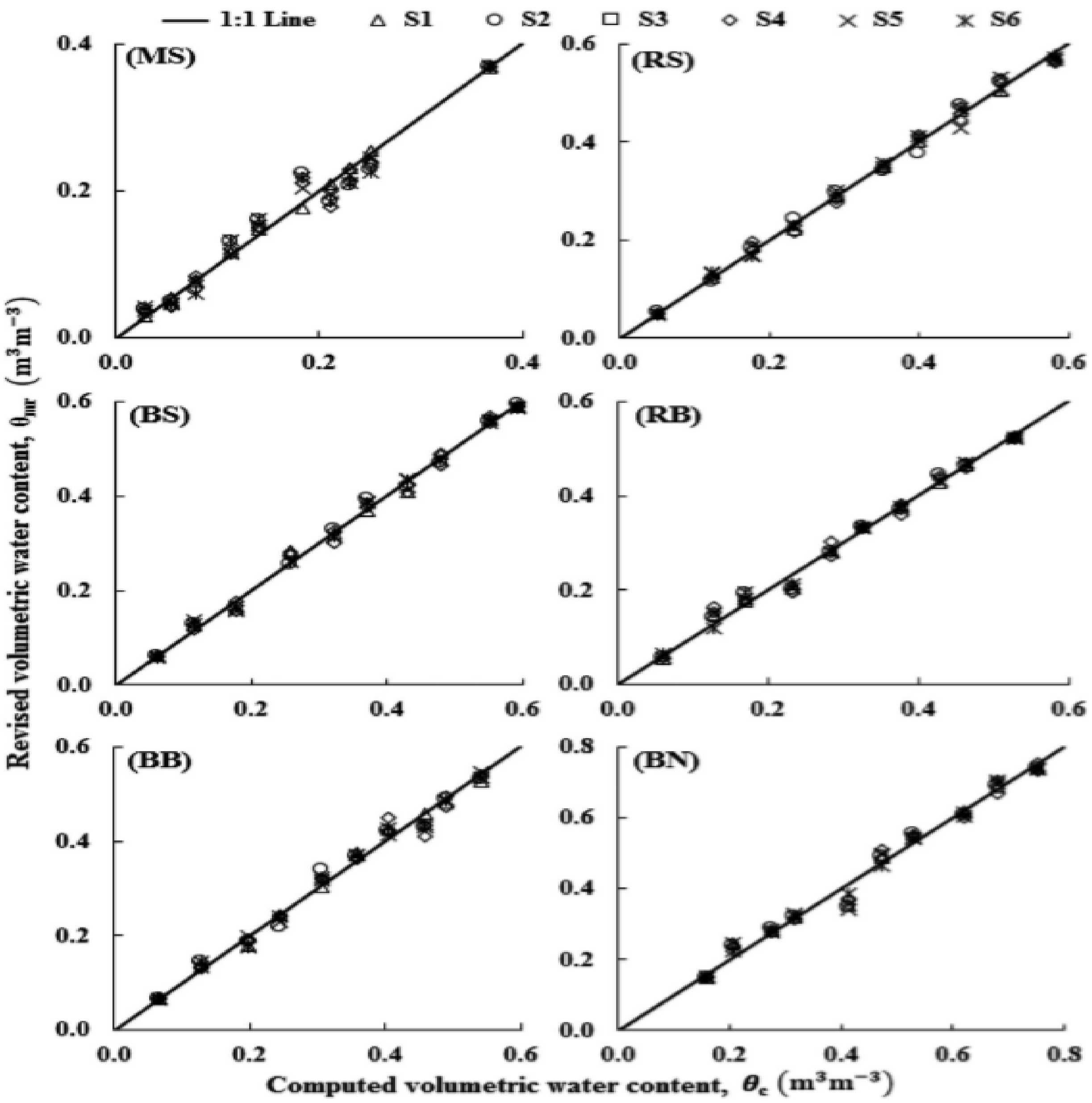

Figure 10: Comparison between Measured (using PP) and Computed VWC (Shaikh et al., 2018)

Figure 11 provides a more straightforward illustration of comparing sensor data before and after calibration for two soils, RS (medium plastic red soil) and RB, with the same compaction condition (mixed soil with bentonite). Without calibration functions, various sensors provided different VWCs for the same VWC at a particular compaction stage; however, after completing sensor- and soil-specific calibrations, the calculated and measured VWCs matched well, and all sensors reported comparable results. Before deploying the PP for field monitoring programs, they urged using their suggested laboratory process for accurate VWC (from 6% to 1% using calibration functions). They determined that soil water content may be continually monitored using a GPR system with many channels.

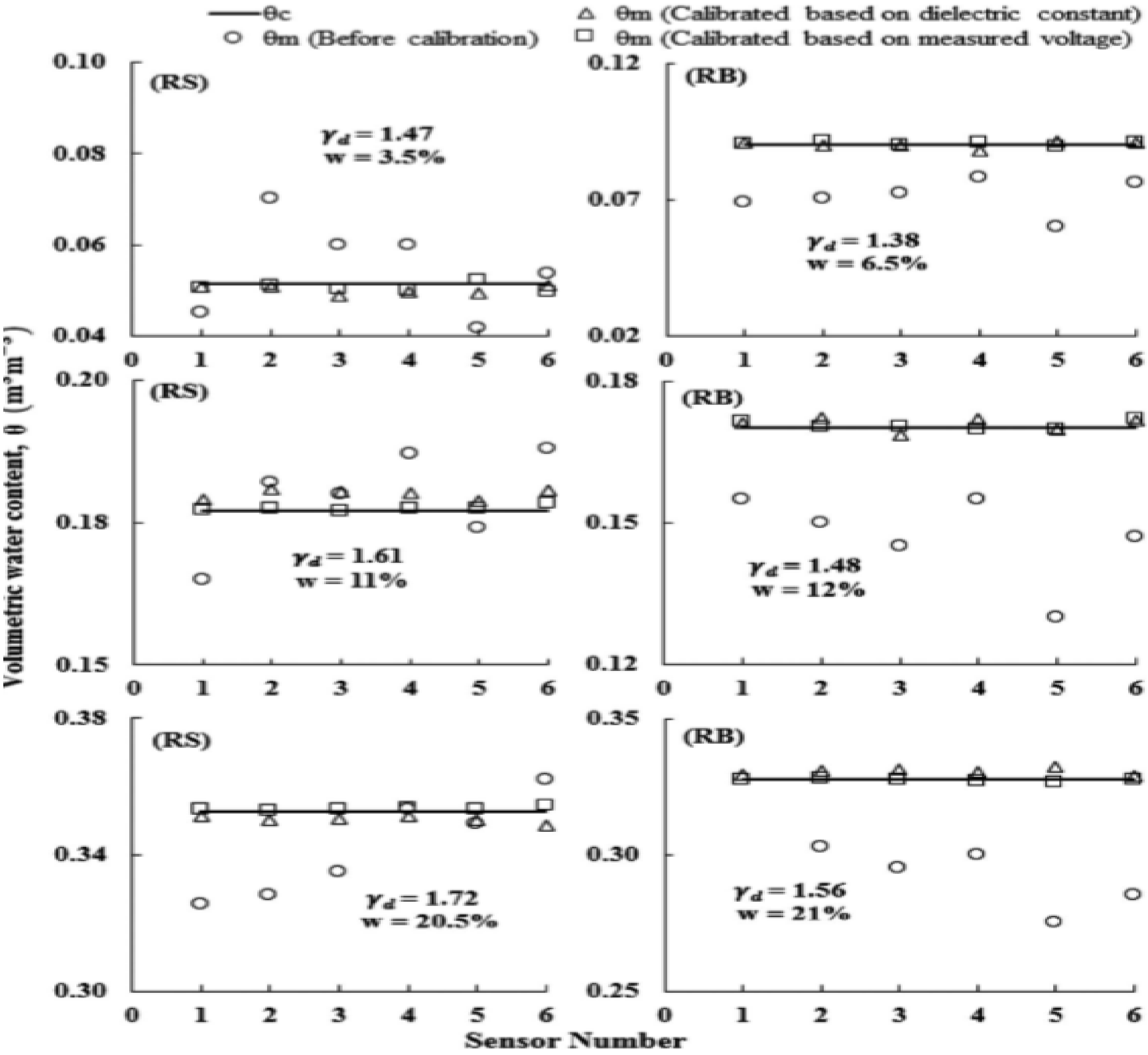

Figure 11: PP Measurements Before and After Calibration at Three Various Compaction States in RS and RB

2.3 Using GPR for Continuous Moisture Content Measurements Over Large Distances

The GPR operates by emitting brief pulses of electromagnetic energy from an antenna into the road structure, which is then reflected to a receiving antenna (Figure 12). The transmission duration and amplitude of the reflected pulse may be correlated with the position and dielectric discontinuities of the material (Maser and Scullion, 1992; Svensson, 1997). As a result of their direct link, the moisture content may also be determined by monitoring the changes in permittivity (dielectric constant). Typically, the equipment is installed on a van for highway studies so that data collection may be conducted at speeds similar to traffic flow (Figure 13). Air-coupled or ground-coupled operations are suited for GPR antennas. The antennas are positioned around 250 mm above the surface for air-coupled mode operating at highway speeds. For a stronger signal, ground-coupled antennas lie on the ground's surface.

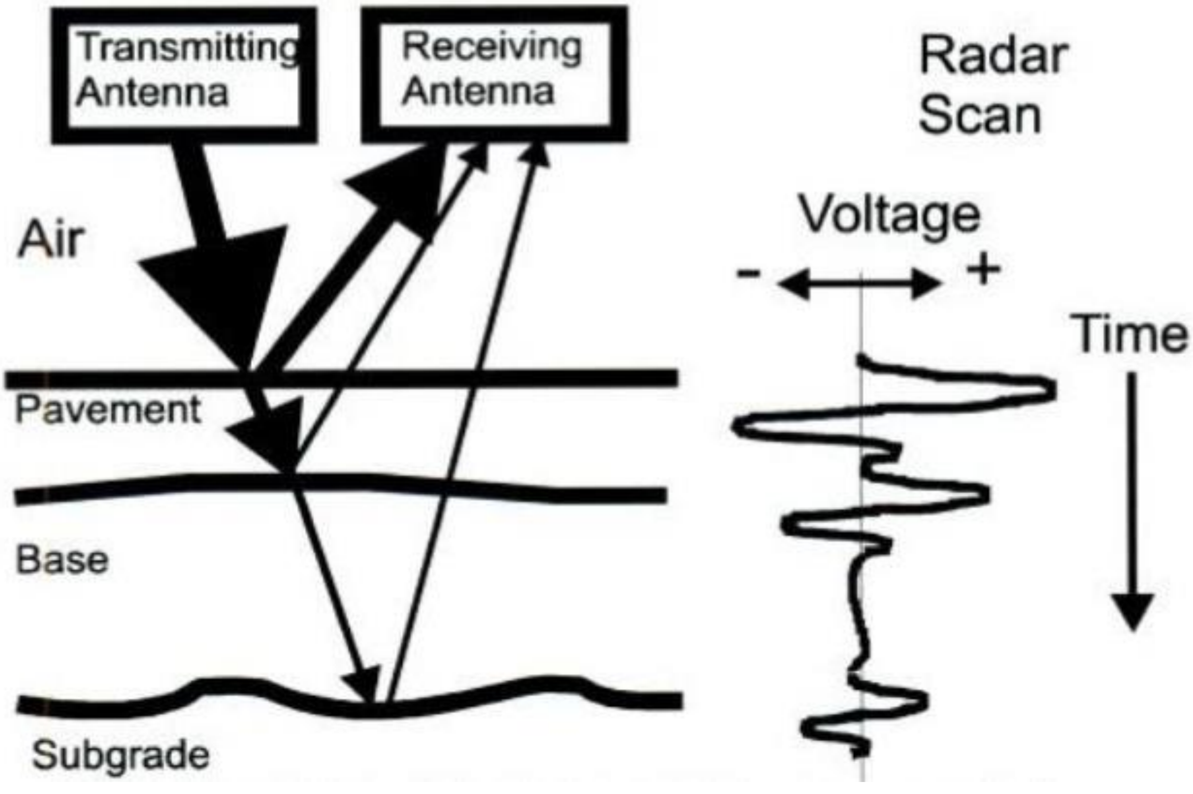

Figure 12: Transmission and Reflections from Interfaces in a Pavement Section

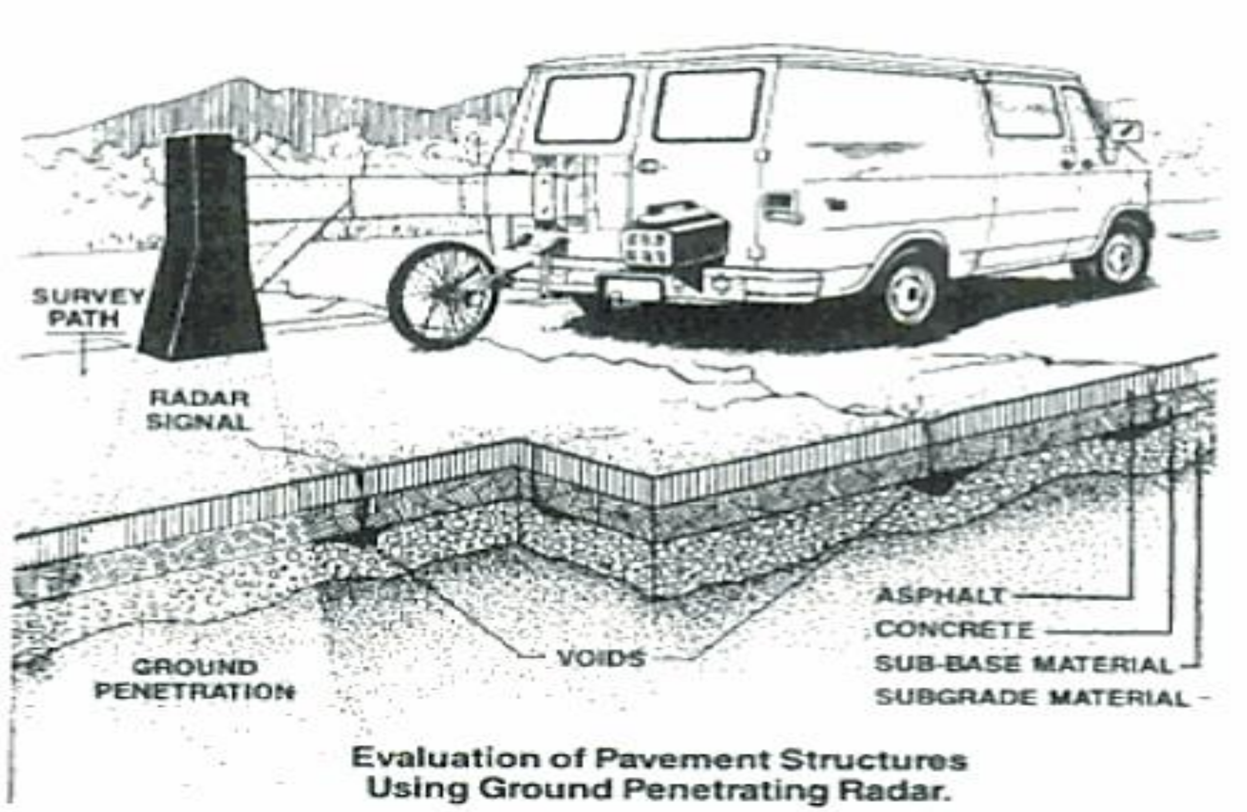

Figure 13: Illustrated Example of Van-mounted GPR System

For many decades, the application of GPR for continuous measurements of soil moisture content on the various strata of a pavement system has been researched. Using a van-mounted horn antenna setup, Maser and Scullion (1992) could effectively derive a moisture profile from radar data. Emilsson et al. (2002) showed that multichannel GPR may be used to measure moisture content in roadbeds continually. As seen in Figure 14a, their study was based on a standard midway technique using an antenna configuration. The antenna spacing in the array ranged from 0.15 m to 4 m for three separate antenna arrays operating at 250, 500, and 800 MHz. The findings in this paper were derived from 500 MHz data. Figure 14b shows an image of the 500 MHz antenna array. They gathered data at speeds between 20 and 40 kilometers per hour and determined the volumetric soil water content at the location. Figure 15 shows the outcomes.

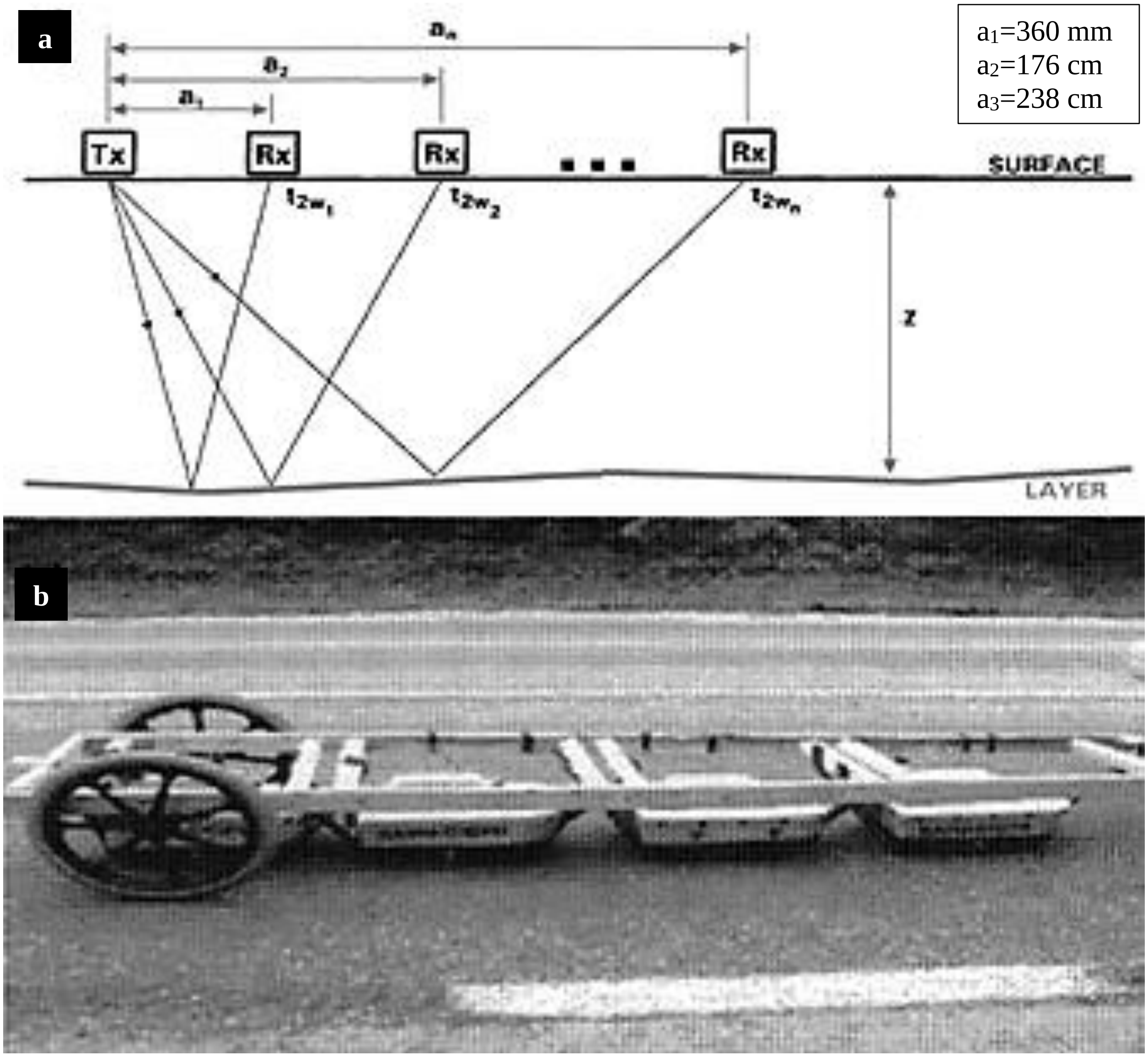

Figure 14: (a) Antenna Setup for Velocity Determination, (b) 500MHz Antenna Array

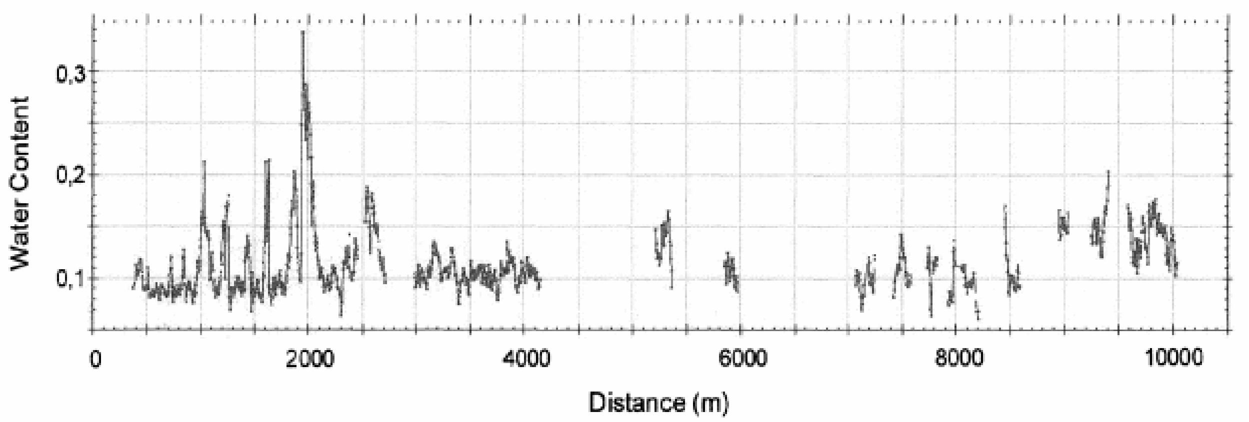

Figure 15: Calculated Soil Moisture Content

Gerhards et al. (2008) proposed a novel method using a multichannel GPR that enabled simultaneous assessment of the depth of a reflector and the average volumetric water content above the reflector with significantly increased operating effort compared to conventional measurement. They used a Mal GeoScience, Sweden-manufactured GPR multichannel device MC4 with a 250-MHz antenna setup. For a straightforward assessment, they employed two trip durations (t2 and t3) from differing antenna separations using a common midpoint (CMP) reflector (Figure 16).

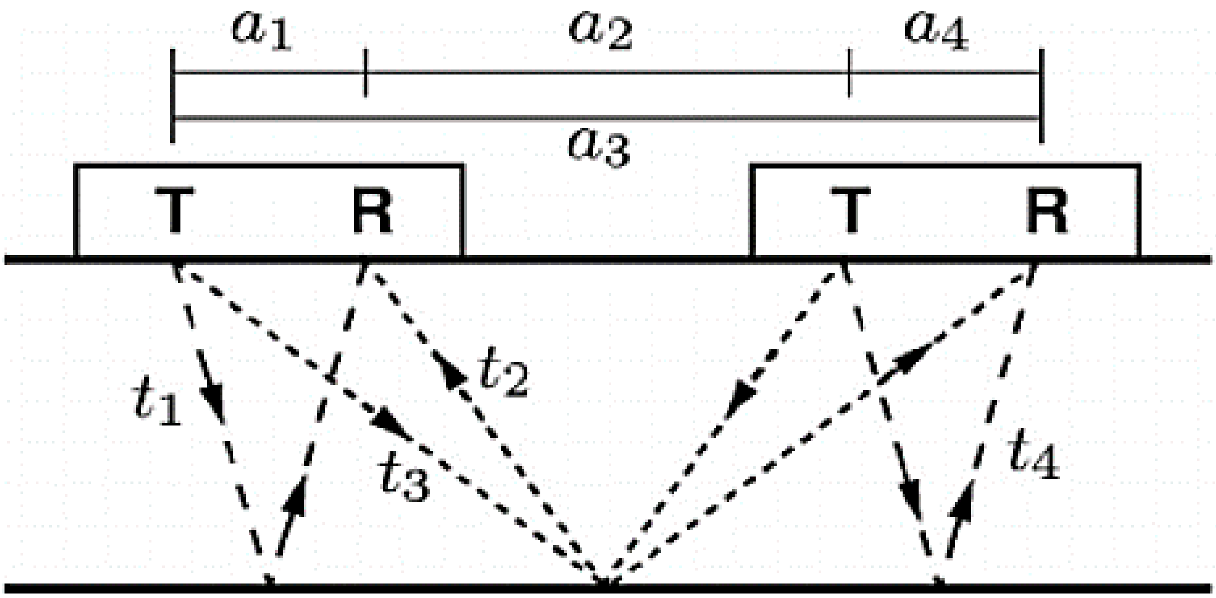

Figure 16: Antenna Setup for Multichannel Measurement

Because four rays and three antenna separations are available for each measurement site, the two-point assessment uses only some available information. In order to determine the reflector depth and average water content, a multipoint assessment with varying numbers of channels was conducted (Figure 17). The gray dashed line represents the multipoint assessment of Channels 1 and 2, whereas the black dashed line represents the multipoint evaluation of all channels. They found that the use of GPR exhibited in their work allowed for the simultaneous measurement of reflector depth and average water content and had a high potential for characterizing subsurface structure.

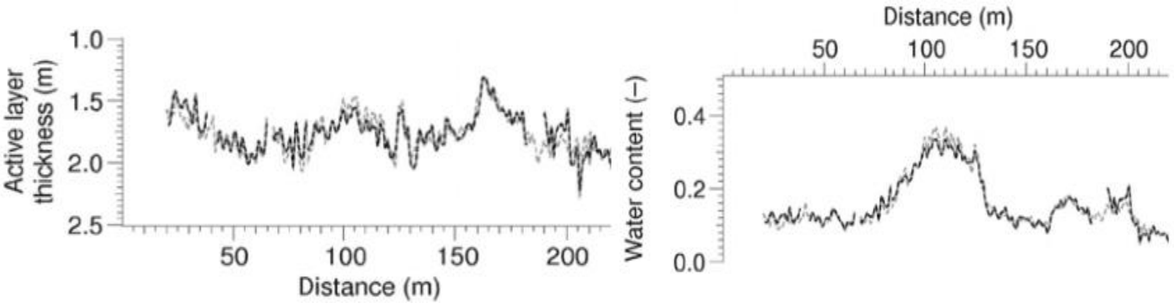

Figure 17: Calculated Reflector Depth and Average Water Content using Different Channels

Wollschlager et al. (2010) used multichannel GPR at a permafrost location to deduce spatial differences in thaw depth and average volumetric water content of the active layer. Their measurements were conducted per a modified version of the method used by Gerhards et al. (2008). Their multichannel GPR system allowed them to collect data from nine "channels" of transmitter-receiver combinations. Using the CMP technique while moving along the radargram, they could accurately estimate relative dielectric permittivity, reflector depth, and average soil moisture content at each position. In addition, they created an inverse evaluation process to improve precision.

The research (Wollschlager et al., 2010) indicated that the multichannel GPR approach covers the scales between standard point measurements and space-based remote sensing. Measurements were undertaken on an area of roughly 85 m by 60 m with surface and soil textural qualities ranging from medium- to coarse- to fine-textured soils, as well as the bed of a gravel road. Figure 18 depicts the topographically corrected reflected depth, relative dielectric permittivity, and average volumetric soil moisture content of the unfrozen active layer obtained from the multichannel analysis. Figure 19 depicts contour plots showing the thickness of the thawed layer, the average moisture content, and the total soil moisture content of the active layer. It is possible to compute the total soil moisture content of the active layer by multiplying the observed thaw depth by the average soil moisture content. This is a crucial parameter for permafrost studies since it offers direct information on the amount of water held in the active layer.

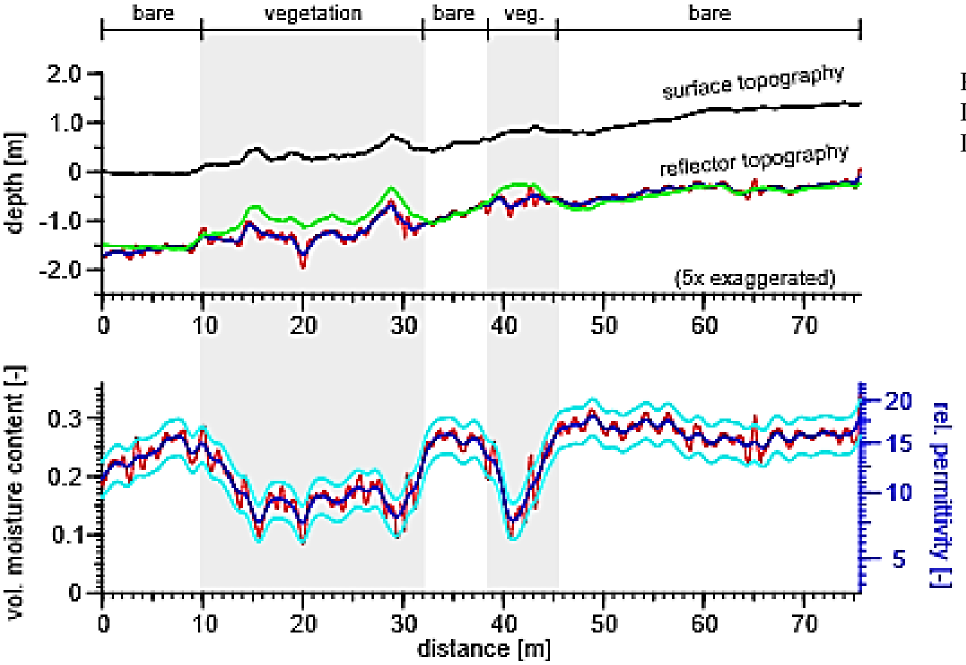

Red: Raw Data
Dark Blue: Averaged Data
Light Blue: Uncertainty

Figure 18: Surface Topography, Reflector Depth, Relative Dielectric Permittivity, and Average Volumetric Soil Moisture Content

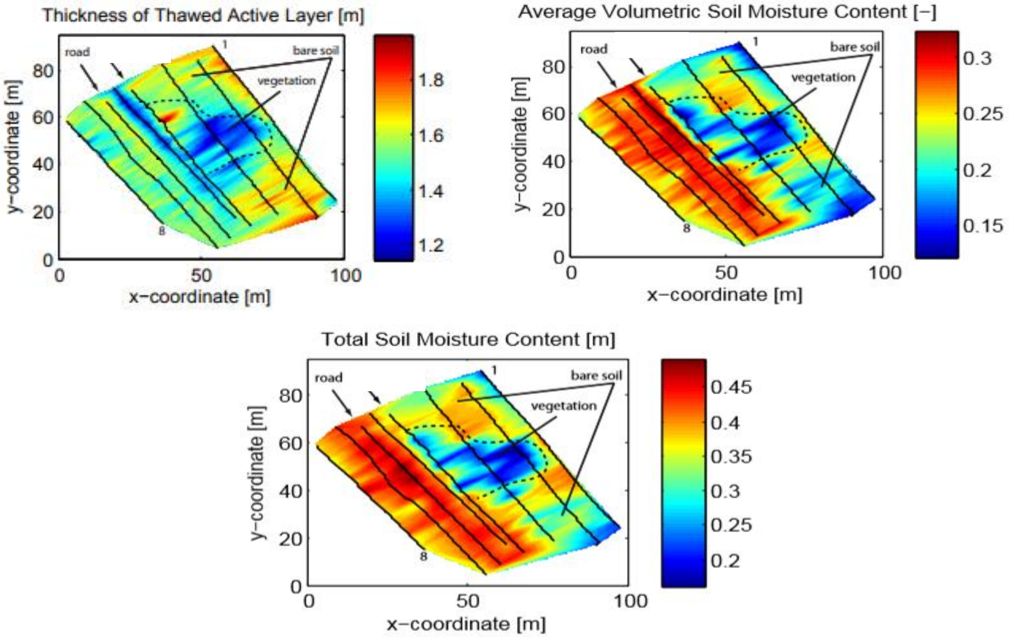

Figure 19: Thickness of Thawed Active Layer, Average Soil Moisture Content, and Total Soil Moisture for the Thawed Active Layer

Muller (2017) showed an automated method using multi-offset ground penetrating radar (GPR) to forecast moisture content continually and layer depth for unbound granular pavements (UBG) at traffic speeds. The initial application of his techniques centered on the investigation of layer depth and moisture content at large project-level scales to assess layer depth as part of pavement rehabilitation investigations and determine the severity of suspected pavement damage caused by excessive moisture in the multilayer structure. Reeves (2010) used a second-generation 3D Noise-Modulated (NM-GPR) instrument for moisture content measurements (Figure 20). This apparatus may gather a sequence of nearby partly overlapping multi-offset measurements with ground coupling.

Figure 20: Second Generation NM-GPR System Incorporating a Traffic-Speed 3D Ground-Coupled Antenna Array

In conjunction with the NM-GPR, a Traffic Speed Deflectometer (TSD) was used to establish the road surface's deflection profile. The TSD is a transportable device that employs Doppler vibrometers and complementing sensors to detect the velocity of the deflecting surface at predetermined offsets in front of the load's rear tire (Ferne et al., 2009; Baltzer et al., 2010; Kelley & Moffat, 2011). While moving down the road, the equipment was designed to collect four nearby wide-angle reflections and refraction (WARR) collects in a quasi-continuous manner. To calibrate the petrophysical relations for UBG pavement materials and create field moisture forecasts, a modified free-space (MFS) permittivity characterization technique was devised. A ray-path modeling-semblance (RM-S1) approach was also used to optimally match all near-transmitter receivers over the breadth of the array.

In June 2015, during the first Site Visit, NM-GPR readings were acquired. The next day, TDR and impulse GPR measurements were taken, and the site bitumen was sealed two days later. The May 2016 Site Visit 2 included the collection of NM-GPR, impulse GPR, and TDR data, as well as several physical samples throughout the length of the site. During Site Visit 2, eight samples (S1 to S8) were dug to estimate the pavement layers' built depth and collect material to measure the location's moisture content. S1 to S4 were taken at 100 mm intervals inside the pavement, and a subgrade sample was also obtained. The other four samples (S4 to S8) were collected from the second half of the site, and the subgrade and individual strata were sampled.

Figure 21 compares the measured response on one of the 32 NM-GPR channels during the first and second site visits with the impulse measurement acquired during the second site visit. Also highlighted are the approximate locations of sample sites S1 through S8.

Figure 22 is a screenshot of the RM-S1 analysis for the measured multi-offset response (Figure 22a), the optimized ray-path model determined for the tested location (Figure 22b), and an image of the calculated layer depth, dipping angle, relative permittivity, and predicted volumetric moisture content (Figure 22c) (Figure 22c). Figure 22d depicts volumetric content projections for previously examined areas along the route. The RM-S method was designed to make processing multi-offset GPR data constantly gathered along a road using 3D GPR equipment more uncomplicated and efficient.

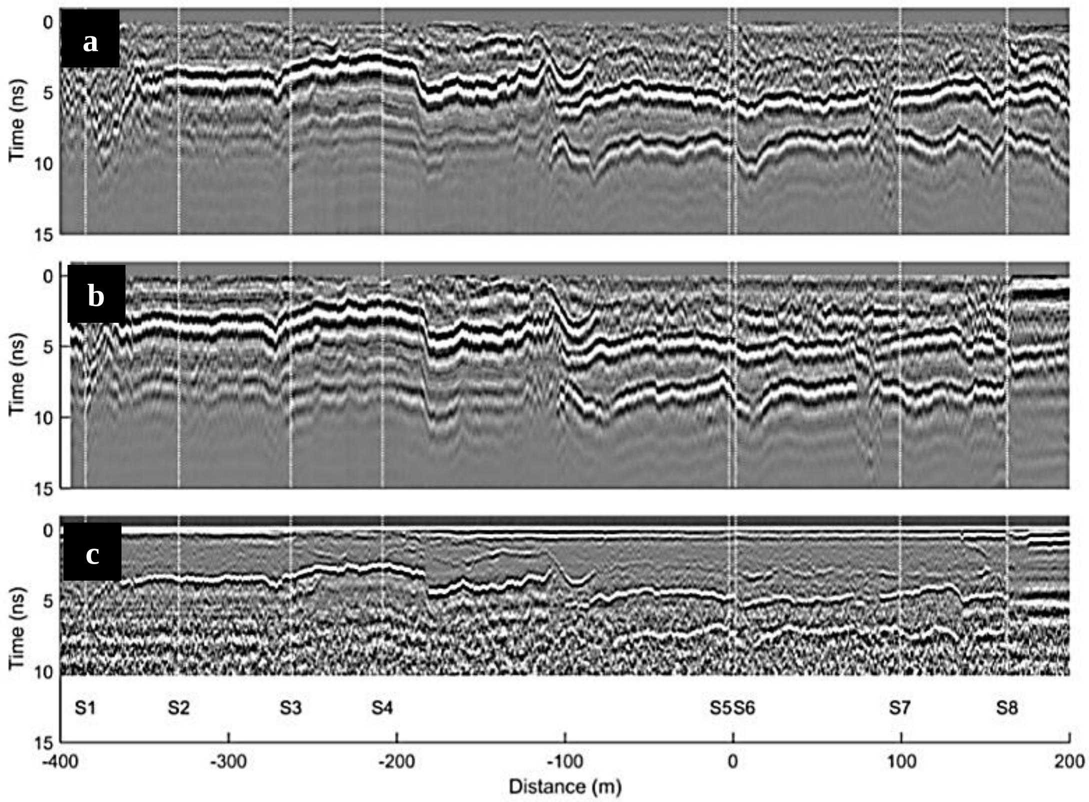

Figure 21: GPR Scans along the Test Site of (a) Site Visit 1 Using NM-GPR, (b) Site Visit 2 using NM-GPR and (c) Impulse GPR

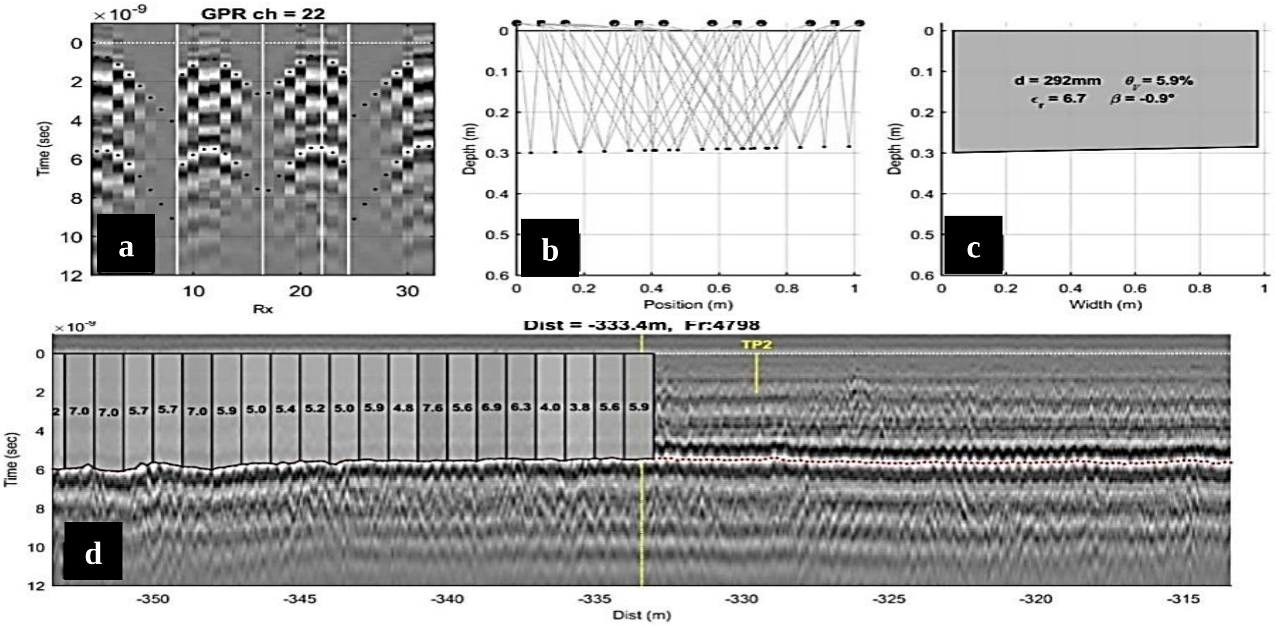

Figure 22: Multi-Offset Analysis using the RM-S1 Approach Showing (a) Measured WARR Response with Airwave and Optimized Ray-Path Travel Time Predictions Overlaid (black dots); (b) Calculated Ray-Path Geometries; (c) Calculated Layer Depth (d), Volumetric Moisture Content

Figure 23 displays the relevant volumetric moisture contents computed using the previously estimated petrophysical relation. The researchers determined a strong connection between the volumetric moisture content predictions of the RM-S1 model and the actual sample findings. Other studies found that TDR and common-offset GPR had a similar tendency to RM-S, although with persistently lower permittivity values. It is crucial to note that using alternative sensor configurations (common midpoint, multiple arrays, standard offset) increases the capability to identify layer interfaces and estimate layer depths. The greater the precision of the depth forecasts, the greater the precision of the permittivity estimate.

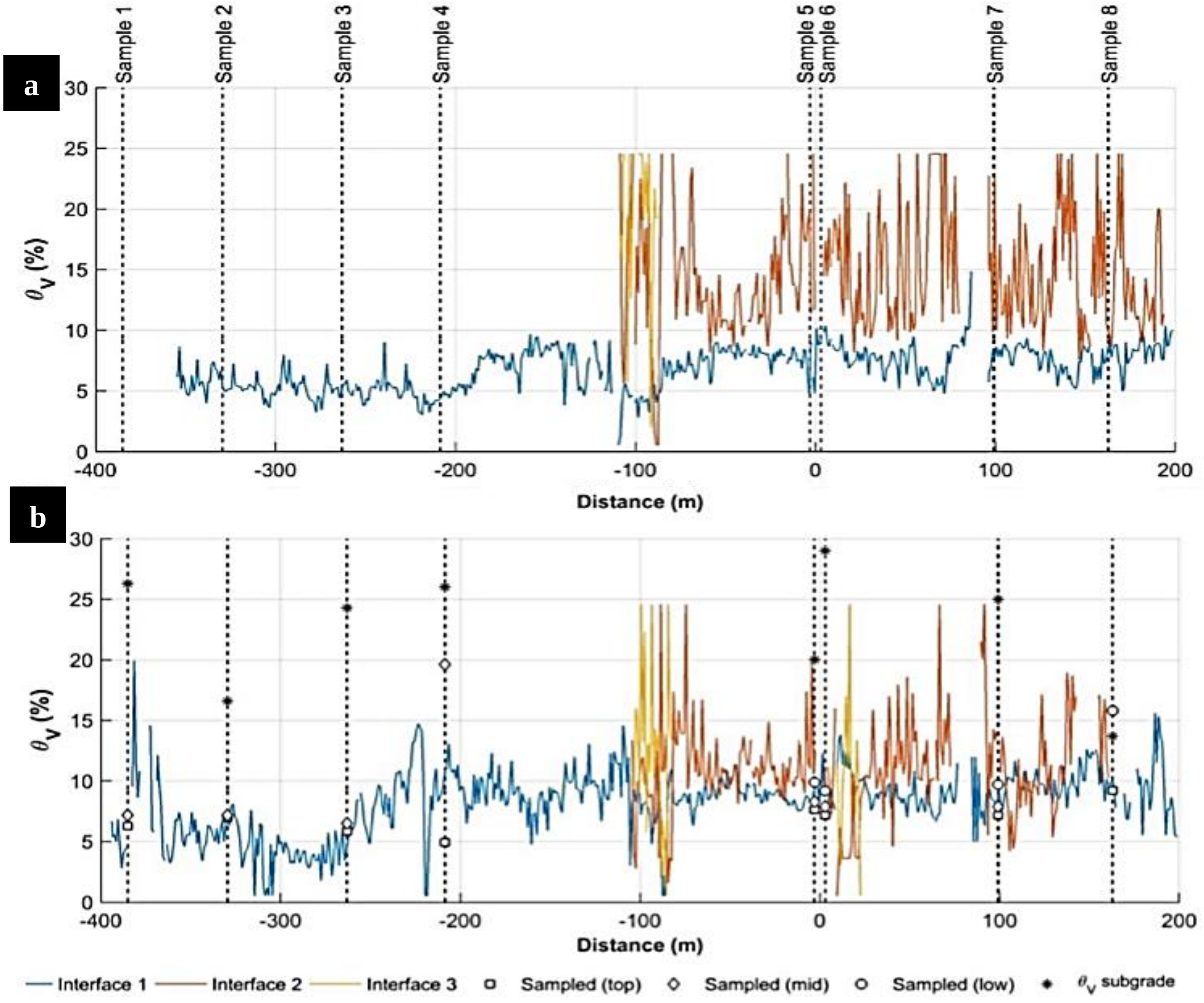

Figure 23: Volumetric Moisture Content Predictions from Permittivity Results during (a) Site Visit 1 and (b) Site Visit 2 (Muller, 2017)

Muller found from this investigation that the predictions of this method corresponded well with actual measurements of layer depth and moisture content of pavement layers. Compared to embedded TDR sensors and common-offset GPR measurements of subsurface reflectors, permittivity predictions followed similar temporal patterns with somewhat lower values. Even though data could be gathered at traffic speeds, layers had to be recognized and monitored, most likely based on spot assessments at intervals along the road, as one of the study's limitations. In addition, it was emphasized that this method could only be used for the subgrade, which was usually the lowest coherent interface. Therefore, integrated TDR or other sensors would still be necessary for subgrade moisture monitoring.

2.4 Further Moisture Measurements

White (2019) researched to optimize pavement laying costs by utilizing material compaction energy and moisture content to enhance the quality by

1. Achieving the minimal critical engineering parameter values throughout the site
2. Limiting variability of critical engineering parameter values over the entire site
3. Restricting spatial areas of non-compliance
4. Control moisture contents to ensure post-placement volumetric stability

The propriety "validated intelligent compaction" (VIC) technology was employed to help the construction process and quality evaluation. They highlighted the variation in QC/QA testing procedures for detecting the water content (Figure 24). Zero shows the optimum moisture content with -4% and +2% limits shown by the orange dashed lines. This demonstrated that 79% of all measurements did not adhere to the stated moisture control limits. Quality evaluation criteria were devised utilizing intelligent compaction to highlight regions of noncompliance (Figure 25a) (Figure 25a). Moisture was measured based on its connection to the density of the material, as illustrated in Figure 25b. Water was added or withdrawn until obtaining the appropriate density.

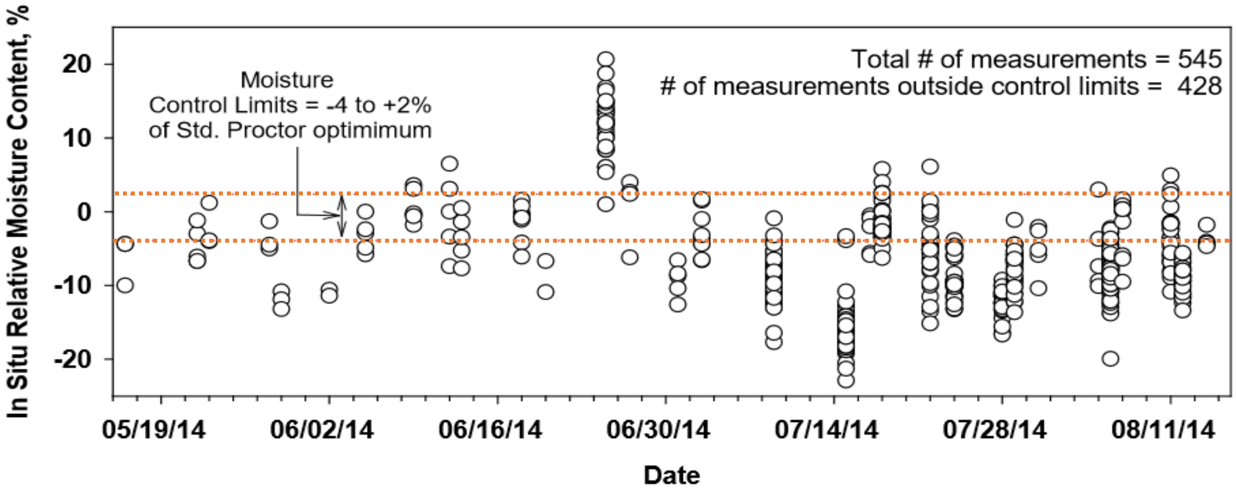

Figure 24: Moisture Content Measurement Variability

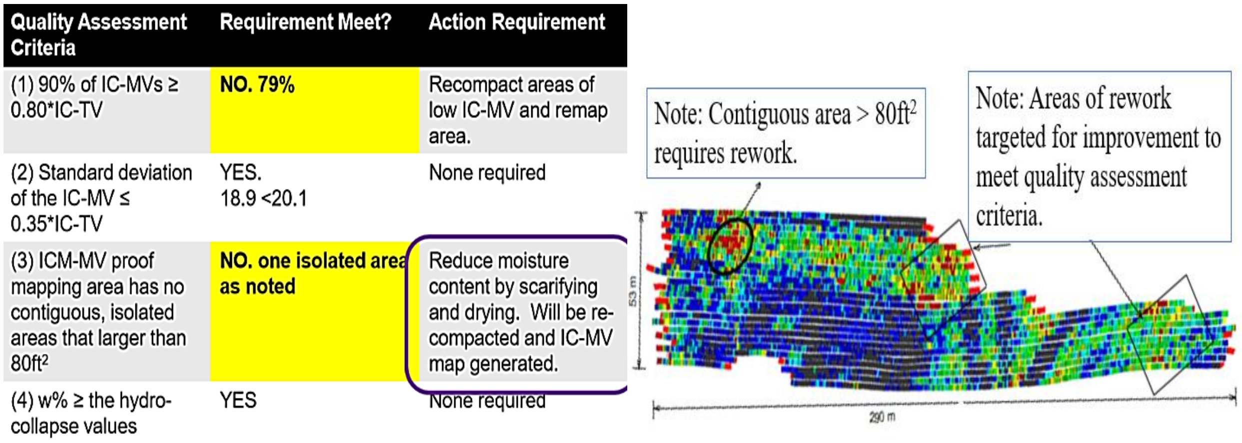

Quality Assessment Criteria	Requirement Meet?	Action Requirement
(1) 90% of IC-MVs ≥ 0.80*IC-TV	**NO. 79%**	Recompact areas of low IC-MV and remap area.
(2) Standard deviation of the IC-MV ≤ 0.35*IC-TV	YES. 18.9 <20.1	None required
(3) ICM-MV proof mapping area has no contiguous, isolated areas that larger than 80ft²	**NO. one isolated area as noted**	Reduce moisture content by scarifying and drying. Will be re-compacted and IC-MV map generated.
(4) w% ≥ the hydro-collapse values	YES	None required

Note: Contiguous area > 80ft² requires rework.

Note: Areas of rework targeted for improvement to meet quality assessment criteria.

Figure 25: (a) Quality Assessment Criteria, (b) Intelligent Compaction Map

Genc et al. (2019) recommended estimating the frost depth and the number of freeze-thaw cycles under a specific highway using continuous meteorological and soil data. Their effort was to produce a method to prevent the occurrence of frost-induced heaving, depressions, fissures, potholes, and unpleasant travel. This work used soil moisture, matric suction, and temperature factors for computational modeling analysis. The chosen test area was instrumented with various soil moisture, matric potential, and temperature sensors implanted in five boreholes at depths ranging from 0 to 8 meters (Figure 26). Several alternatives were tested to determine the best practical sensor for measuring the soil’s moisture content. After an exhaustive study of commercially available devices, they opted to employ the GS1 sensor by Meter Environment. Due to its calibration technique and precision, the Decagon Devices MPS-6 sensor was chosen to detect the soil's matric potential. The selected test area had a weather station for measuring air temperatures. The sensors and weather stations used for this experiment are shown in Figure 27. After installation and data collection, a remote connection was established with the data logger, and the stored information was retrieved. Ultimately, continuous moisture content, matric potential, and temperature measurements were acquired. Figure 28 illustrates an example of the obtained data for continuous moisture measurements for sensors set at a depth of 1 foot in the five boreholes in this area.

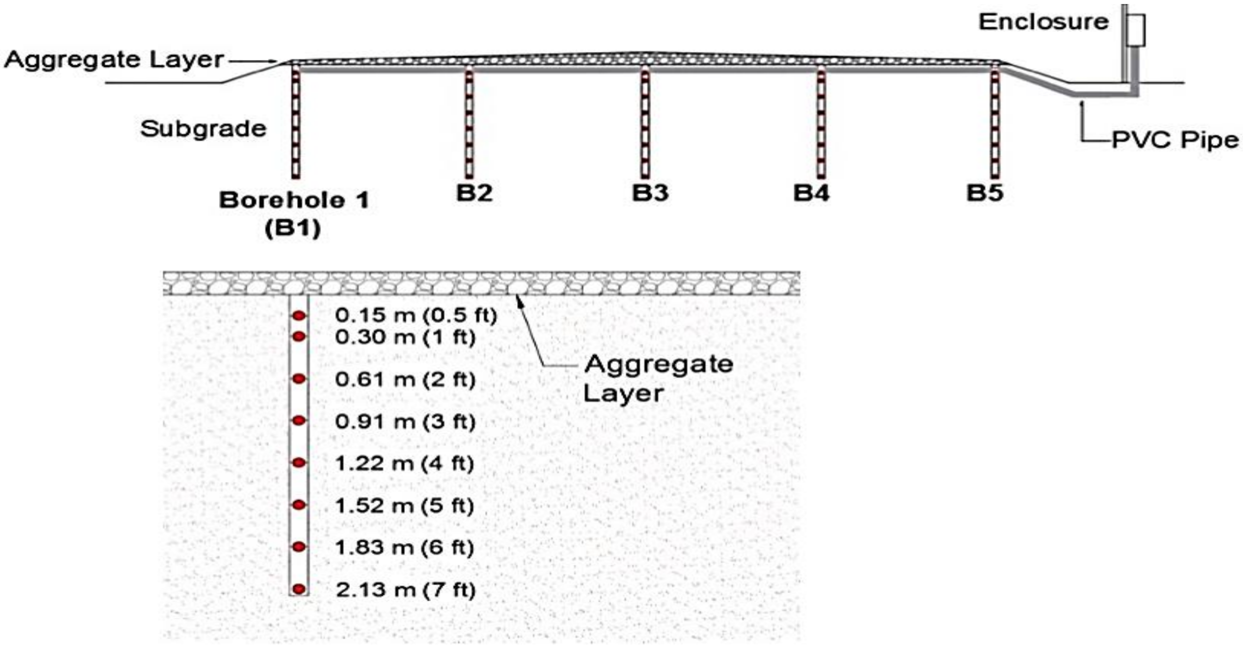

Figure 26: Cross-Sectional View of Roadway and One Borehole

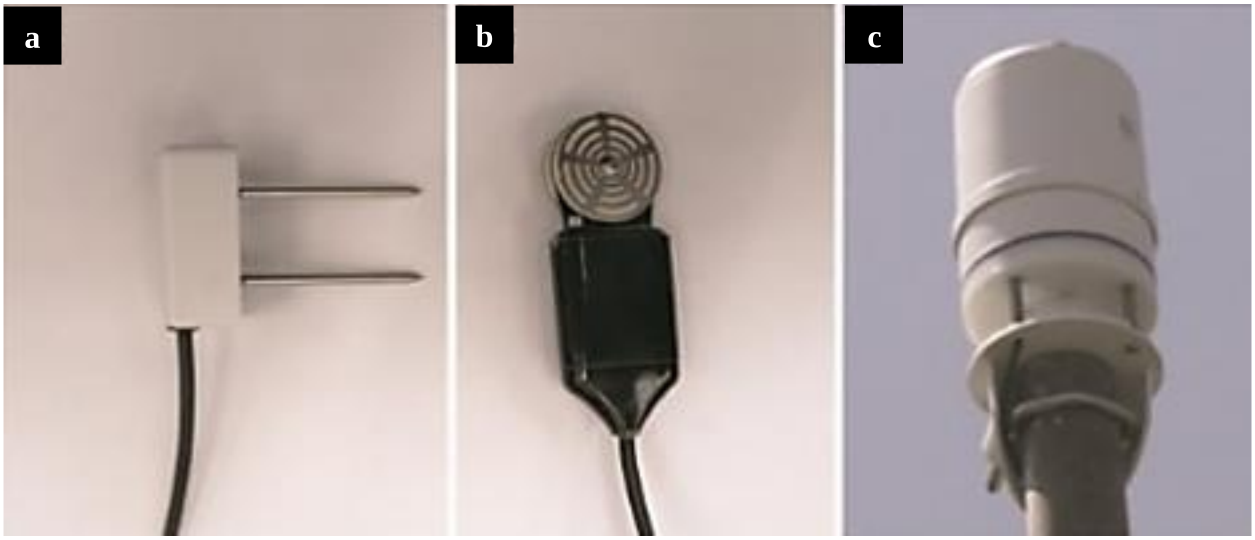

Figure 27: (a) GS1 (b) MPS-6 (c) Weather Station

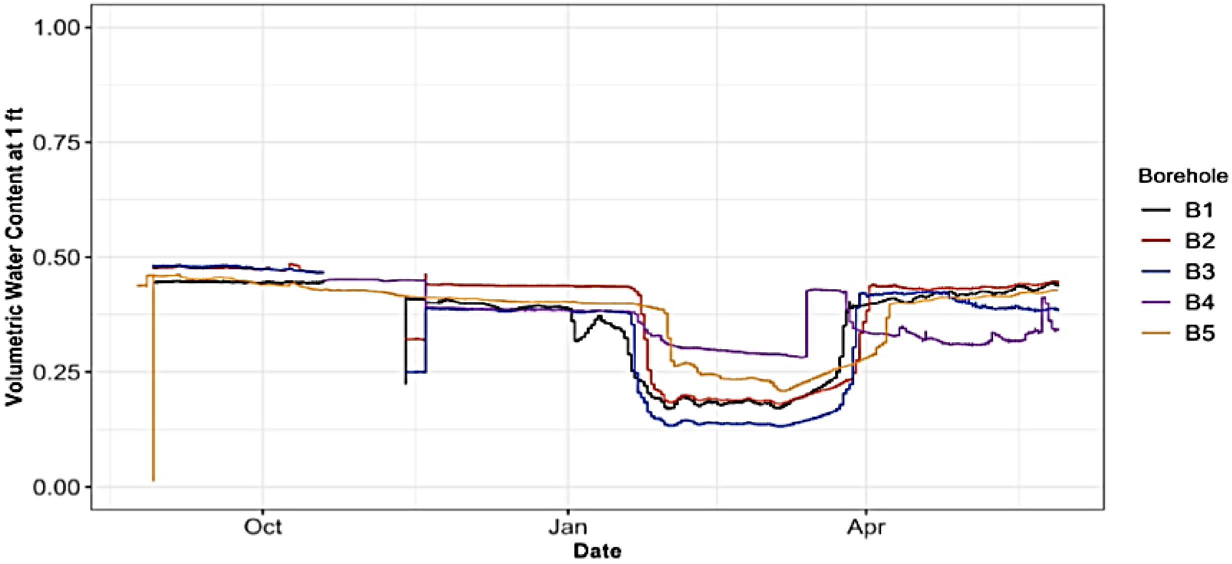

Figure 28: Continuous Moisture Measurement

Campbell (2019) described advances altering how soil moisture is assessed. This study's primary purpose was to install a moisture and temperature system to provide the required data for a model to estimate road weight constraints. Three sensors positioned at distances of 6 inches, 18 inches, and 30 inches were used to measure the relative humidity. In addition, a comprehensive weather station was installed at the site for temperature observations. Fourteen days of continuous moisture measurements at 6 inches were generated for various regions (Figure 29).

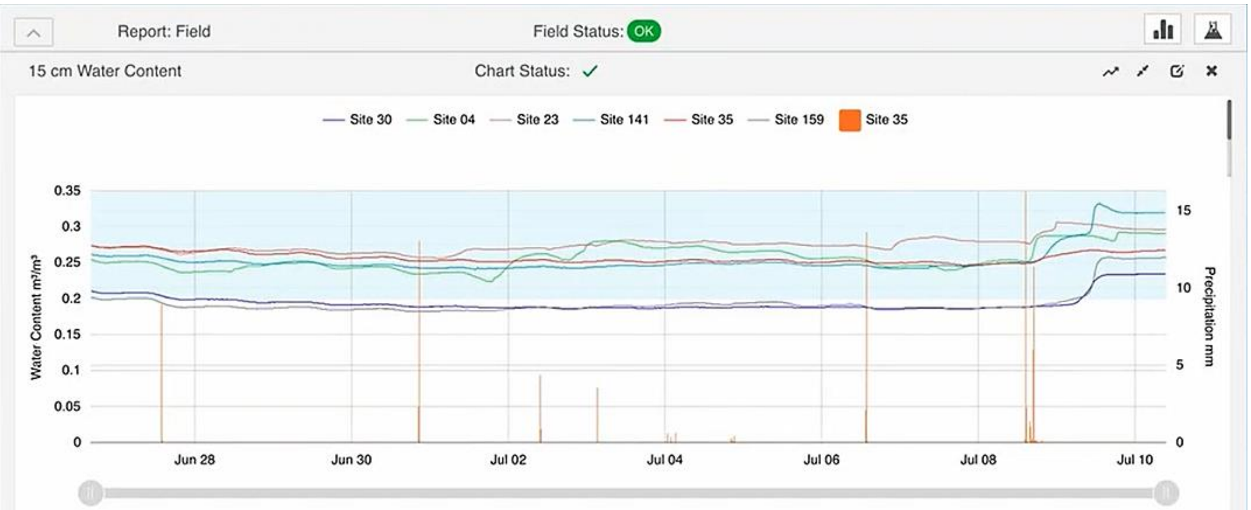

Figure 29: Example of a Continuous Moisture Measurement

Grabe and Mahutka (2005) established via modeling and field measurements that the regional variation of soil stiffness and pavement roughness displayed the same statistical properties. In addition to the number of vehicle passes and their load characteristics, they discovered that the geographical variation influenced the pavement's uniformity in soil stiffness. They determined that the variation in the foundation layers' stiffness affected the pavement's durability.

Brand et al. (2013) performed a historical review of research about the effects of nonuniform foundations on the performance of pavements, particularly rigid pavements. They determined that "certain nonuniform support of concrete slabs may cause much larger tensile stresses than uniform support, especially when varied loading locations and curling circumstances, soft support along the pavement edge, and preexisting fractures are considered." Several case studies illustrating the effect of nonuniform pavement foundations were also presented.

White et al. (2016) did a comprehensive analysis of the uniformity of earthwork in Iowa and the efficacy of their current requirements in delivering a consistent end product. One of their results was that the variable moisture content contributed significantly to the lack of homogeneity of the foundation layer of the pavement. They suggested the following three approaches to enhance uniformity:

1. Enhance the current moisture and moisture-density specifications
2. Develop Alternative DCP/LWD-based (strength/stiffness-based) QC/QA specifications
3. Incorporate intelligent compaction (IC) measurements into QC/QA specifications

Quoting from a comprehensive study performed by White et al. (2021), the following key challenges in terms of uniformity of foundation in general and moisture content in particular:

1. Substantial spatial variability (nonuniformity) exists in newly constructed pavement foundations for the range of materials tested

The overlying aggregate base layer will be nonuniform if the subgrade layer is nonuniform

2. Limited geotechnical testing (covering less than 1% of a given work area) is used to accept the engineering support values of pavement foundations, resulting in low reliability
3. Limited technology is available to help earthwork and paving contractors improve the field control of pavement foundation layers during construction
4. Most methods for quality inspection testing do not qualify as direct mechanistic measurements

CHAPTER 3 – LABORATORY METHODOLOGY

3.1 Testing Program

The experimental plan consisted of laboratory testing and small-scale testing. The flowchart of testing and analysis of each geomaterial is shown in Figure 30. As soon as the geomaterial arrived in the laboratory, it was processed, dried, and subjected to index tests such as particle size distribution (sieve analysis, ASTM 6913), Atterberg limits (ASTM D4318), and specific gravity (ASTM C127/128). These index results were used to classify the geomaterial according to the Unified Soil Classification System (USCS, ASTM D2487).

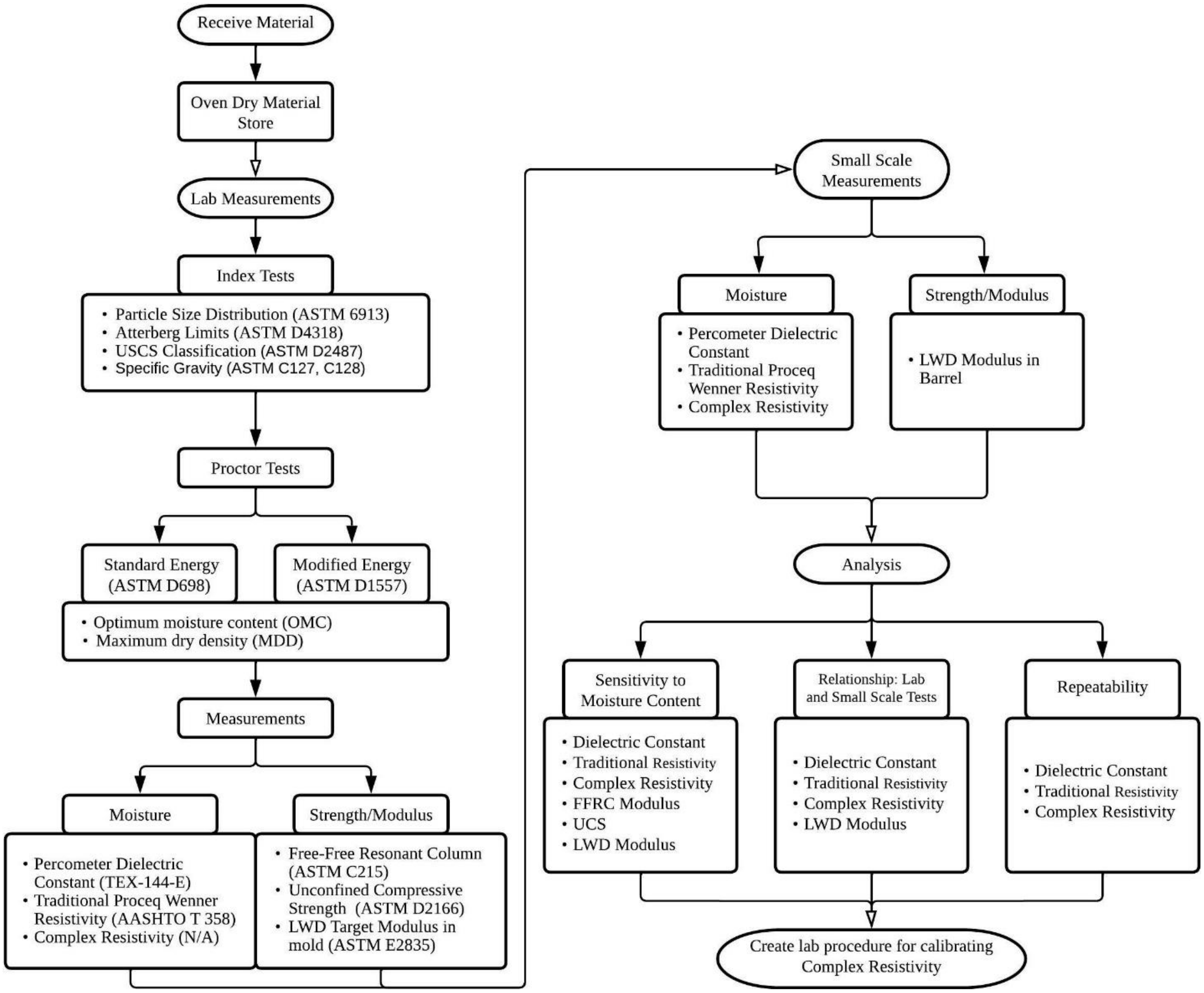

Figure 30: Testing Flowchart

The next step consisted of the Proctor tests to obtain the optimum moisture content (OMC) and the material's maximum dry density (MDD). The specimens prepared for this step and the subsequent laboratory testing were prepared in different sizes and with different compaction efforts depending on the texture of the geomaterial. The fine-grained soils and sandy materials were compacted per the Standard Proctor test energy (ASTM D698). The coarse-grained materials were compacted as per the Modified Proctor test energy (ASTM D1557). The specimens were prepared at longer lengths than those prescribed in the standard while maintaining the compaction energy to ensure rigorous strength and modulus test results. The fine-grained specimens were compacted in molds of 4 in. diameter by 8 in. height, and the coarse-grained specimens were compacted in 6 in. in diameter and 8.5 in. length.

3.2 Material Selection

Six geomaterials were selected as a baseline for verification of the outcomes of this study, as shown in Table 2; two fine-grained soils, both classified as CL, two sandy materials classified as SM and SP, and two coarse-grained materials classified as GW, were used in this study. These geomaterials provide a reasonable basis for materials with different characteristics in terms of their interaction with moisture, levels of suction, levels of moduli, and their use as compacted geomaterials.

Table 2: Geomaterials Used

Soil Type	Classification	Source
Fine-Grained	CL-1	Texas
	CL-2	MnROAD
Sandy	SM	Texas
	SP	MnROAD
Coarse-Grained	GW-1	Texas
	GW-2	Texas

3.3 Laboratory Measurements

As soon as the OMC and MDD were established, a series of five specimens were prepared at the following five nominal moisture contents: OMC, OMC±10%×OMC (or OMC±1% if the OMC is less than 10%), and OMC±20%×OMC (or OMC±2% if the OMC is less than 10%). These specimens were demolded and then subjected to a series of moisture content tests, namely Dielectric Constant using a Percometer (Tex-144-E, https://www.humboldtmfg.com/datasheets/Percometer.pdf), Traditional Resistivity using a Wenner probe (AASHTO T 358, https://www.screeningeagle.com/en/sales-flyers/SF-resipod), Complex Resistivity using the prototype being developed in this study.

Since all these tests are non-destructive and rapid, each specimen was subjected to the free-free resonant column (FFRC, ASTM C215) test to obtain the seismic modulus and then the unconfined compressive strength test (ASTM D2166).

A series of five specimens were prepared in a separate mold used in conjunction with the newly suggested method for estimating the target modulus of LWD to obtain the lab LWD modulus.

3.3.1 Dielectric Constant (DC)

A Percometer, shown in Figure 31, measured each specimen’s dielectric constant (DC). The percometer emits a frequency of 40-50 MHz into the soil and then records the capacitance change between the probe and soil from the change in water content and ion polarization on grain surfaces. Five measurements on top of the specimens and five on the bottom were conducted and averaged to obtain the representative DC of each specimen. Four measurements followed around the sample’s top and bottom surface areas, and the fifth was recorded in the middle of the surface.

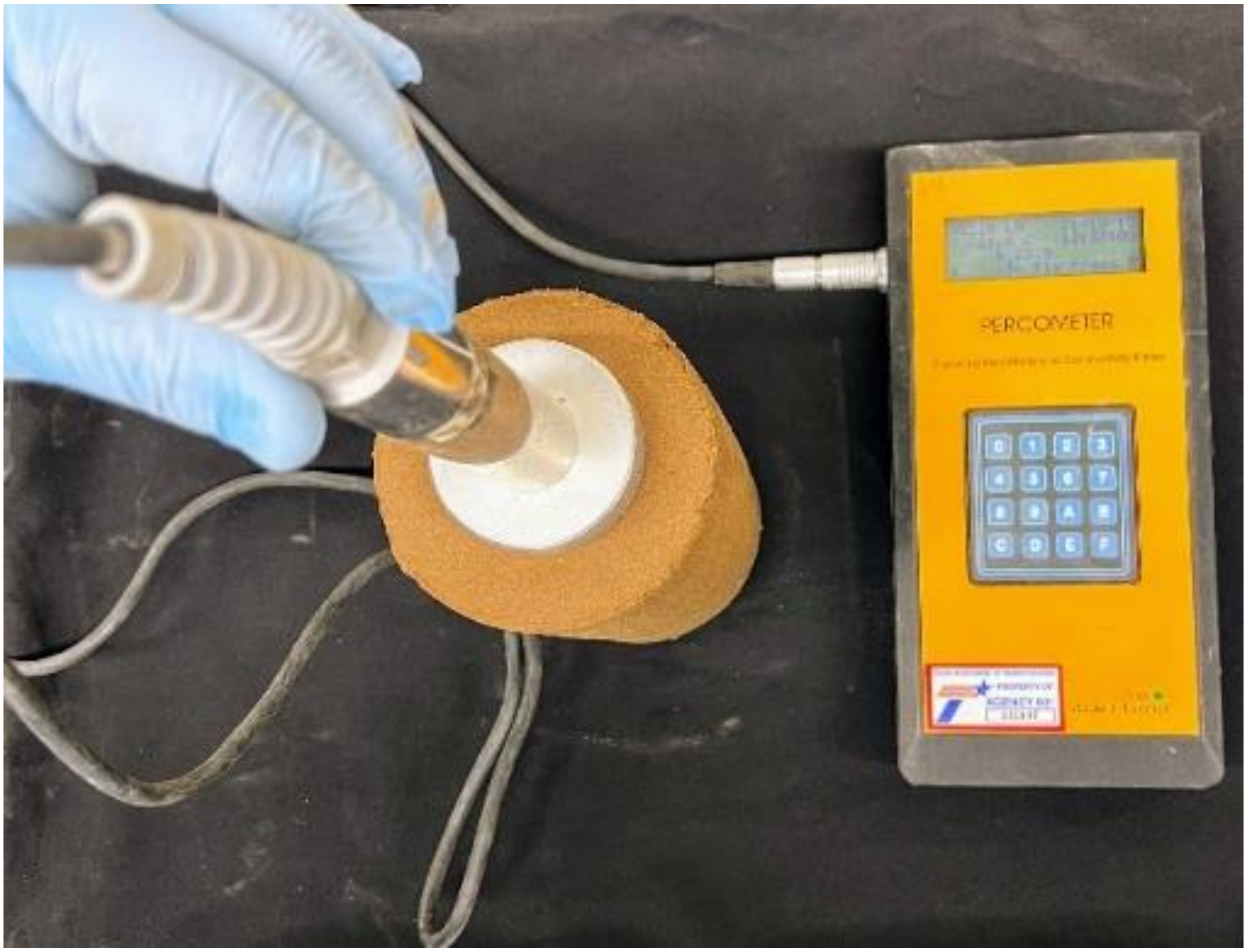

Figure 31: Percometer used for Measuring Dielectric Constant

3.3.2 Traditional Resistivity (TR)

A Wenner probe developed for measuring concrete resistivity, as shown in Figure 32a, was used to measure each specimen’s resistivity. The probe operates at a frequency of 40 Hz, a current of 10 µ-amps to 50 µ-amps, and computes the resistivity in kohm×cm. Current is injected into the soil from the two outer electrodes, where the two inner electrodes measure the passing current. Five measurements were taken at 60-degree intervals around the diameter of the specimen. The representative resistivity was the average of the five readings. The TR meter was saturated on low-resistivity soils as the instrument used its highest current setting and had voltages below its measurement threshold. A customized device with the same frequency and currents but a larger voltage measurement range was developed (Figure 32b). After proper calibration, the two devices provided almost identical readings.

Figure 32: (a) Traditional Wenner Array (b) Laboratory-Created Array

3.3.2.1 Correction Factors

The Wenner array functions on the expectation that current is being injected into a homogenous half-space (a large plane such as the ground). The voltage through the half-space is expected to decrease with distance; however, with the dimensions of the laboratory specimens, using a fixed probe spacing impacts the resistivity measurements. By using a finite-difference model, Cartesian coordinates, and a 50-mm node spacing, the geometric adjustment factors were determined to be 2.74 for the 4 in. diameter specimens and 1.82 for the 6 in. diameter specimens. The obtained resistivity values are divided by these correction factors.

3.3.3 Seismic Modulus (SM)

After the two moisture tests, the seismic modulus of the specimen was found using the free-free resonant column testing (per ASTM C215), as shown in Figure 33. An impulse is imparted to the specimen with a small hammer equipped with a load cell. The vibration of the signal within the specimen is measured with an accelerometer. Those two signals are transformed into the frequency domain to measure the resonant frequency of the specimen. The resonant frequency of the specimen is determined from those measurements that can be readily converted to a seismic modulus. Nine measurements on each surface (top/bottom) were averaged to obtain the representative seismic modulus.

Figure 33: Free-Free Resonant Column Testing for Seismic Modulus

3.3.4 Unconfined Compressive Strength (UCS)

Figure 34 demonstrates a clay specimen being tested using a Sigma 1 Automated Load Test System at a strain rate of 1% per minute. After the UCS tests were determined, each specimen’s moisture content was obtained via oven drying.

3.3.5 Lightweight Deflectometer Modulus (LWD)

The lightweight deflectometer modulus of each soil was obtained by preparing another set of specimens in a 6-in. by 8.5-in. mold provided by the LWD manufacturer, as shown in Figure 35. The diameter of the LWD plate measured 6 in. (150 mm), and the load applied was nominally 800 lbs. (3535 N). The average LWD deflections were obtained from three consecutive drops after three conditioning LWD drops. The average deflections were then converted to moduli.

Figure 34: Unconfined Compressive Strength Testing

Figure 35: Lightweight Deflectometer Testing

3.4 Complex Resistivity (CR)

Complex Resistivity (CR), is a measurement of electrical impedance as a complex number that uses the same four-electrode geometries as the TR measurement in Section 3.3.2. Two outer electrodes inject current, and the inner electrodes measure voltage difference. Resistivity is a complex number that can be calculated by dividing voltage and current. The CR measurement is more stringent than TR in the four main conditions.

1. The CR equipment allows measurement at up to ten frequencies ranging from 60 Hz to 40 kHz.
2. The CR equipment injects current at up to ten amperage levels ranging from 1 µA to 1 A. These current levels are fixed, not auto-ranged, as in the TR equipment.
3. The magnitude and phase of the injected current and the voltage are directly measured to monitor possible electrode/material interaction complications.
4. The frequency dependence of electrode and saturation polarization becomes an approximation to a diffusion equation model[1] rather than the simpler Poisson's equation[1].

Figure 36 shows the two complex resistivity prototypes. Figure 36a was the first laboratory prototype (version 6 electronics), and Figure 36b (version 8 electronics) was used in the last 6 months of testing. Both functioned similarly, measuring numerous frequencies and currents with square or sine waves. The Version 6 device operated at too high of a current range to function on the coarse/dry bases. Version 8 had an improved analog-to-digital (A/D) convertor, a better dynamic range at lower currents on the voltage channels for the dry/coarse bases, and improved ruggedness/reliability while making access and maintenance easier.

---

[1] Diffusion equation ($\nabla^2 V=K\ \delta V/\delta t$) where V is voltage, K represents a spatial function of resistivity and polarization and t is the time.

[2] Poisson's equation ($\nabla^2 V=f$) where V is voltage and f represents a spatial function of resistivity.

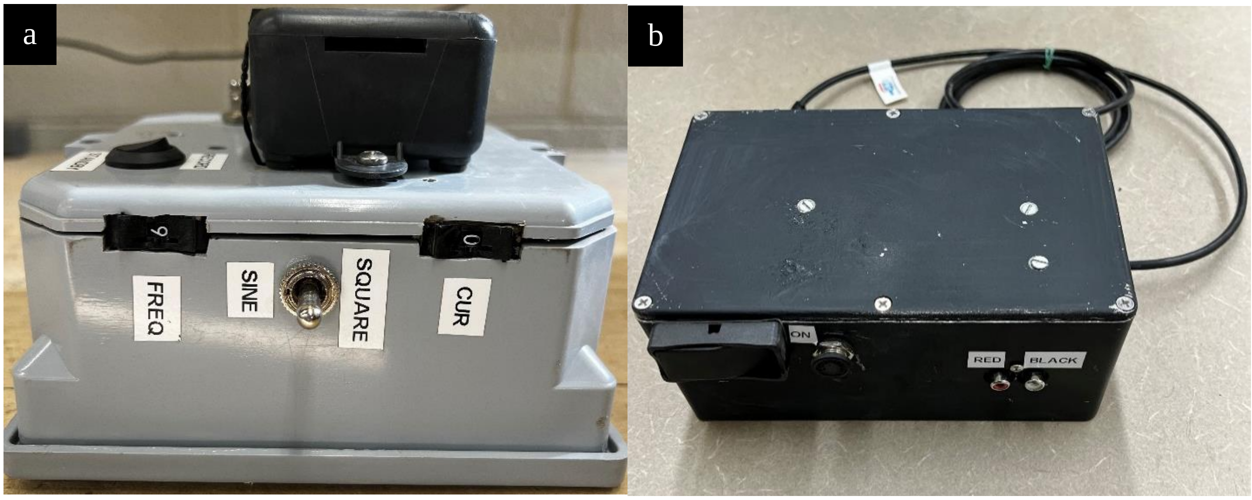

Figure 36: Complex Resistivity Prototypes and Arrays

Two arrays were made to meet laboratory compaction standards. The cradle array was used to test Proctor specimens by allowing them to sit on four solder-coated brass electrodes, as shown in Figures 37a, and 37b. With a larger electrode contact area and uniform support across the specimen surface, the more delicate and wet specimens performed better compared to the earlier design of the four-probe electrode in Figure 37c. The larger distributed electrodes required a separate geometric correction factor calculated by finite difference modeling. The two Wenner arrays (Figure 37c-d) were used to test large-scale specimens. The three arrays function the same. The measurements are taken with a phase-sensitive detector that multiplies the voltage and current signals measured by an in-phase sine-wave and a 90° delay sine-wave. Hardware multiplication using the in-phase or 90° delay square waves produces a real-time Fourier transform of the measured signal (real and imaginary). The imaginary value measures polarization, while the real value measures resistivity. This measurement rejects nonlinear distortion and noise more strongly than the simpler TR circuitry, which combines them into one resistivity value. The data collection procedure is as follows:

1. The specimen is set on top of the brass electrodes and power button is switched on
2. Desired frequency is selected, (starting frequency was set to 3)

3. The record and square wave are turned on
4. Run through all currents, 0-9, then finish with 0 (typically .5 to 1 sec. between change)
5. Turn square wave off, then the record switch,
6. Change frequency and repeat from step 3

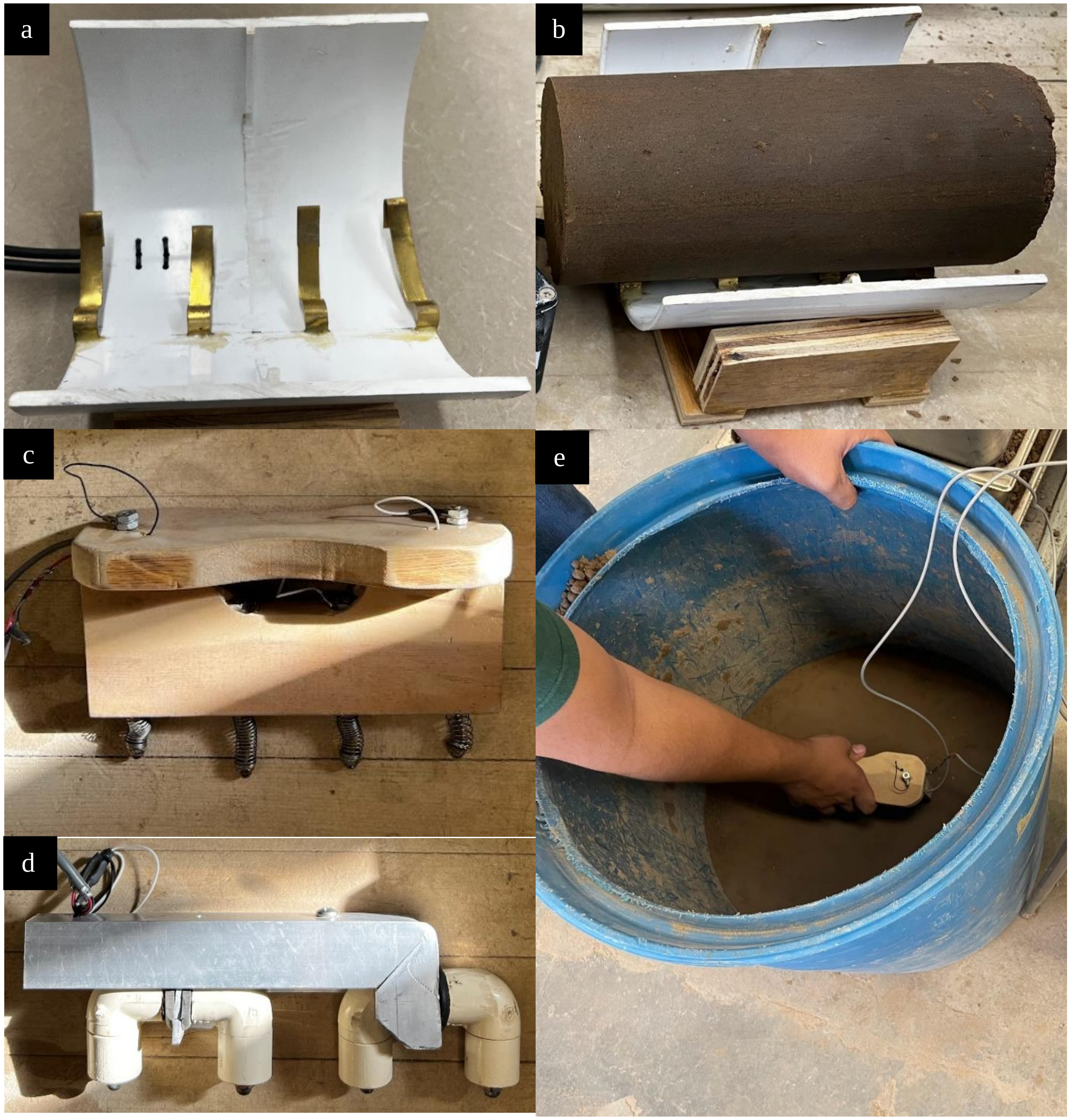

Figure 37: (a-b) Cradle Array and (c-d) Wenner Arrays

3.5 Large-Scale Measurements

The small-scale tests were carried out in the laboratory by preparing 18-in. diameter by 24-in. height specimens constructed within a 35-gallon barrel, as shown in Figure 38. Five specimens at the five target moisture contents (OMC, OMC±10%×OMC or OMC±1% if the OMC is less than 10%, and OMC±20%×OMC or OMC±2% if the OMC is less than 10%) were compacted and measured.

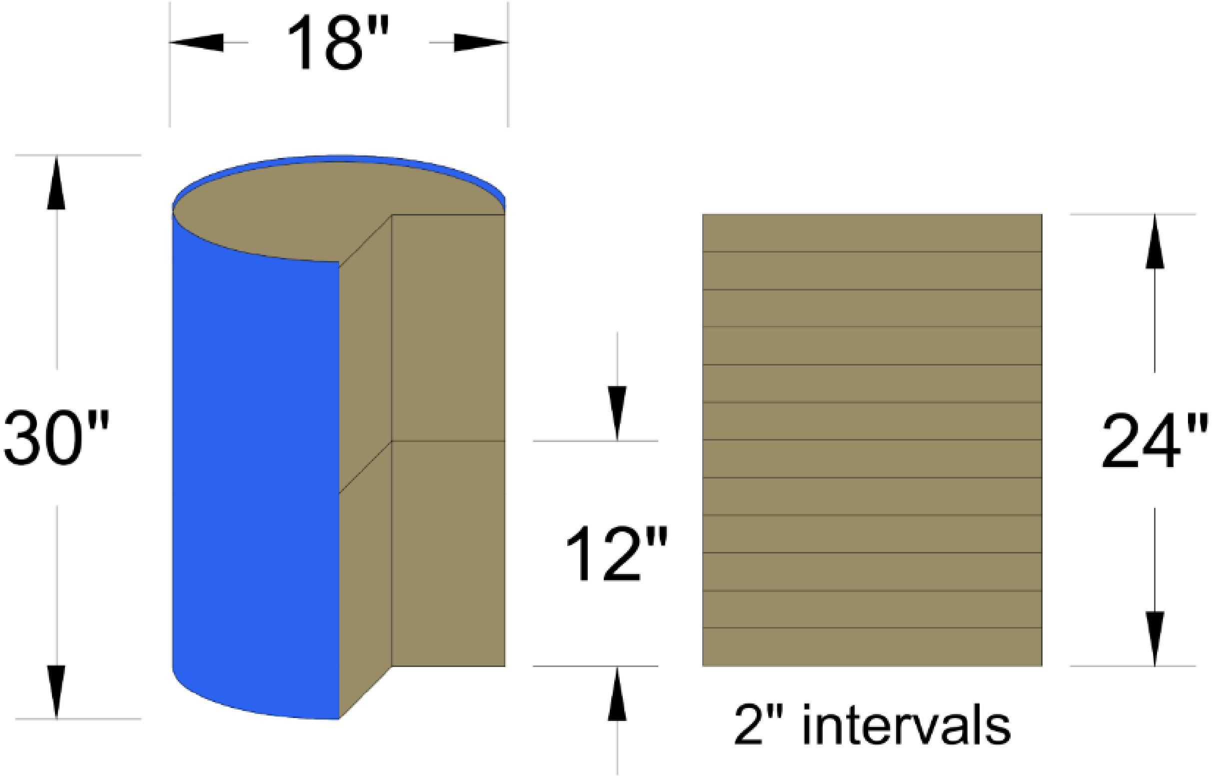

Figure 38: Schematic Diagram of Large-Scale Test Specimen Set-up

A concrete mixer (Figure 39) was used to prepare the materials to the desired moisture content. An adequate amount of dry geomaterial necessary to achieve the desired density for volume of a 2-in. lift was placed in the mixer, and a precise amount of water was added to the soil with a water sprayer to ensure accurate moisture content. The moist material was then transferred into the container and compacted to the desired density with a concrete stamper. This process was repeated until a height of 12 in. was achieved. At that height, the moisture content measurements (with the

Percometer, traditional resistivity probe, and the complex resistivity probe) and LWD measurements were obtained at three separate locations. Each specimen was then built up to its final height of 24 in. using 2-in. lifts and tested using the three moisture probes and LWD. Soil samples were extracted at every 4 in. height to obtain oven-dry moisture contents.

Figure 39: (a) Mixer and (b) Concrete Stamper with Barrel Used to Prepare Large Scale Specimens

The laboratory measurements were taken at the sixth layer (12-in height) and the 12th layer (24-in height). Five readings of the dielectric constant, pictured in Figure 40a, are recorded and averaged—one reading in the middle and four between the barrel's center and perimeter. The traditional resistivity is measured next. Five readings are recorded in the middle of the barrel and averaged, as shown in Figure 40b. Using numerical analysis, a correction factor is not necessary for the barrels. Next, the complex resistivity is recorded in the middle of the barrel, with a Wenner array pictured in Figure 40c. Lastly, the LWD modulus, Figure 40d, is recorded. The average of three different positions is taken and averaged to find the corresponding LWD modulus.

Figure 40: Large Scale Measurements (a) DC (b) TR (c) CR (d) LWD

3.6 Normalization of Data

Using the degree of saturation instead of moisture content is desirable. Since the determination of the degree of saturation requires an accurate measurement of the specific gravity of the materials, it was deemed impractical for this study. Instead, an alternative normalization process proposed in the NCHRP 10-84 was pursued. The ordinate (y-axis) parameters were normalized by dividing the given parameter at a given moisture content by the corresponding value at OMC. The abscissa (x-axis) was normalized using Equation 1.

$$\text{Normalized Moisture Content} = \frac{\text{Actual Moisture Content} - OMC}{OMC} \qquad (1)$$

CHAPTER 4 – RESULTS OF LABORATORY MEASUREMENTS

This section discusses the results from three diverse geomaterials in detail. The raw data from all tests on the six geomaterials are represented in the Appendix. Presented in Table 3 is a summary of the soil parameters of the six materials tested, including their Atterberg limits and gradations.

Table 3: Summary of Index Properties

Soil		Atterberg Limits		Constituents, % (dry sieve)			Compaction Parameters		Properties at OMC[1]			
Type	**Classification**	**LL**	**PI**	**Gravel**	**Sand**	**Fines**	**OMC[1] (%)**	**MDD[2] (pcf)**	**DC[3]**	**R[4] (Kohm-cm)**	**SM[5] (ksi)**	**UCS[6] (psi)**
Fine-Grained	CL-1	33	13	0.0	27.6	72.4	14.1	109.2	26.5	0.7	8.7	9.8
	CL-2	27	8	3.0	38.6	58.4	14.4	118.9	13.5	1.2	7.0	11.9
Sandy	SM	No PI		0.0	83.2	16.8	9.5	118.0	14.2	2.1	6.6	5.5
	SP	20	2	17.7	79.9	9.1	9.8	130.6	21.0	3.0	32.4	22.8
Coarse-Grained	GW-1	16	2	60.1	39.9	0.0	4.7	148.3	16.5	3.2	16.7	3.0
	GW-2	18	3	52.9	43.1	4.0	5.3	149.6	13.1	10.6	16.5	3.3

[1]Optimum Moisture Content, [2]Maximum Dry Density, [3]Dielectric Constant, [4]Traditional Resistivity, [5]Seismic modulus, [6]Unconfined Compressive Strength

Figure 41 demonstrates the moisture density curves of the CL-1, SM, and GW-1 geomaterials. The CL-1 and SM soils were tested at more moisture contents than the five target moisture contents to understand better the testing scheme and anticipated trends of the dielectric constant, traditional resistivity, and complex resistivity. The GW-1 was tested only at the five nominal moisture contents.

4.1 Dielectric Constant

Presented in Figure 42 are the variations of the dielectric constants of the three geomaterials with moisture content. The error bar for each data point corresponds to the ±1 standard deviation bound to demonstrate the consistency of the test method at different moisture contents. A conclusive pattern cannot be observed for the SM and CL-1 materials. The GW-1 material was the most susceptible to moisture increases as its dielectric constants increased with moisture. Due to the high variability, the dielectric constant data for the large-scale specimens are presented in the appendix.

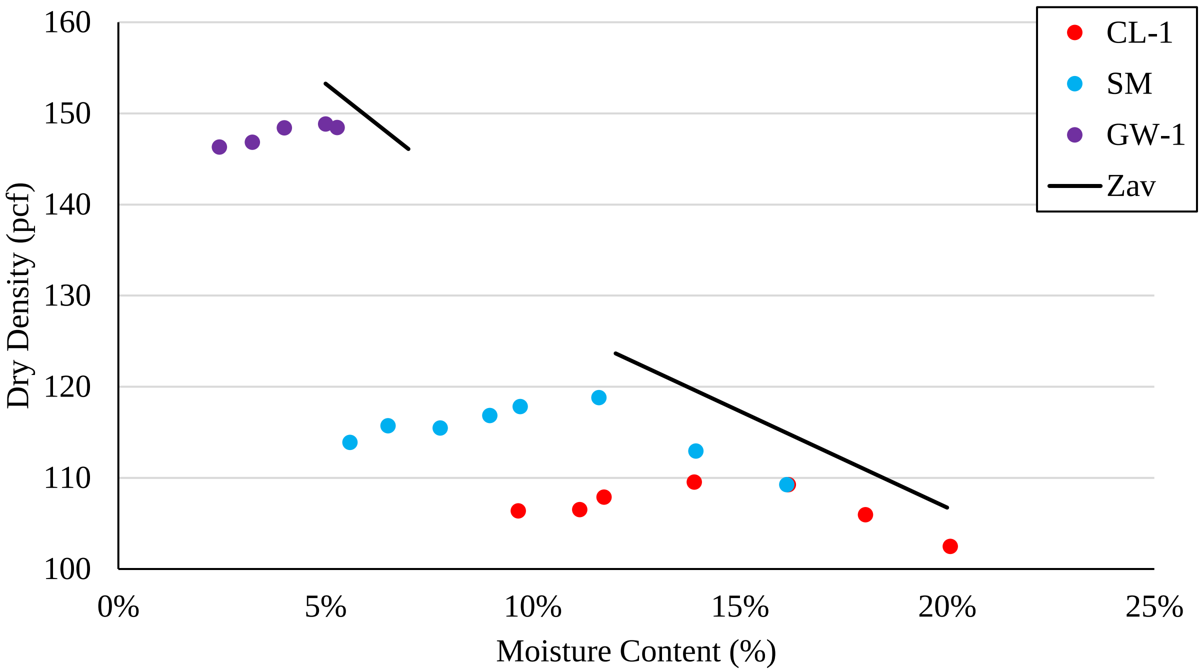

Figure 41: Moisture-Density Curve of CL-1, SM, and GW-1

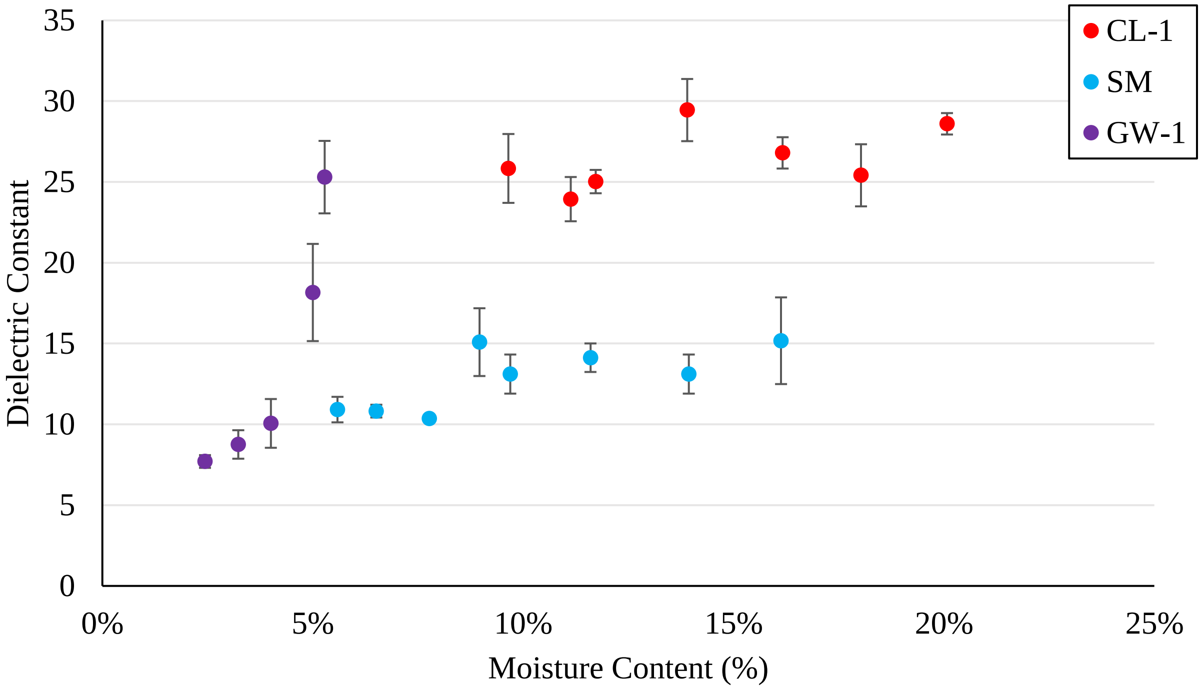

Figure 42: Dielectric Constant Data of CL-1, SM, and GW-1

4.2 Traditional Resistivity

4.2.1 TR of Proctor Specimens

Figure 43 shows the variations of the resistivity measurements with moisture content for the three materials. A consistent pattern is observed among the three materials but over different ranges. The resistivity change with moisture content is large at lower saturation and becomes nearly insensitive as saturation increases above OMC. This variability is higher for the GW material. The moisture-resistivity curve shape and higher variability for the larger aggregate are consistent with the expected volumetric decrease in double-layer conduction as the surface area decreases with grain size increase.

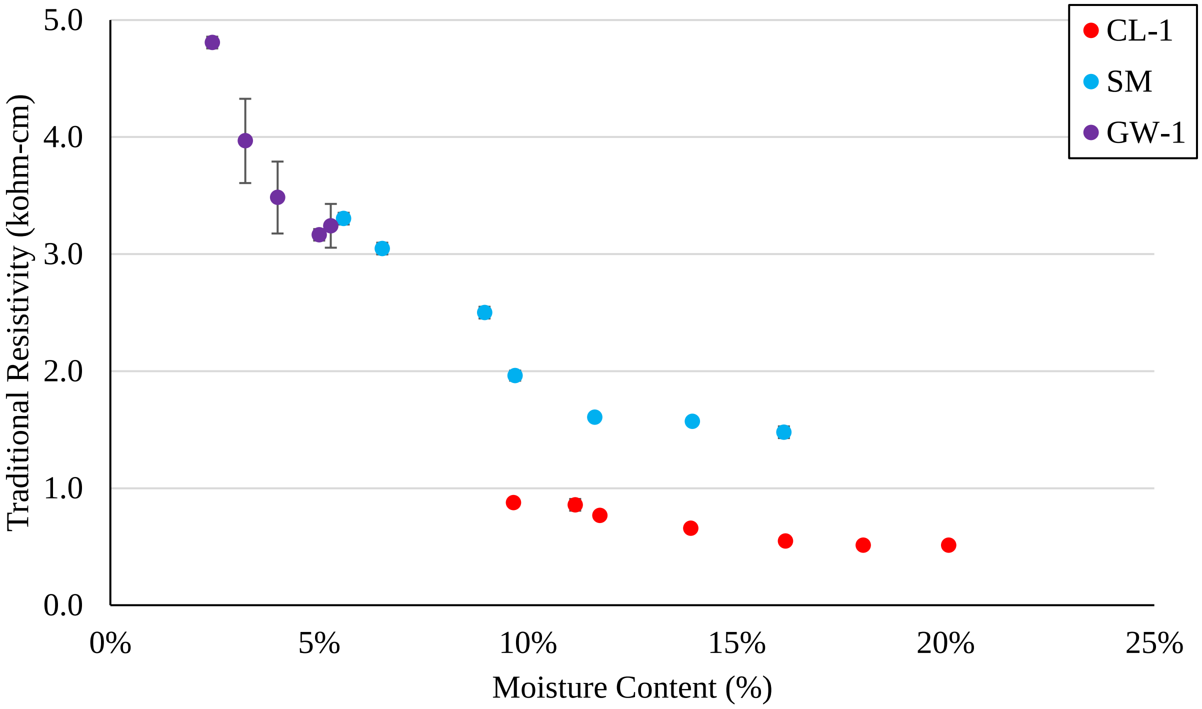

Figure 43: Traditional Resistivity Data of CL-1, SM, and GW-1

Figure 44 shows the variations of the normalized traditional resistivity of the geomaterials with normalized moisture content. The vertical line passing through zero indicates the optimum moisture content. The specimens with negative normalized moisture contents are dry of OMC, and the positive ones are wet of OMC. The solid line indicates the trend that all soils follow with some anticipated dispersion. For specimens prepared dry of OMC, a rather steep decrease in the normalized resistivity with an increase in the normalized moisture content is observed. However, for the specimens prepared wet of OMC, the normalized resistivity is less sensitive to the change in the moisture content. This trend makes sense since, at moisture contents wet of OMC, the electrical properties of the water dominate the response. The data dispersion among different soils indicates the need for thorough laboratory calibration of the resistivity-moisture content relationship before field implementation.

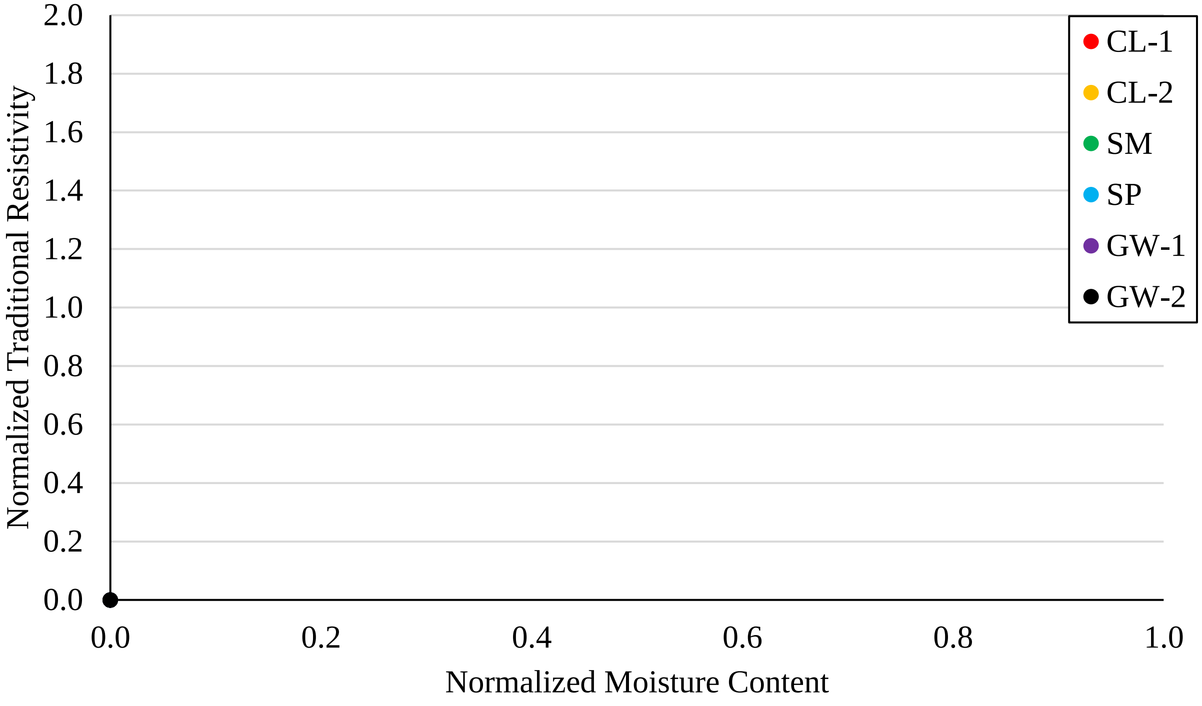

Figure 44: Normalized Traditional Resistivity Data of all Geomaterials

4.2.2 TR of Large-Scale Specimens

The variations of the traditional resistivity with moisture content for the three geomaterials are summarized in Figure 45. The moisture measurements were repeated at five points to document the variability of the results. The measurements made at 12 in. and 24 in. heights yielded similar results. The measurements were also repeatable as judged by the lengths of the error bars representing ±1 standard deviation.

The normalized resistivity of the measurements conducted in the large-scale specimens with moisture content is presented in Figure 46. Due to the similarity of the results from the 12-in. and 24-in. heights, the averages of the two measurements are shown in the figure. The solid black curve is the lab measurements' trend (Figure 44). That trendline represents the lab data quite well, indicating that the lab and large-scale specimen results follow the same trends as long as an appropriate calibration process is implemented.

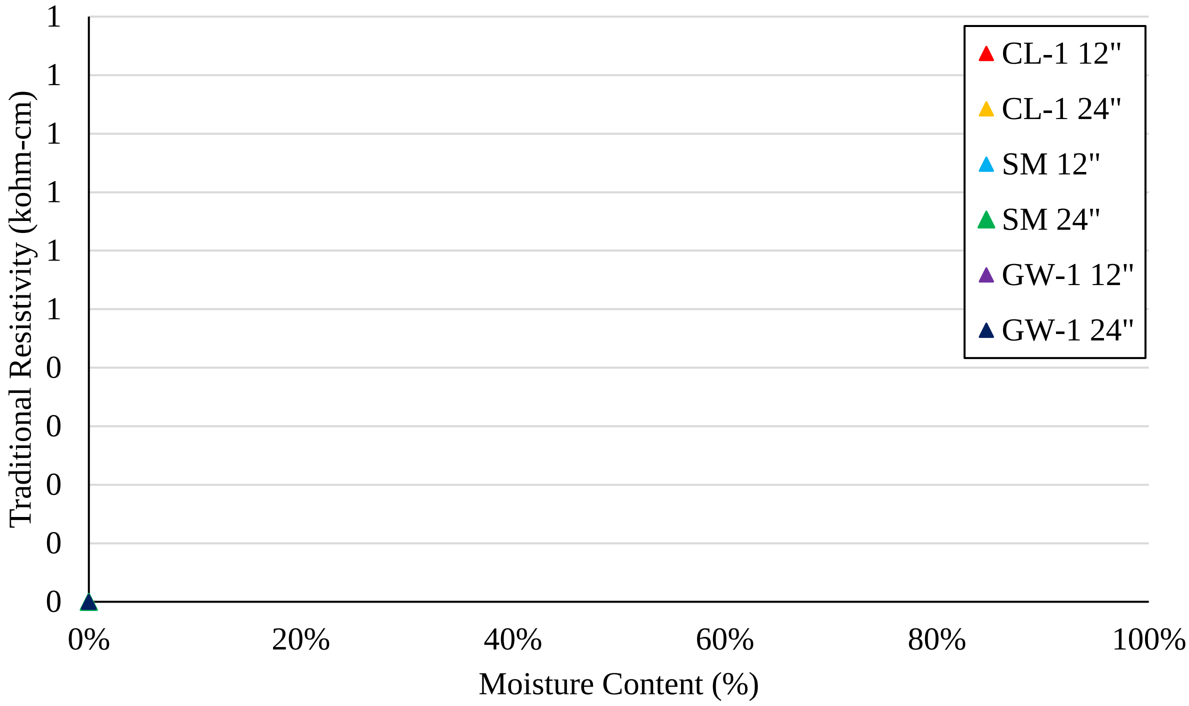

Figure 45: Traditional Resistivity Data of CL-1, SM, and GW-1 in Large Scale Specimens

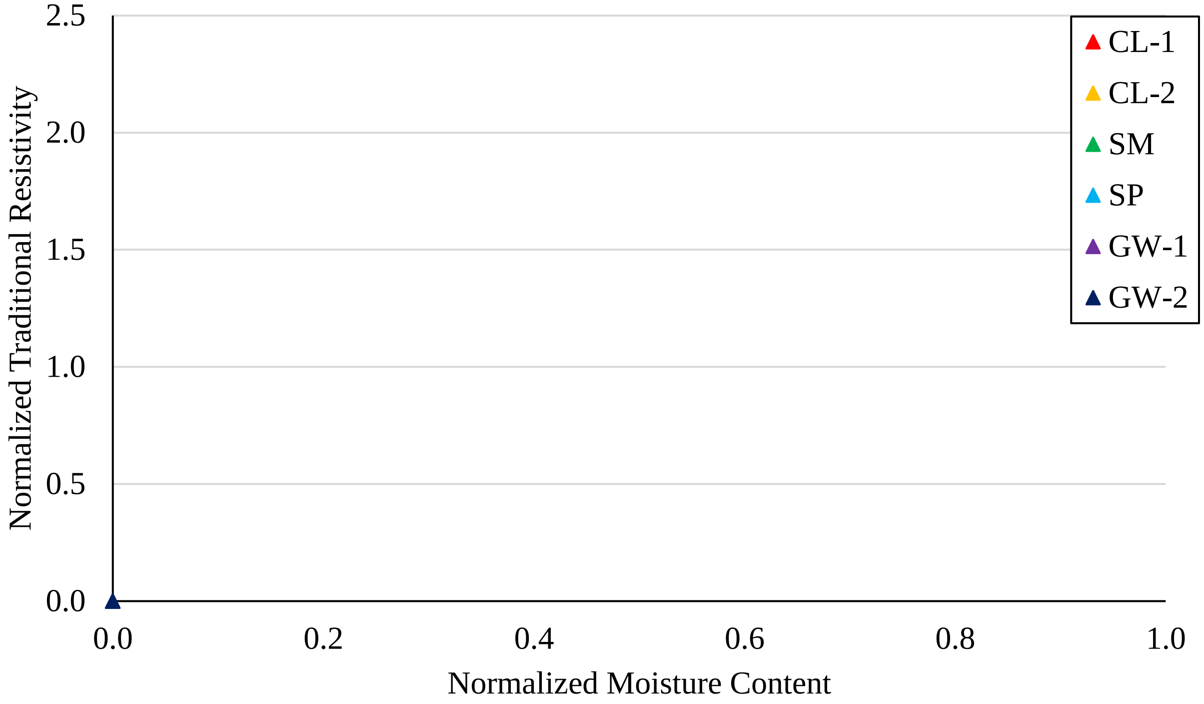

Figure 46: Normalized Traditional Resistivity of Soils in Large-Scale Specimens

To emphasize the importance of proper calibration, the measured resistivity's for the six materials are shown in Figure 47. A systematic difference between the mold and barrel measurements can be observed that can be attributed to the differences in compaction method and energy, among several other factors that were not considered in the adjustment factors. Nevertheless, the rate of change in resistivity with moisture content is the same between the laboratory and field data.

4.2.3 Impact of Specimen Size on TR

Comparing the different sizes of the specimens was critical in understanding the impact of moisture on the different measurements. Since for all materials (except the two GW materials), 4 in.-diameter and 6 in.-diameter specimens were prepared, the results from these two tests are reported below. As shown in Figure 48, the resistivity measurements adjusted for the geometry for the 6 in.-diameter specimens are close to corresponding values from the 4 in.-diameter specimens.

Some dispersion is noticed that may be contributed to the inevitable variation in moisture contents among specimens.

4.3 Repeatability

Five replicate specimens were made at three different moisture contents per material using the CL-1, SM, and GW-1 geomaterials to assess the repeatability of the moisture tests. The three moisture contents comprised OMC, OMC±20%×OMC for the clay, and OMC±2% for the sand and gravel. Table 4 shows the variability of the dielectric and resistivity measurements. The dielectric constant measurements showed a coefficient of variation between 10% and 32%, with a typical variability of about 20%. The coefficients of variation of the measurements with the traditional resistivity were 8.5% or less for all the specimens tested. Given the level of variability of the dielectric measurements, further analysis was not carried out in this report. The results are, however, documented in Appendix A. The coefficients of variation of the complex resistivity and phase change are shown at the 600 Hz frequency. The typical variability of the complex resistivity was under 20% but could range to a maximum of 26%. The phase changes showed a slightly higher variability with a maximum coefficient of variation of 28%.

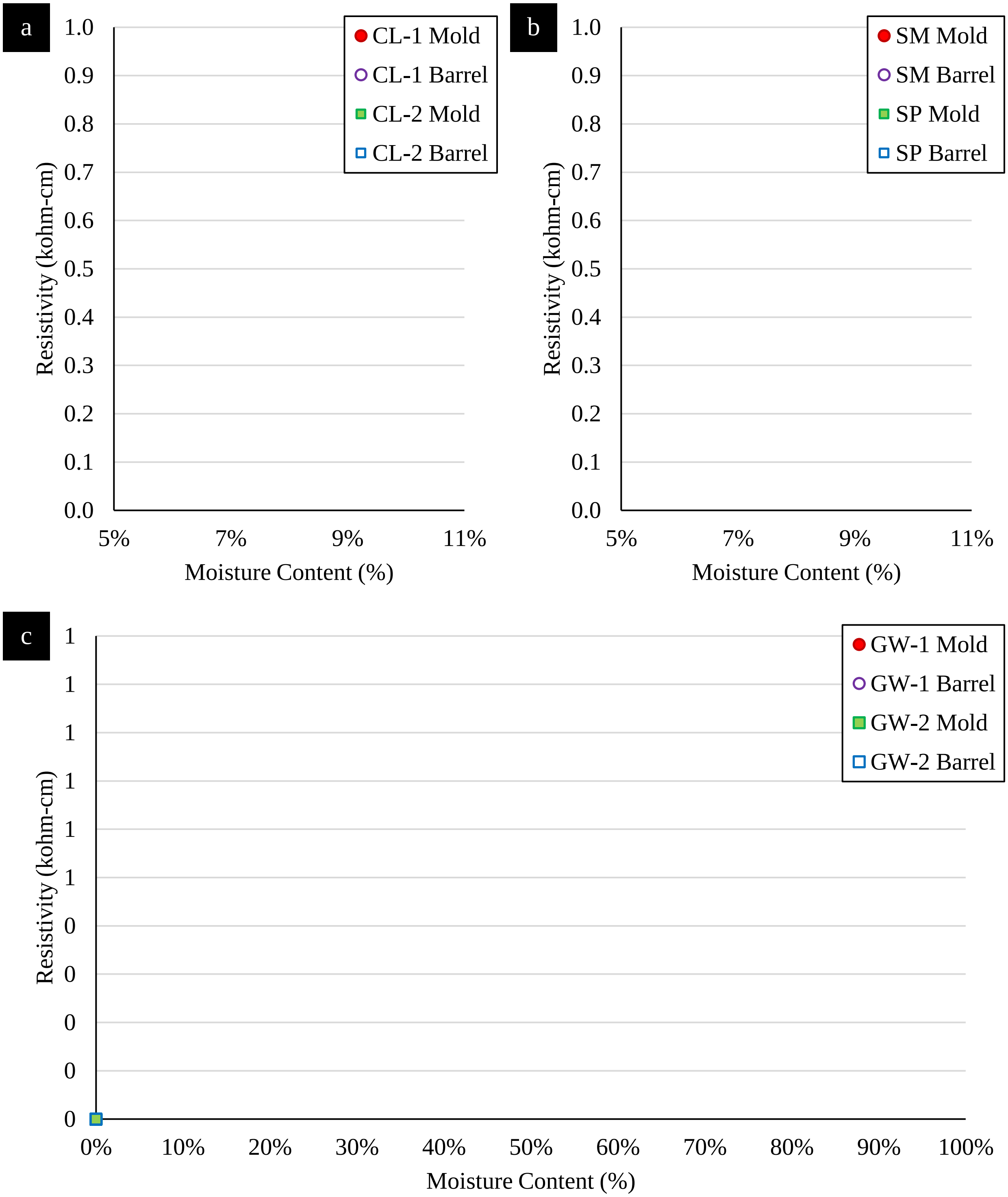

Figure 47: Comparison of TR of Lab and Large-Scale Specimens (a) Clays (b) Sands (c) Gravels

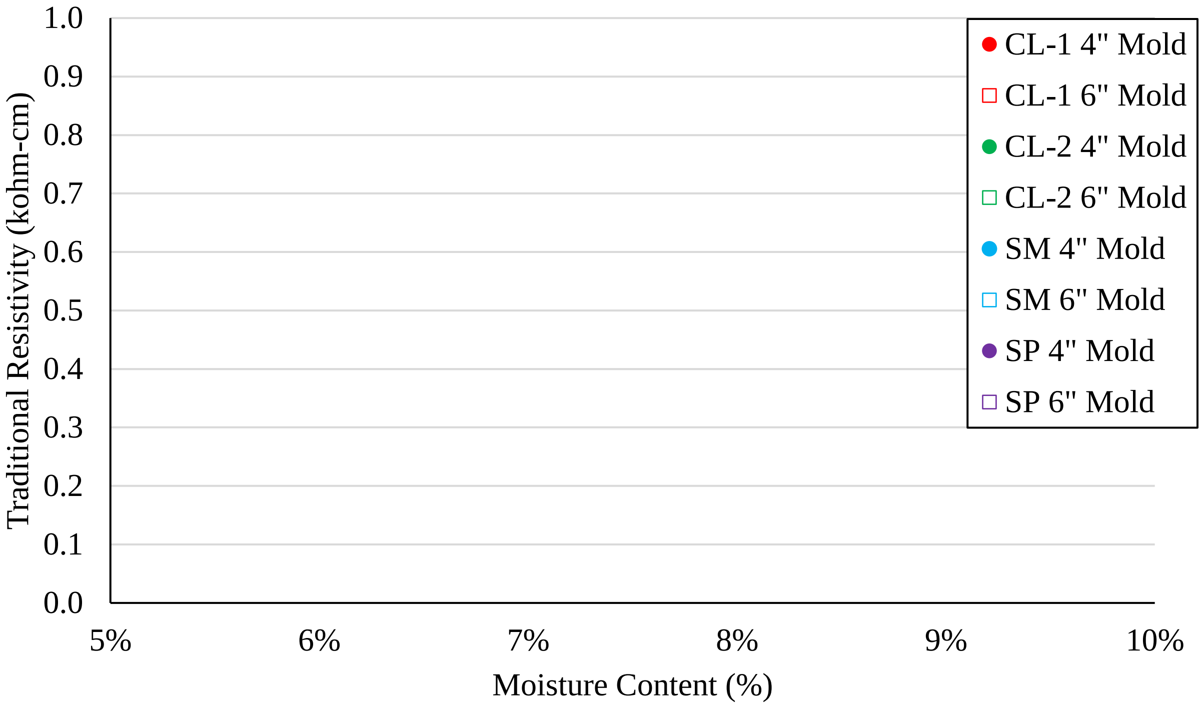

Figure 48: Comparison of Resistivity Measurements from Different Specimen Sizes

Table 4: Coefficient of Variation of Replicate Specimens

Measurement	**Soil**	**Dry**		**OMC**		**Wet**	
		Average	**Max**	**Average**	**Max**	**Average**	**Max**
Dielectric Constant	**CL-1**	19.7	21.6	20.7	32.3	13.7	18.2
	SM	9.8	11.7	14.1	27.0	10.6	18.0
	GW-1	13.4	22.0	26.0	32.1	20.4	28.0
Traditional Resistivity	**CL-1**	3.2	4.9	4.7	7.0	3.7	5.0
	SM	2.4	4.3	4.2	7.7	5.0	6.0
	GW-1	6.0	7.3	4.9	8.5	5.1	5.8
Complex Resistivity	**CL-1**	17.8	20.5	13.9	15.5	15.5	15.8
	SM	15.9	16.3	11.4	11.9	7.8	8.6
	GW-1	14.4	15.9	9.4	13.2	6.0	6.2
Complex Phase Change	**CL-1**	8.6	11.9	12.0	13.4	22.0	25.7
	SM	14.2	16.9	13.3	14.8	17.0	18.7
	GW-1	23.8	28.1	25.1	28.2	13.7	16.6

4.4 Complex Resistivity

The frequency and current operating parameters must be carefully chosen to distinguish saturation polarization from electrode-surface interactions when designing a measuring system for moisture management using CR. Figure 49 displays CR readings for CL-2 specimens in the cradle at four different moisture contents, seven frequencies labeled on the abscissa, and ten current levels at each frequency. The error bars represent one standard deviation estimation based on at least ten measurements at each current and include an uncertainty when the measured current deviates from the design current. Lower frequencies and low currents show high variation and low precision where electrode interactions are significant. Resistance magnitudes and resistance phase values with measurements impacted by electrode effects removed are depicted in Figures 50a and 50b, respectively. The upgraded version 8 electronics were used for these measurements.

About 20 current and voltage measurements per frequency and multiple currents are saved to a CSV file. The averages and standard deviations of these currents and voltages are then read, computed, and estimated in post-processing software. This step also calculates the ratio of the real and imaginary electrode voltages to the real and imaginary driving current. The software needs a calibration factor for resistivity magnitude and phase, followed by electrode geometry and sample shape calibration factors. The errors indicated for resistivity and phase are computed using randomized perturbations to observed voltages and currents due to the nonlinearity and dependencies in the computation. When fixed ideal resistors are connected to the cradle or array electrodes, this same measurement procedure provides calibration constants. The following four major features in the measurements shown in Figure 49 are apparent:

1. Although electrode polarization dominates measurements at low frequencies (60, 120 Hz: TR measurement domain), they exhibit consistent moisture and current dependency patterns. As we switch to a Wenner array with a reduced contact area, this electrode polarization reduces (higher current density).

2. There was an improvement in the measurement errors from version 6 to version 8 of the CR device; however, there is still error in the first few currents of each of the higher frequencies.
3. The fraction of ions polarizing at the air-water interface, which rises as moisture content drops, is measured by the phase change with moisture and frequency. At 600 Hz and above frequencies, resistivity and phase values exhibit consistent and substantial variations in moisture content. In general, the resistivity decreases with frequency as moisture content rises, reflecting that ions in the fluid move farther at lower frequencies while the potential water path increases. As the moisture content of the same sample varies, phase value should be able to distinguish saturation variations more accurately than resistivity. It needs to be clarified how resistivity/phase will alter when the texture changes during compaction.
4. By not being the highest while displaying the higher phase value anticipated for the lowest saturation, the blue curve at the lowest moisture content (11.4%) deviates from the expected resistivity pattern. The phase shifts in this specimen response happen less frequently than anticipated from published data on controlled samples. More significant scale deviations from uniformity are expected and likely cause the low-frequency phase irregularities at low moisture levels. Textural and gradation homogeneity is crucial in addition to moisture content.

A study in progress is the simplification of the CR data to infer moisture-sensitive parameters. Comparing the full spectrum CR tests for samples of the GW-2 and CL-2, with high uncertainty values eliminated, in Figure 50 demonstrates how difficult it is to simplify. First, a low-frequency CR estimate, an uncertainty, and the slopes of normalized CR with frequency and current were utilized to summarize each resistivity and phase curve’s characteristics. This comprehensive technique may be helpful in the lab or while making static diagnoses in the field; however, a more straightforward measurement and analysis are needed for field measurement in a continuous mode.

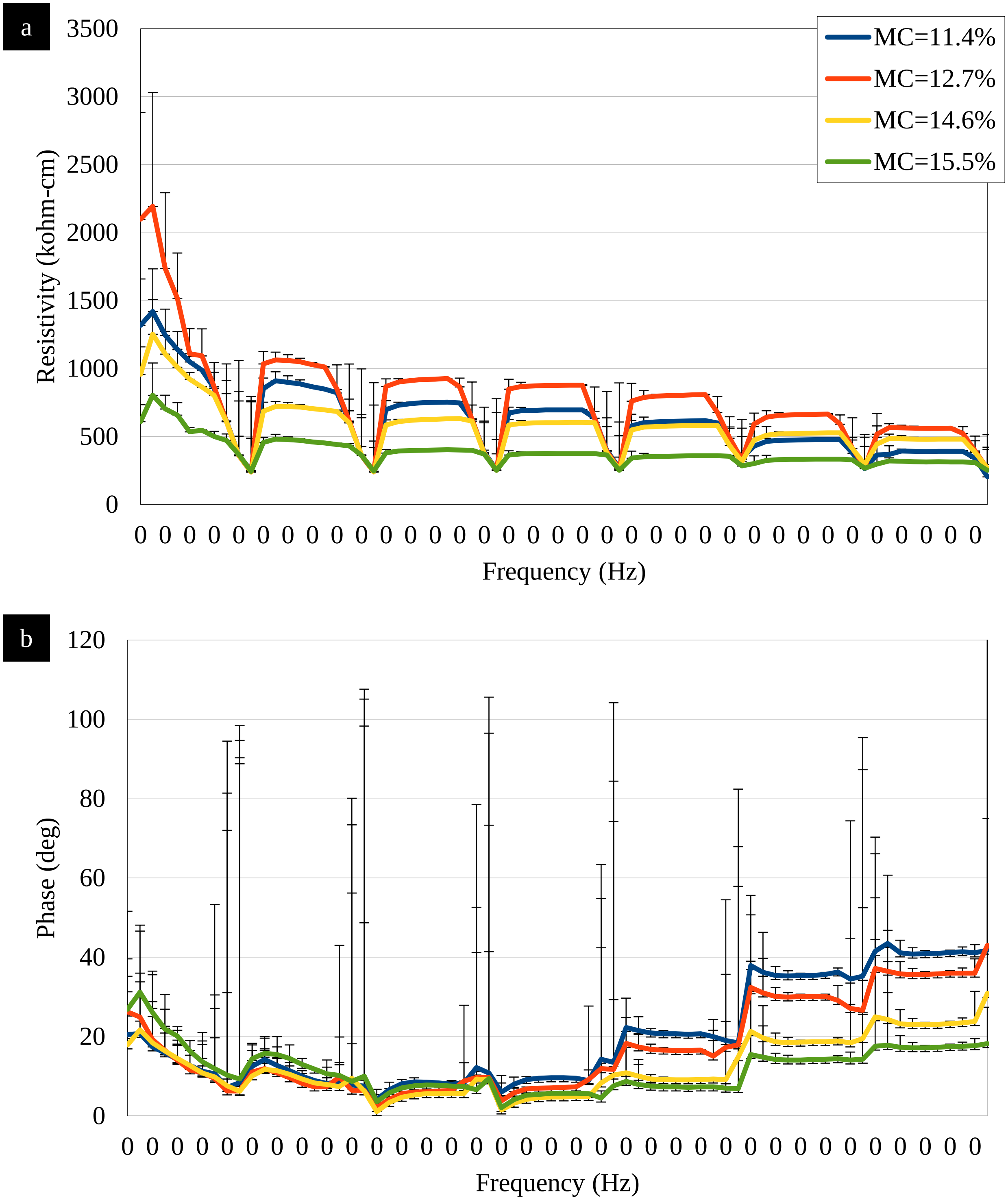

Figure 49: Sample Measurement of CL-2 of (a) CR and (b) Phase at Several Moisture Contents (MCs)

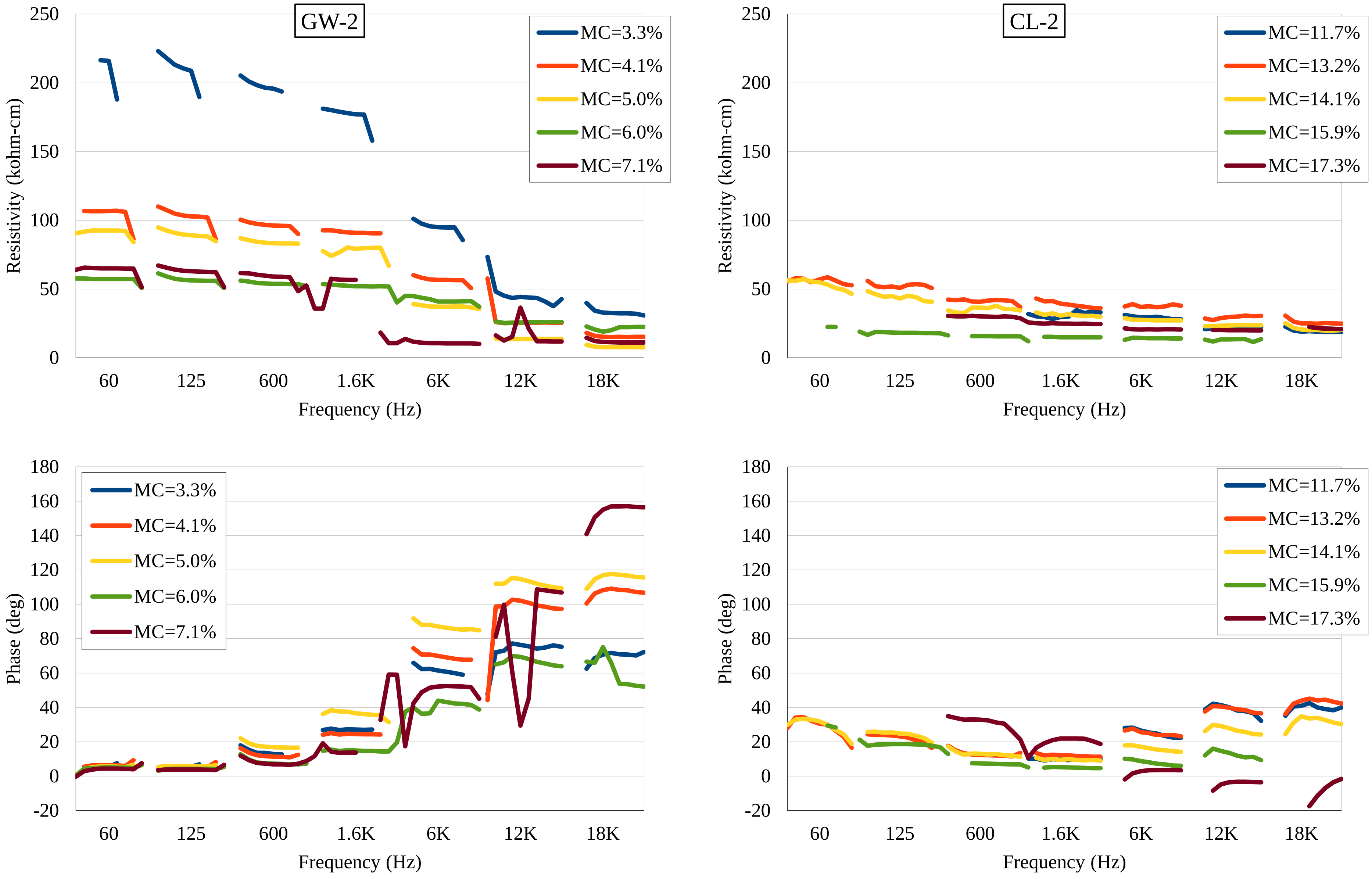

Figure 50: Large Scale Full Spectrum Tests of GW-2 and CL-2 of CR and Phase at Several Moisture Contents (MCs)

A composite plot of the CL-1, SM, and GW-1 measurements of resistivity and phase slope with frequency is shown in Figure 51 for comparison with the TR measurements in Section 4.2. Figure 52a shows the normalized complex resistivity, and Figure 52b shows the normalized phase values normalized to OMC. Both of the repeatability. There is more variation in the CR measurements, but the curve shapes are consistent with the moisture-resistivity relations previously discussed. There is more variability in the CR measurements; however, there is a correlation between resistivity and phase slope within each material type at a particular moisture level, which is consistent with the expectation that gradation changes in compaction are as crucial as moisture level changes to the CR measurements.

4.5 Seismic Modulus

The variations of the seismic modulus with moisture content for the fine-grained and sandy geomaterials are presented in Figure 53. There was difficulty obtaining the seismic moduli of the gravelly specimens due to the length-to-diameter ratios of the specimens. For all geomaterials demonstrated, the modulus decreases significantly with an increase in moisture content. The two CL soils exhibited significantly different moduli, despite demonstrating similar index properties and MDDs. This pattern demonstrates the importance of modulus measurements.

4.6 Unconfined Compressive Strength

The variations of the unconfined compressive strength with moisture content for each of the six geomaterials are demonstrated in Figure 54. Again, similar clays demonstrate different strengths, as was the case for the seismic modulus measurements.

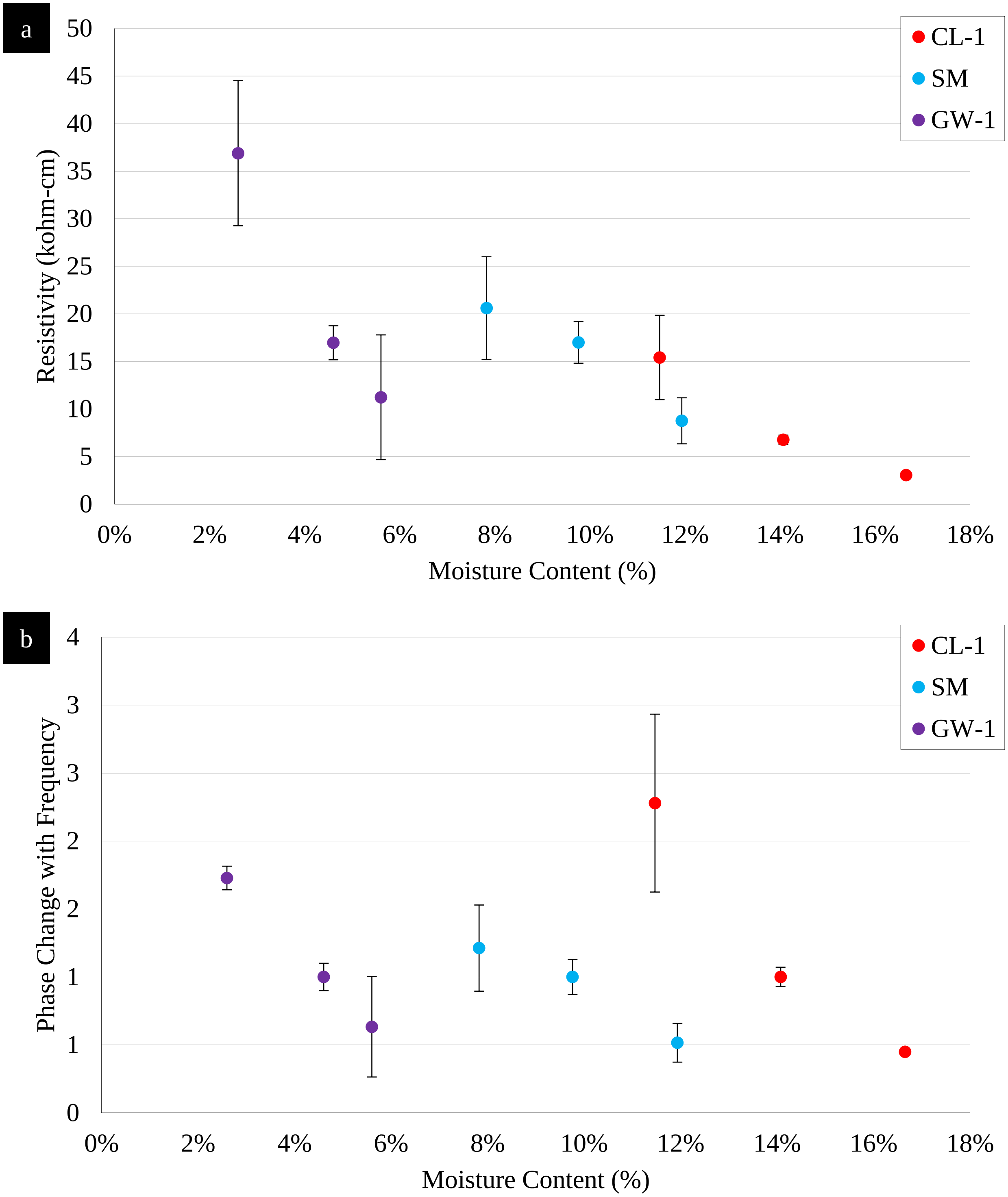

Figure 51: CR Data of CL-1, SM, and GW-1 (a) Resistivity (b) Phase-Change

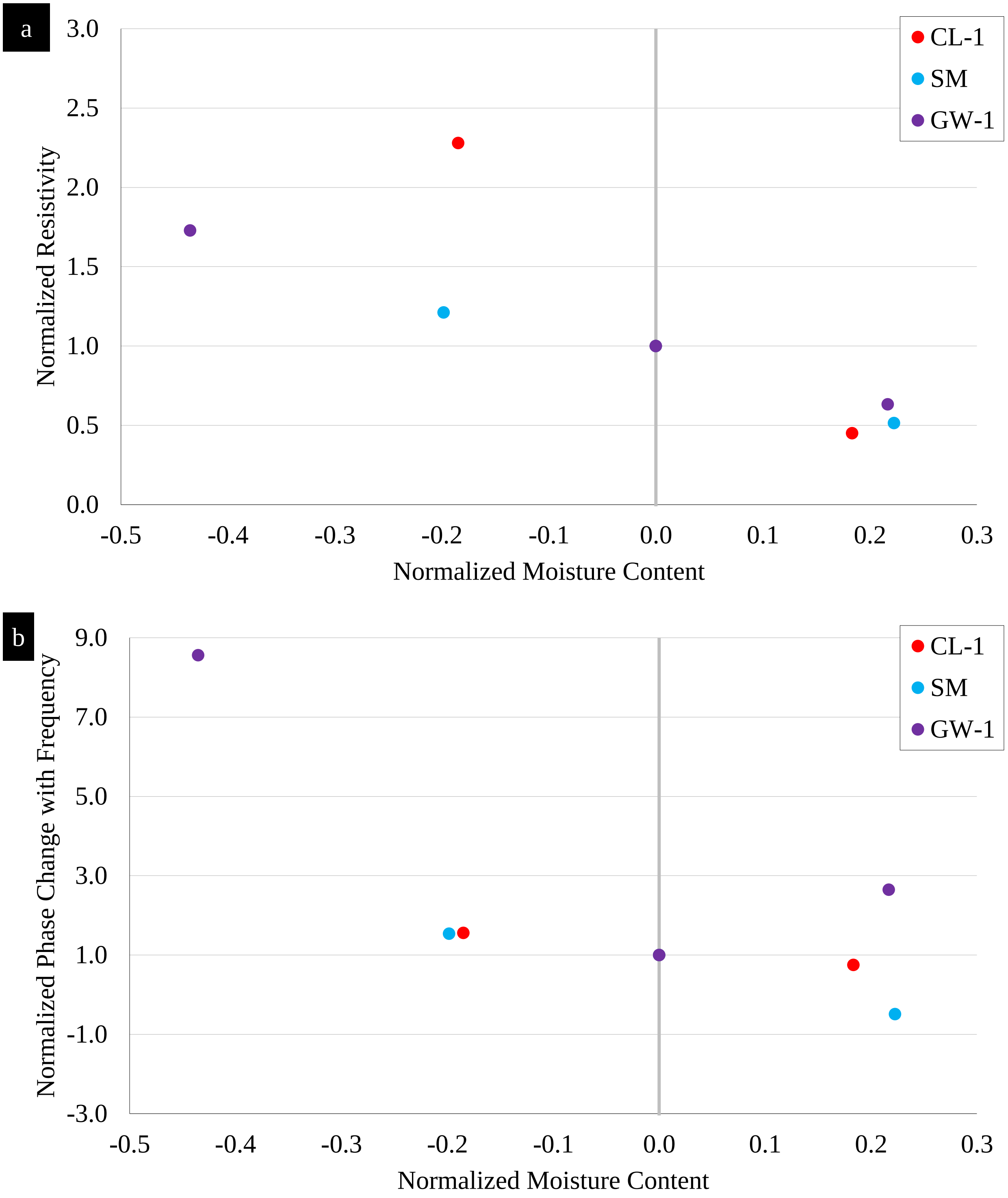

Figure 52: Normalized CR Data of CL-1, SM, and GW-1 (a) Resistivity (b) Phase-Change

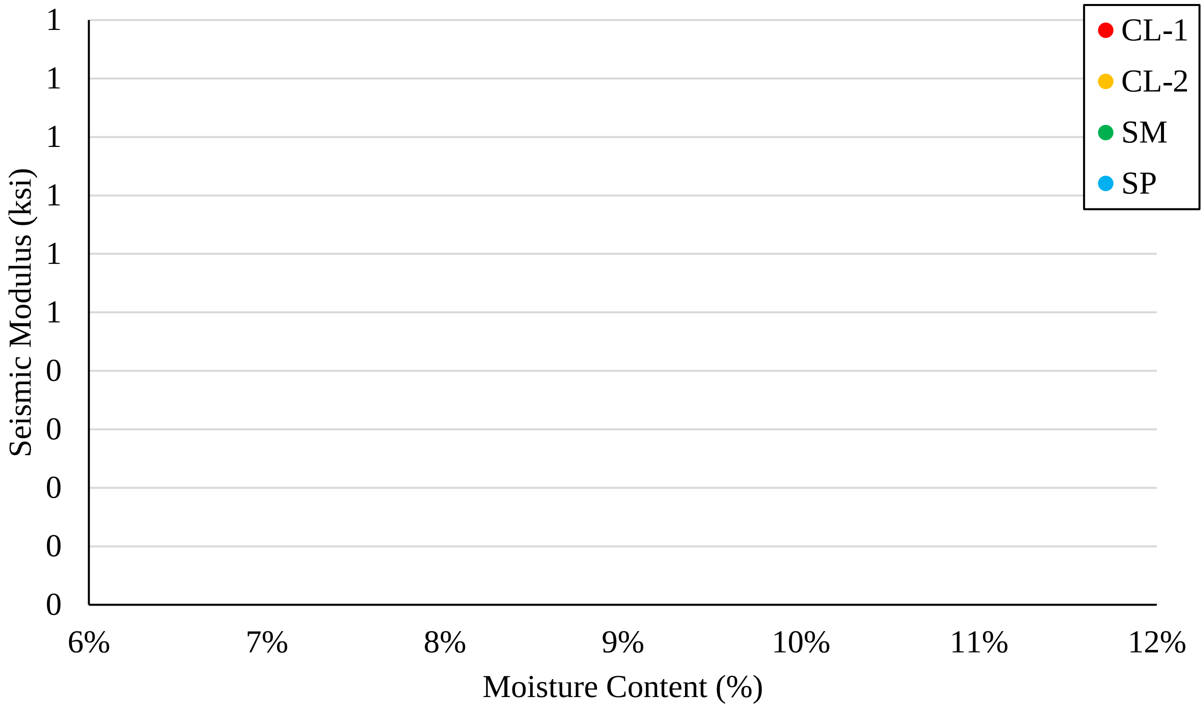

Figure 53: Seismic Modulus Data of Geomaterials

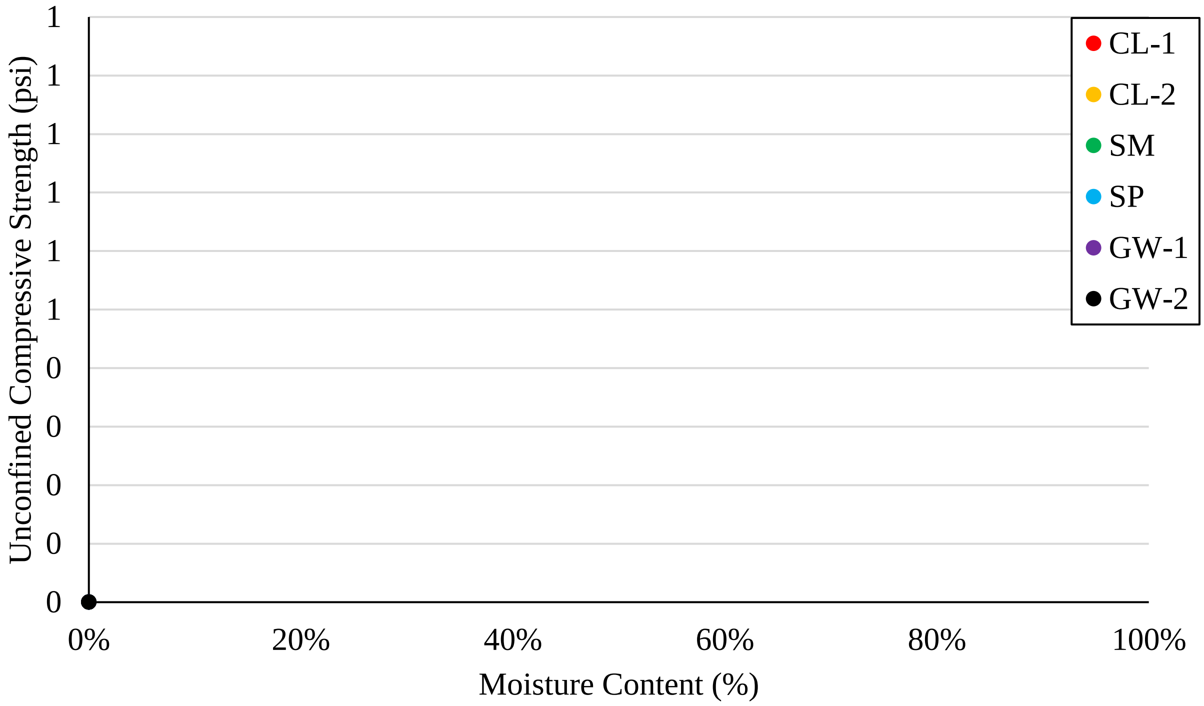

Figure 54: Unconfined Compressive Strengths of Geomaterials

4.7 Lightweight Deflectometer Moduli

The variations of the LWD modulus with moisture content for the six geomaterials using the special setup recommended for determining the target modulus are shown in Figure 55. The moduli of the sands tended to decrease as moisture increased. The height at which the large-scale specimens were tested played a factor in the measured moduli. The LWD moduli of both clays and the SP geomaterial followed similar patterns between the laboratory and large-scale specimens. The modulus of the SM had high variability at different heights. The modulus of the barrels for the gravels minimally changed or increased slightly.

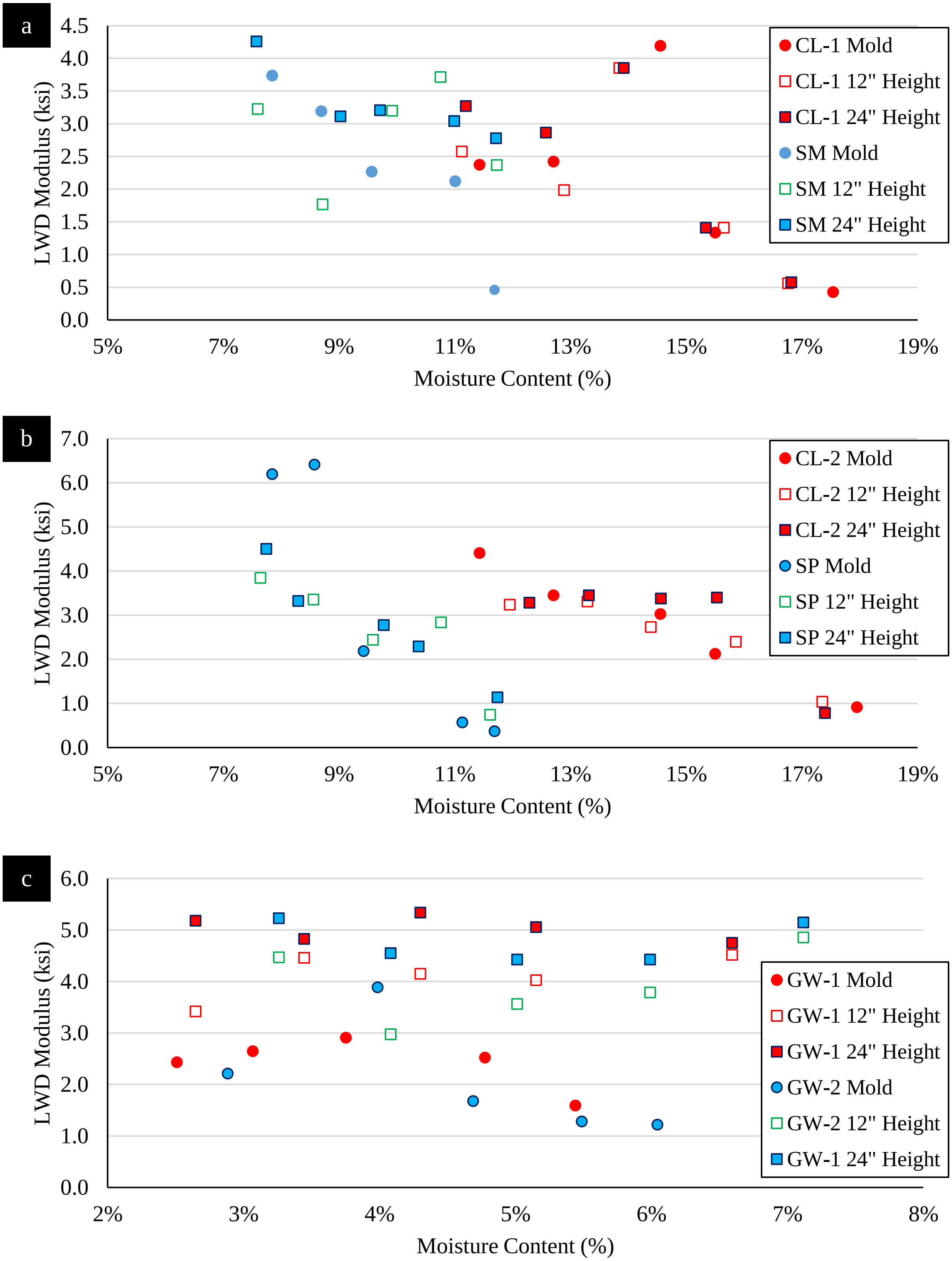

Figure 55: Laboratory-Measured Lightweight Deflectometer Moduli of Geomaterials

CHAPTER 5 –CONCLUSIONS AND RECOMMENDATIONS

In this study, six geomaterials were compacted to standard/modified proctor specifications and subjected to laboratory measurements to study the variations in their electromagnetic and electric properties with moisture content. The relationships between the seismic modulus, unconfined compressive strength, and moisture content for the same geomaterials were also established. Large-scale replicate specimens were also compacted and subjected to numerous measurements. The following lessons were learned from completing these measurements:

1. The complex resistivity showed promise in supplementing the information obtained from the traditional resistivity; however, work is still required to improve the hardware and technician-friendly software.
    a. Aside from moisture content, grain size and specimen homogeneity play a more significant role in measuring resistivity than previously expected. Future work could look at how important each feature holds on resistivity.
2. The dielectric constants measured with a Percometer were less sensitive and more uncertain about the moisture content variations than the resistivity values measured with a Wenner probe.
3. Traditional resistivity measurements were repeatable and consistent among different types of soils used in this study. Also, a good correlation was observed between the laboratory compacted specimens and corresponding measurements in a large-scale specimen of the same soil.
4. The resistivity changes are less pronounced for the materials at moisture contents wet of OMC.
5. The seismic modulus values were the most sensitive parameter to the moisture content for all materials.

6. The unconfined compressive strengths also changed significantly with the moisture contents wet of OMC and generally plateaued when the moisture contents were dry of OMC.
7. The lightweight deflectometer modulus showed little to no correlation to moisture content.
    a. For many of the specimens, after the initial 3 drops, there was significant deformation in the vertical height of the specimens.
8. The normalization scheme helps collapse the variations of the parameters with moisture content into a narrow band for easier comparison independent of the material type.

5.1 Recommendations

As DOTs begin and continue to use reclaimed asphalt pavements (RAP) and recycled concrete aggregate (RCA) in base and subbase mixes, the high polarizing nature of binder and calcium carbonate, found in RAP and RCA, respectively, is something that must be studied if resistivity is to be used in monitoring moisture.

The grain size of the large base materials exhibited similar complex and traditional resistivity measurements to the finer-grained soils; however, due to the calcium carbonate found in the tested bases, complex resistivity polarization occurred frequently and coated the different arrays. The calcium carbonate coating created numerous anomalies requiring frequent cleaning of the contact electrodes. Also, during the summer of 2022, a rolling array was tested on a subbase and base containing different RAP and RCA percentages. The hydrophobic nature of the RAP caused enormous resistivities and strange polarization not expected nor measured within the laboratory setting.

REFERENCES

Baltzer, S., Pratt, D., Weligamage, J., Adamsen, J., and Hildebrand, G. (2010). "Continuous bearing capacity profile of 18,000 km Australian road network in 5 months." In 24th ARRB Conference, Melbourne, Australia.

Bell, J.P., Dean, T.J., and Hodnett, G.C. (1987). "Soil moisture measurement by an improved capacitance technique, Part II. Field techniques, evaluation and calibration." J. of Hydrology 93 (1-2): 79-90

Bogena, H. R., Huisman, J. A., Oberdörster, C., & Vereecken, H. 2007. "Evaluation of a low-cost soil water content sensor for wireless network applications." Journal of Hydrology, 344(1-2), 32-42.

Brand, A.S., Roesler, J.R., Chavan, H.L., and Evangelista F. (2013). "Effects of a nonuniform subgrade support on the responses of concrete pavement." Report No. ICT-13-027, University of Illinois at Urbana-Champaign, 142 p.

Campbell, C. (2019). "Improving the Outcomes of Geomaterial Field Monitoring Campaigns" Transportation Research Board, Washington, D.C.

Cole, S., & Buis, A. "NASA soil moisture radar ends operations, mission science continues." SMAP. URL: https://smap. jpl. nasa. gov/news/1247/nasa-soil-moisture-radarends-operations-mission-science-continues/(visited on 09/08/2017).

Emilsson, J., Englund, P., and Friborg, J., (2002). "Simple method for estimation of water content of roadbeds using multi-offset GPR." In Ninth International Conference on Ground Penetrating Radar (Vol. 4758, pp. 422-426). International Society for Optics and Photonics.

Entekhabi, D., Yueh, S., O'Neill, P. E., Kellogg, K. H., Allen, A., Bindlish, R., and Das, N. (2014). "SMAP handbook–soil moisture active passive: Mapping soil moisture and freeze/thaw from space."

Evett, S. R., Heng, L. K., Moutonnet, P., and Nguyen, M. L. (2008). "Field estimation of soil water content: A practical guide to methods, instrumentation, and sensor technology." IAEA: Vienna.

Ferne, B. W., Langdale, P., Round, N., and Fairclough, R. (2009). "Development of a calibration procedure for the UK highways agency traffic-speed deflectometer." Transportation research record, 2093(1), 111-117.

Genc, D., Ashlock, J. C., Cetin, B., and Kremer, P. (2019). “Development and pilot installation of a scalable environmental sensor monitoring system for freeze-thaw monitoring under granular-surfaced roadways.” Transportation Research Record, 0361198119854076.

Gerhards, H., Wollschläger, U., Yu, Q., Schiwek, P., Pan, X., & Roth, K. (2008). Continuous and simultaneous measurement of reflector depth and average soil-water content with multi-channel ground-penetrating radar. Geophysics, 73(4), J15-J23.

Grabe, J., and Mahutka, K.-P. (2005). “Long-term evenness of pavements with respect to soil deformations.” Proceedings Seventh International Conference on the Bearing Capacity of Roads, Railways and Airfields.

Hansen, B.J. and Nieber, J.L. (2013). “Performance-based measurement of optimum moisture for soil compaction.” Report MN/RC 2013-28, University of Minnesota, 53 p.

Jones, S. B., Wraith, J. M., a.”nd Or, D. 2002. “Time domain reflectometry measurement principles and applications.” Hydrological processes, 16(1), 141-153.

Kelley, J., and Moffat, M., 2011. “Review of the Traffic Speed Deflectometer-Final Project Report.” ARRB Group, Melbourne, Australia, Austroads Report AT1613.

Kurtz, L. 2019. “How to measure moisture content”. Wikihow. URL: https://www.wikihow.com/Measure-Soil-Moisture

Liang, R. Y., Al-Akhras, K., and Rabab'ah, S. 2006. Field monitoring of moisture variations under flexible pavement. Transportation research record, 1967(1), 160-172.

Maser, K. R. and Scullion, T., (1992). “Automated pavement subsurface profiling using radar: case studies of four experimental field sites.”

McNairn, H., Jackson, T. J., Powers, J., Bélair, S., Berg, A., Bullock, P., ... and Pacheco, A. 2016. “Experimental plan SMAP validation experiment 2016 in Manitoba, Canada (SMAPVEX16-MB).”

Mittelbach, H., Casini, F., Lehner, I., Teuling, A. J., and Seneviratne, S. I. (2011). “Soil moisture monitoring for climate research: Evaluation of a low-cost sensor in the framework of the Swiss Soil Moisture Experiment (SwissSMEX) campaign.” Journal of Geophysical Research: Atmospheres, 116(D5).

Muller, W., (2017). “Characterizing moisture within unbound granular pavements using multi-offset Ground Penetrating Radar.”

Robinson, D.A., Jones, S.B., Wraith, J.M., Or, D., and Friedman, S.P. (2003). “A review of advances in dielectric and electrical conductivity measurement in soils using time domain reflectometry.” Vadose Zone J. 2, 444–475

Saïd, M. N. A. (2007). “Measurement methods of moisture in building envelopes–a literature review.” International Journal of Architectural Heritage, 1(3), 293-310.

Sebesta, S., Taylor, R., and Lee, S. I., 2013. 0-6676: “Rapid field detection of moisture content for base and subgrade: (No. 0-6676).” Texas. Dept. of Transportation. Research and Technology Implementation Office.

Shaikh, J., Yamsani, S. K., Sekharan, S., and Rakesh, R. R. (2018). “Performance Evaluation of Profile Probe for Continuous Monitoring of Volumetric Water Content in Multilayered Cover System.” Journal of Environmental Engineering, 144(9), 04018078.

Singh, J. (2017). “Performance Assessment of Electromagnetic Soil Water Sensors in Different Soil Textural, Temperature, and Salinity Conditions.”

Sotelo, M. J., (2012). “Evaluation of non-nuclear devices in measuring moisture content and density of soils.”

Svensson, J. (1997). “Moisture content in road pavements: state of the art and development of a simple moisture measurement equipment.” Swedish National Road and Transport Research Institute., VTI Meddelande 809A.

Topp, G.C., Davis, J., and Annan, A.P. (1980). “Electromagnetic determination of soil water content: Measurements in coaxial transmission lines.” Water Resources Research 16(3): 574-582

University of Sherbrooke (2012). “SMAP Validation Experiment (SMAPVEX12).”

UTEST. 2016. “RoadReader nuclear density gauges”.

Viyanant, C., Rathje, E. M., and Rauch, A. F. (2004). “Compaction control of crushed concrete and recycled asphalt pavement using nuclear gauge.” In Geotechnical Engineering for Transportation Projects (pp. 958-966).

White, D.J., Li S., and Vennapusa P. (2016). "Embankment Quality and Assessment of Moisture Control Implementation," Report IHRB Project TR-677, Center for Earthworks Engineering Research, Iowa State University, 225 p.

White, D.J. (2019). "Optimizing Placement Cost using Material Specific Compaction Energy and Moisture Content" Transportation Research Board presentation, Washington, D.C.

White, D.J., Vennapusa P., and Cetin B. (2021). "Improving the foundation layers for concrete pavements: lessons learned and a framework for mechanistic assessment of pavement foundations" Report 09-352, Iowa State University, 141 pp.

Wollschläger, U., Gerhards, H., Yu, Q., and Roth, K. (2010). "Multi-channel ground-penetrating radar to explore spatial variations in thaw depth and moisture content in active layer of a permafrost site." The Cryosphere, 4(3), 269.

Yu, X., and Yu, X. (2009). "Time domain reflectometry automatic bridge scour measurement system: principles and potentials." Structural Health Monitoring, 8(6), 463-476.

Yueh, S., O'Neill, P. E., Butler, R., Osornia, L. M., Hu, W., Hanna, M., Ballard, C., and Mizukami, M., Mission Description SMAP. URL: https://smap.jpl.nasa.gov/news/1247/ nasa-soil-moisture-radar-ends-operations-mission-science-continues/(visited on 09/08/2017).

APPENDIX A- COMPREHENSIVE DATASETS

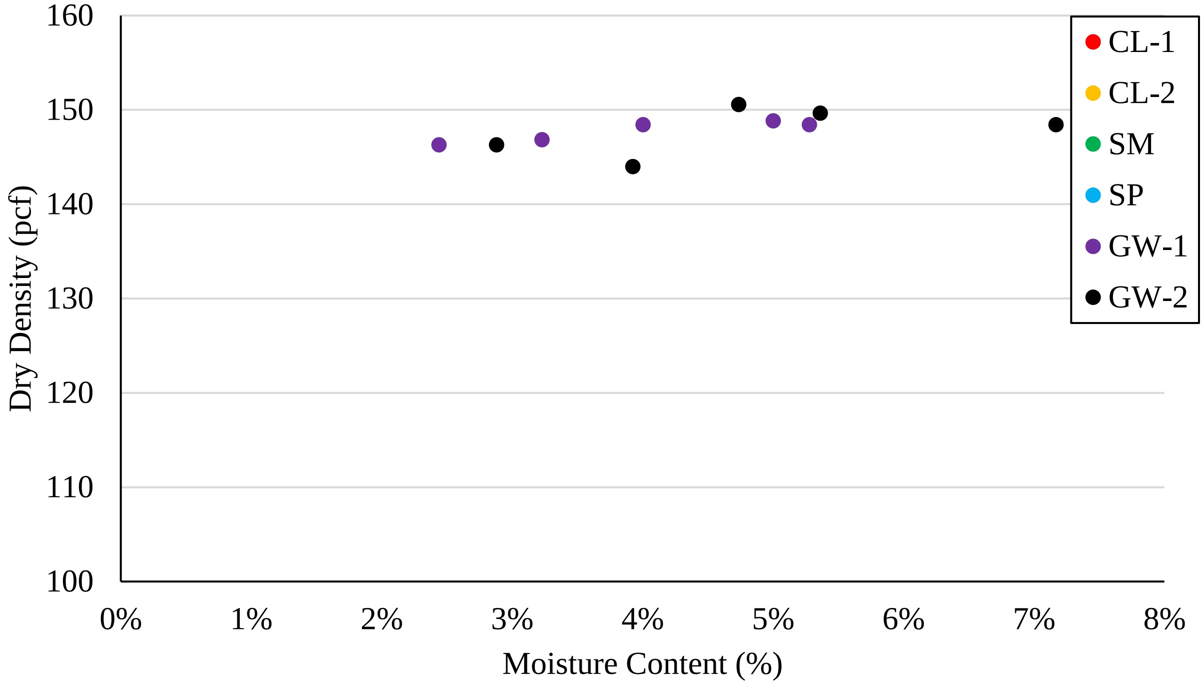

Figure A- 1: MD Curves of 4 in. Specimens and 6 in. Gravel Specimens

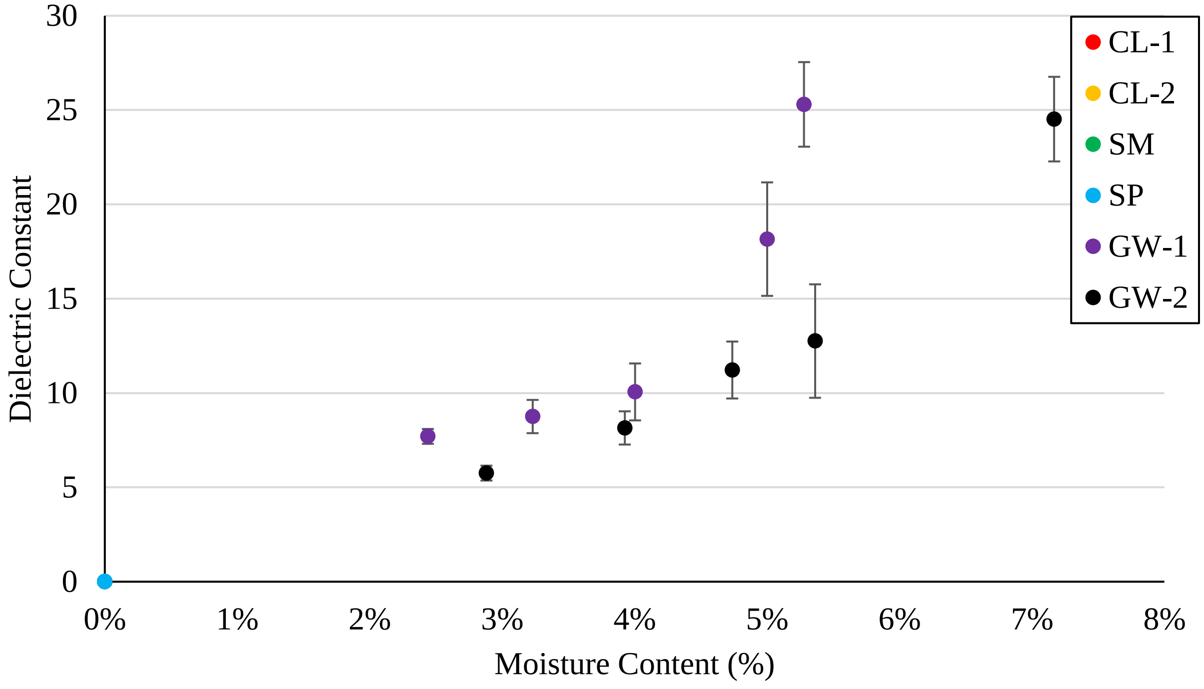

Figure A- 2: Dielectric Constant of 4 in. Specimens and 6 in. Gravel Specimens

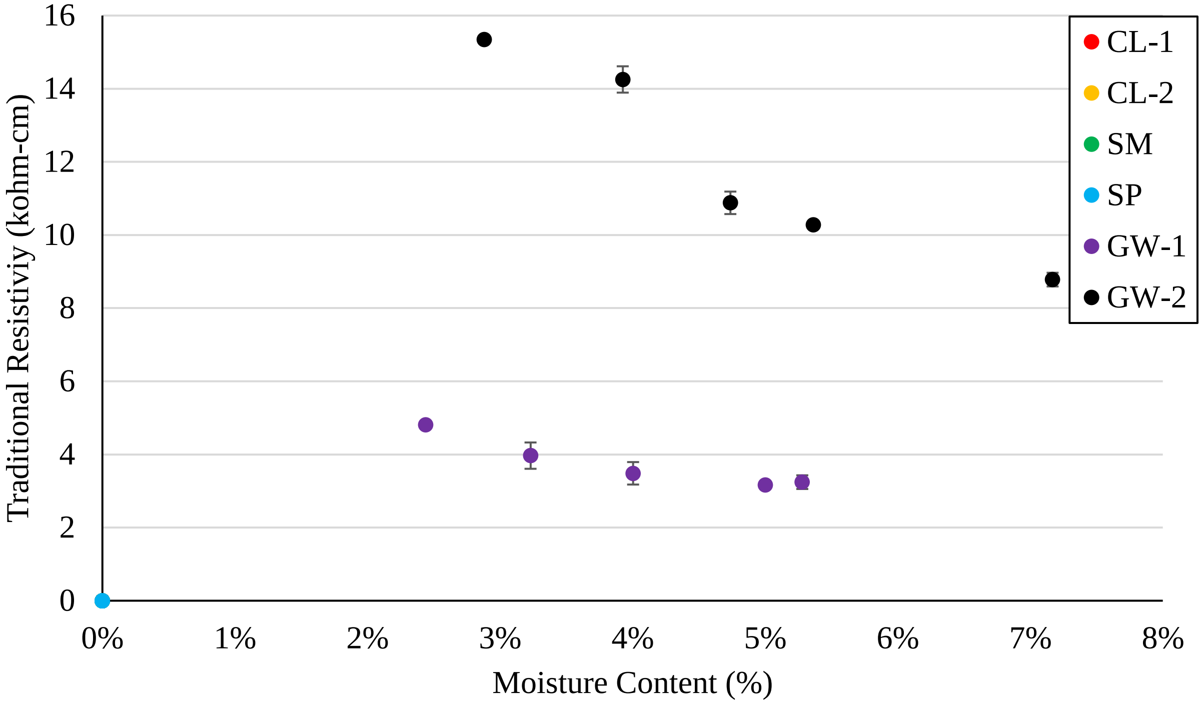

Figure A- 3: Traditional Resistivity of 4 in. Specimens and 6 in. Gravel Specimens

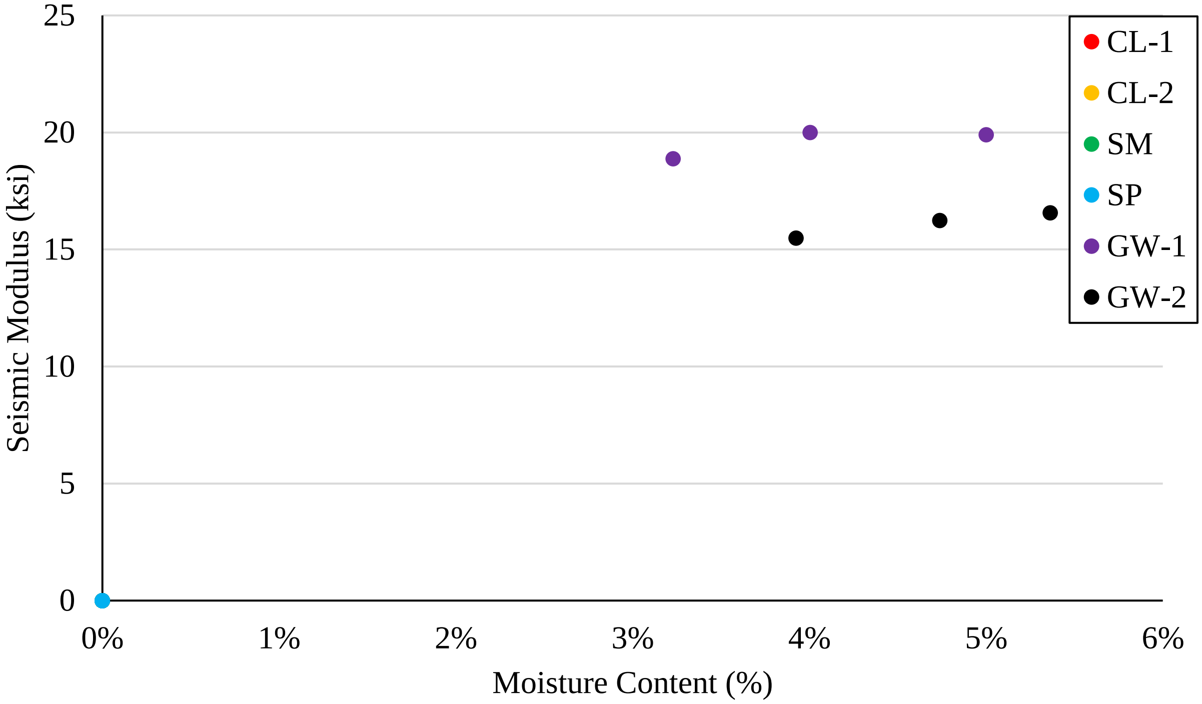

Figure A- 4: Seismic Modulus of 4 in. Specimens and 6 in. Gravel Specimens

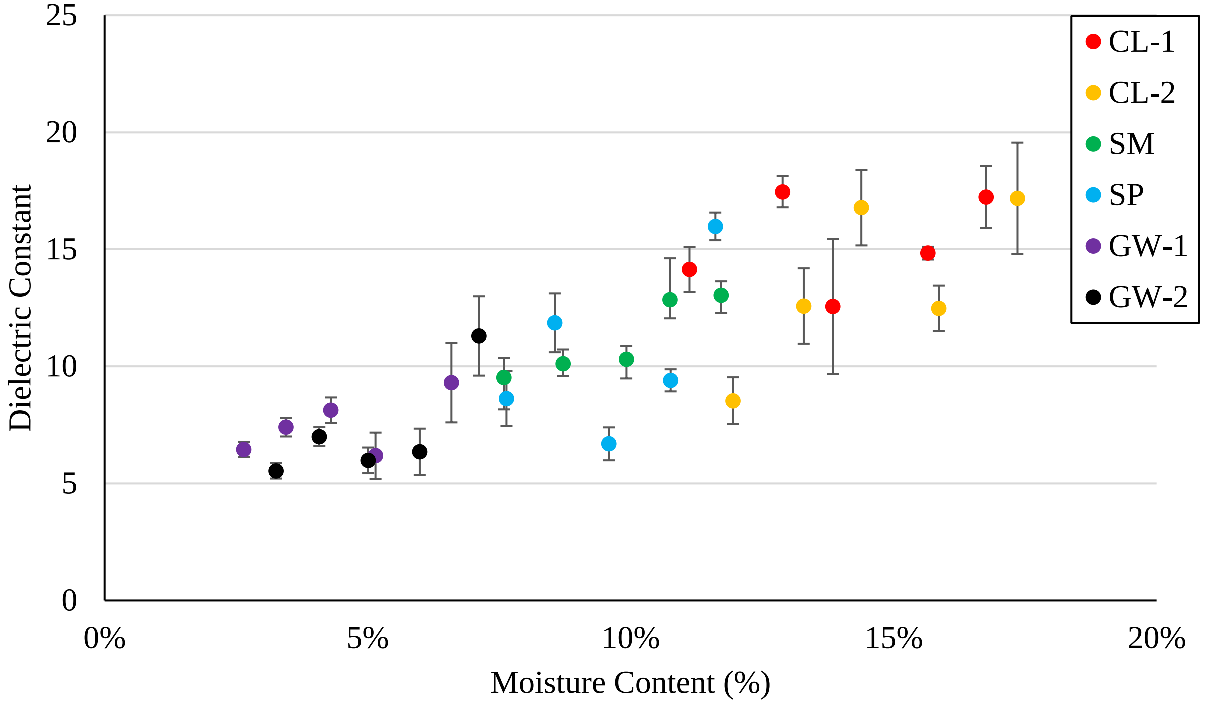

Figure A- 5: Dielectric Constant Measurement in Large Scale Specimen at 12 in. Height

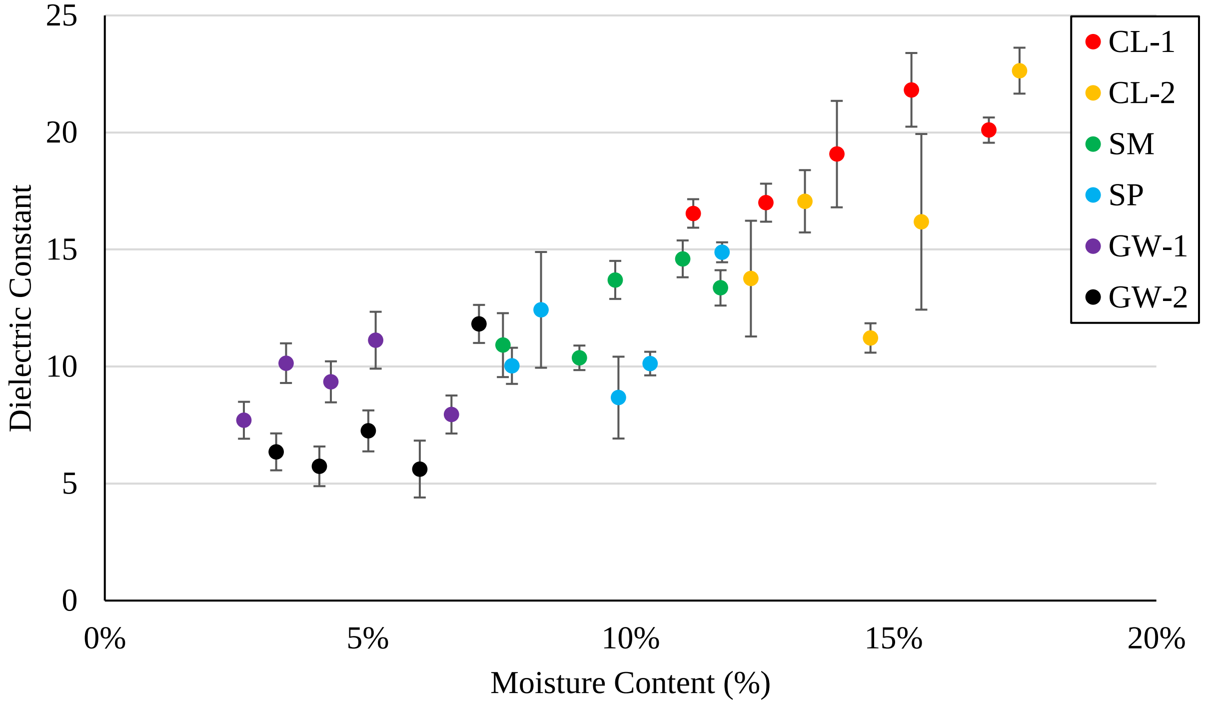

Figure A- 6: Dielectric Constant Measurement in Large Scale Specimen at 24 in. Height

Table A- 1: Coefficients of Variation of Measurements of Lab Specimens

Measurement	Soil	Dry		OMC		Wet	
		Average	Max	Average	Max	Average	Max
Seismic Modulus	**CL-1**	5.4	8.5	3.5	4.0	3.9	9.1
	SM	4.0	7.6	2.8	4.7	8.1	12.9
	GW-1	Not Tested		13.8	19.9	Not Tested	
Unconfined Compressive Strength	**CL-1**	7.5	N/A*	8.5	N/A*	8.1	N/A*
	SM	25.6		24.9		7.9	
	GW-1	Not Tested		21.0		Not Tested	
Lightweight Deflectometer	**CL-1**	1.6	3.3	0.4	0.7	2.2	6.0
	SM	1.1	1.7	3.0	5.5	3.8	7.3
	GW-1	3.0	5.6	1.4	2.3	1.9	4.3

*** Not applicable since only one test can be done per specimen**

Table A- 2: Coefficients of Variation for Measurements on Large Scale Specimens at 12 in. Height

Measurement	Soil	Dry		OMC		Wet	
		Average	Max	Average	Max	Average	Max
Lightweight Deflectometer	**CL-1**	6.9	14.0	6.4	14.3	4.2	6.3
	SM	9.7	10.3	9.9	16.3	10.5	16.9
	GW-1	7.1	12.7	5.5	13.9	7.8	10.0
Dielectric Constant	**CL-1**	7.1	10.5	7.4	10.1	18.0	26.4
	SM	5.0	7.0	7.2	7.9	6.5	12.7
	GW-1	17.4	29.8	20.8	31.8	24.7	41.1
Traditional Resistivity	**CL-1**	3.5	4.5	5.3	7.4	6.6	10.2
	SM	1.0	2.1	2.3	4.3	3.1	4.0
	GW-1	4.8	5.7	6.7	10.0	7.2	9.1

Table A- 3: Coefficients of Variation for Measurements on Large Scale Specimens at 24 in. Height

Measurement	Soil	Dry		OMC		Wet	
		Average	Max	Average	Max	Average	Max
Lightweight Deflectometer	**CL-1**	8.6	18.8	5.1	9.2	3.4	5.5
	SM	7.3	15.9	13.7	18.6	8.2	15.0
	GW-1	4.4	8.3	6.8	14.0	7.4	14.6
Dielectric Constant	**CL-1**	4.6	8.9	11.1	14.1	4.9	10.0
	SM	7.5	7.6	6.3	8.5	4.7	6.7
	GW-1	7.0	10.1	17.1	19.6	29.8	43.9
Traditional Resistivity	**CL-1**	3.3	3.6	3.2	6.3	5.6	8.0
	SM	0.9	1.8	1.8	3.9	2.3	2.8
	GW-1	4.1	5.5	4.9	7.1	8.5	10.2

CURRICULUM VITA

Isaac Zuniga was born in the Central Valley of California in August of 1998. He is the first son of three. He graduated from the University of Texas at El Paso (UTEP) with a bachelor's degree in Civil Engineering in the spring of 2021. He entered into the graduate program at UTEP the subsequent fall. He joined the Center for Transportation Infrastructure Systems (CTIS) as an Undergraduate Research Assistant and continued as a Master's Research Assistant during the master's program. His graduate work was titled "Continuous Moisture Measurement during Pavement Foundation Construction," funded by the National Road Research Alliance. He can be contacted at blankzuniga@gmail.com.